Universidade de Lisboa

Faculdade de Ciências

Departamento de Física

Experimental Investigation of Newly Developed Zeolite Membranes for Tritium Process in the Breeding Blanket

Rodrigo Nuno Mendes Antunes

Dissertação

Mestrado Integrado em Engenharia Física

Setembro 2014

Universidade de Lisboa

Faculdade de Ciências

Departamento de Física

Experimental Investigation of Newly Developed Zeolite Membranes for Tritium Process in the Breeding Blanket

Rodrigo Nuno Mendes Antunes

Dissertação

Mestrado Integrado em Engenharia Física

Supervisors:
Doctor David Demange[1]
Prof. Doctor Teresa Madeira Amorim[2]

Setembro 2014

[1]Institute for Technical Physics, Karlsruhe Institute of Technology
[2]Departamento de Física, Faculdade de Ciências, Universidade de Lisboa, 1749-016 Lisboa

Abstract

Tritium (hydrogen radioactive isotope) is proposed as fuel for nuclear fusion energy, and shall be produced directly in the machine inside the so-called Breeding Blanket (BB). An advanced two-step process for extracting tritium from the BB of the DEMOnstration reactor was recently proposed by the Tritium Laboratory Karlsruhe (TLK), where a pre-concentration stage with membranes is followed by a catalytic membrane reactor. A dedicated experimental program has been started at TLK to search for the most promising membranes, using a specifically built facility. This work presents the results of the gas permeation experiments performed on three zeolite (MFI-ZSM5, NaA and SOD) and one carbon membranes. The SOD and carbon membranes evidenced to be considerably defected to provide any gas separation. The single helium, nitrogen and hydrogen experiments on the MFI-ZSM5 demonstrated that the latter is the most permeable and a H_2/He ideal selectivity of 2.11 ± 0.10 at room temperature was obtained. The H_2/He binary mixture experiments on the MFI-ZSM5 showed that the separation factor reaches a maximum of 1.68 ± 0.10 at 0.3 cut without any significant dependence on the H_2 concentration between 0.10% and 10%. 1% H_2O/He binary mixtures experiments were performed on the NaA and MFI-ZSM5 and a strong increase of the separation factor with the decrease of the temperature was observed for the two membranes. From the 1%/1% H_2/H_2O/He ternary experiments on the MFI-ZSM5 at 32 °C, it was measured that the H_2/He separation factor (3.05 ± 0.31) is higher than the results obtained in the single and H_2/He experiments. The use of such membranes appear to be very attractive for tritium recovery from He if it is in oxidised form, but the separation performances towards tritium in molecular form seems to be not sufficient for application in a single stage configuration.

Keywords

breeding blanket, tritium extraction system, inorganic membranes, permeation experiments, separation efficiency

Resumo

O isótopo radioativo do hidrogénio, o trítio, é proposto como combustível para a energia de fusão nuclear, e deverá ser produzido diretamente no reator, no interior da camada fértil (CF). Um processo avançado de duas etapas para a extração de trítio da CF do reator DEMOnstration foi recentemente proposto pelo Tritium Laboratory Karlsruhe (TLK), onde um estágio de pré-concentração com membranas é seguido de um reator de membrana catalítica. No TLK, foi iniciado um programa experimental dedicado para investigar as membranas mais promissoras, usando uma instalação concebida especificamente para este fim. Este trabalho apresenta os resultados das experiências de permeação com gases realizadas em três membranas de zeólito (MFI-ZSM5, NaA e SOD) e uma de carbono. As membranas SOD e de carbono evidenciaram conter demasiados defeitos estruturais internos para providenciar separação de gases. As experiências em modo simples de hélio, azoto e hidrogénio na membrana MFI-ZSM5, demonstraram que o último é o mais permeável e foi obtida uma seletividade ideal H_2/He de 2.11 ± 0.10 à temperatura ambiente. Das experiências binárias H_2/He na MFI-ZSM5 conclui-se que o fator de separação atinge um máximo de 1.68 ± 0.10 com um corte de 0.3, sem qualquer dependência significativa na concentração de H_2 entre 0.10% e 10%. Foram realizadas experiências binárias 1% H_2O/He nas NaA e MFI-ZSM5 e foi observado para ambas um forte crescimento do fator de separação com o decréscimo da temperatura. Das experiências ternárias 1%/1% H_2/H_2O/He na MFI-ZSM5 a 32 °C, o fator de separação H_2/He (3.05 ± 0.31) é superior aos obtidos nas experiências simples e H_2/He. Estas membranas apresentam desempenhos muito atrativos para a recuperação de hélio na sua forma oxidada, mas os rendimentos de separação na forma molecular parecem não ser suficientes para aplicação em modo de estágio único.

Palavras Chave

camada fértil, sistema de extração de trítio, membranas inorgânicas, experiências de permeação, eficiência de separação

Acknowledgments

My first words go to my portuguese supervisor, prof. Doctor Teresa Amorim. Without her, I would have never applied to work in this project, and I would have never had this great experience in my life. Furthermore, professor Teresa while showing a enormous character and human sense was always available to help me, whenever I needed and whatever was the issue. I also would like to specially mention my masters' coordinator, prof. Doctor Margarida Godinho, that was always available to give me the best advises and to support me in all decisions I made.

Secondly, I want to thank all the support and availability of Doctor David Demange, my supervisor in TLK. His informal and friendly way to communicate made easier to get fruitful brainstorming sessions in our periodic meetings. I also want to thank him for the wise guiding and for all the sincer comments about my work and improvements, not mentioning the relieving optimistic way he always looked to the results and achievements.

I want also to thank Doctor Hannes Richter for his availability for the very productive and interesting discussion we had about the results we obtained with the membranes produced by IKTS.

The Karlsruhe Institute of Technology and in particular the Tritium Laboratory Karlsruhe are specially acknowledged since they provided me financial support and gave me the opportunity to work in a world-level R&D environment. Furthermore, I want to thank all the TLK staff and colleagues, always available to help me with a very pleasant friendly spirit.

The person who I was with most of the time in TLK was the phD student Olga Borisevich. She helped me with every experimental difficulty, showing an infinite patience. I have also to thank her for all the honest opinions she gave me about my work. All the efforts we made to go through the experimental problems made us a really good team. Moreover, I am truly glad to call her my friend. Thank you for all the interesting and enjoyable conversations we had. In addition, I am sure that the friendships I created with Aleksandra, András, Christoph, Olga and Zoltan will last forever. Thank all of you for all the great and unforgettable moments.

Since this work is a culminating point of a 5-years project in my life, I want to thank all the friendships and colleagues I have made during this period. A special mention goes to Raquel and Rita, my course colleagues and friends since the very first year of my course. I will never forget our really great, funny and unforgettable moments. I am also thankful to my long date friends, with whom I had probably the best moments of my life.

Finally, I want to thank all my family. Without them these years would have never been

possible. Thank all of you for all the patience you had with me, when I was several times stressed with the work and not pleasant to be with. Many thanks for all the situations you believed in my capabilities more than myself. It really helped me to have the required strength to be succeded in all the academic challenges I had to go through.

The work I now present was only possible with all of you. Thank you.

Contents

List of Figures

List of Tables

List of Acronyms

AH	*Absolute Humidity*
BB	*Breeding Blanket*
CPS	*Coolant Purification System*
CT	*Cold Trap*
DEMO	*DEMOnstration reactor*
GS	*Gas Separation*
GT	*Gas Translational*
HCS	*Helium Cooling System*
HF	*Hollow Fiber*
H-SOD	*Hydroxy Sodalite*
IKTS	*Institut für Technologie und Keramische Systeme*
ITER	*International Thermonuclear Experimental Reactor*
KIT	*Karlsruhe Institute of Technology*
LN_2	*Liquid Nitrogen*
LTA	*Linde Type A*
MF	*Micro-Filtration*
MFI	*Mordenite Framework Inverted*
MFC	*Mass Flow Controller*
MFR	*Mass Flow Register*
MM	*Membrane Module*
MSB	*Molecular Sieve Bed*
PC	*Pressure Controller*
PR	*Pressure Register*
PERMCAT	*PERMeator and CATalyst*
QMS	*Quadrupole Mass Spectrometer*

RH	*Relative Humidity*
RO	*Reverse Osmosis*
RT	*Room Temperature*
SOD	*Sodalite*
TBM	*Test Blanket Module*
TES	*Tritium Extraction System*
TLK	*Tritium Laboratory Karlsruhe*
UF	*Ultra-Filtration*
WDS	*Water Detritiation System*
ZIMT	*Zeolite Inorganic Membranes for Tritium*

List of Symbols

A	*membrane's surface area* [m^2]
α	*alpha particle (helium's nucleus)*
$\alpha_{i/j}$	*ideal selectivity* or *permselectivity* [no dim]
$\alpha_{i/j}^{K_n}$	*selectivity for Knudsen mechanism* [no dim]
$\alpha_{i/j}^{*}$	*separation factor* [no dim]
β	*coordination number of the zeolite crystal*
$c_{\mathrm{H_2O}}$	*concentration of water in wet streams* [no dim]
γ	*ratio of the permeate pressure to the feed pressure* [no dim]
$d_k(i)$	*kinetic diameter of the gas i* [nm]
d_p	*diameter of the membrane's (active layer) porous* [nm]
D	*deuterium*
$D_{i,\mathrm{GT}}$	*diffusion coefficient for gas i for gas translational diffusion* [$m^2\ s^{-1}$]
$D_{0_i,\mathrm{GT}}$	*pre-exponential factor for the diffusion coefficient* $D_{i,GT}$ [$m^2\ s^{-1}$]
$\widetilde{D}_{i,s}$	*diffusion coefficient for gas i for surface diffusion* [$m^2\ s^{-1}$]
$\widetilde{D}_{0_i,s}$	*pre-exponential factor for the diffusion coefficient* $\widetilde{D}_{i,s}$ [$m^2\ s^{-1}$]
ΔH	*isosteric heat of sorption (enthalpy)* [J mol^{-1}]
Δp_i	*partial pressure difference of gas i* [Pa]
$E_{D_i,s}$	*activation energy for surface diffusion* or *flow of gas i* [J mol^{-1}]
$E_{D_i,\mathrm{GT}}$	*activation energy for gas translational diffusion* [J mol^{-1}]
ϵ	*porosity of the zeolite membrane* [no dim]
F_i	*rate of permeation* or *flow of gas i* [mol s^{-1}]
F_F	*total flow in feed* [mol s^{-1}]
F_P	*total flow in permeate* [mol s^{-1}]
$J_{i,\mathrm{GT}}$	*gas translational diffusion flux of gas i* [mol $m^{-2}\ s^{-1}$]

$J_{i,s}$	*surface diffusion flux of gas i* [mol m^{-2} s^{-1}]
$J_{i,\mathrm{tot}}$	*total flux of gas i as a result of surface and GT diffusion* [mol m^{-2} s^{-1}]
K_i	*Langmuir constant* [Pa^{-1}]
K_{0_i}	*pre-exponential factor for Langmuir constant* [Pa^{-1}]
K_n	*Knudsen number* [no dim]
l	*average mean-free path of a given gas* [m]
λ	*distance between two adsorption sites* [m]
M_i	*molecular mass of the gas i* [kg mol^{-1}]
n	*neutron*
ν	*cut* [no dim]
p	*proton*
p_F	*total pressure in feed* [Pa]
$\mathrm{P_F}$	*output power of the fusion reactions within the plasma* [W]
$\mathrm{P_H}$	*input heating power to the plasma* [W]
P_i	*permeability of gas i* [mol m^{-1} s^{-1} Pa^{-1}]
p_P	*total pressure in permeate* [Pa]
Π_i	*permeance of gas i* [mol m^{-2} s^{-1} Pa^{-1}]
q_i	*amount of adsorbed gas i in the membrane* [mol g^{-1}]
q_{sat}	*adsorption capacity of a membrane* [mol g^{-1}]
Q	*represents the three hydrogen isotopes*: H, D and T
Q	*Q-value of a fusion machine* [no dim]
R	*ideal gas constant* [J K^{-1} mol^{-1}]
R^2	*coefficient of determination* [no dim]
ρ_z	*density of the zeolite* [g m^{-3}]
σ	*cross-section* [barn]
$\langle \sigma v \rangle$	*reaction parameter* [m^3/s]
T	*tritium*
T	*temperature* [°C or K]
T_{D_p}	*dew point* [°C or K]
θ_i	*fraction of occupied adsorption sites* [no dim]
t_m	*membrane's active layer thickness* [m]
x_i	*concentration of the gas i in the feed stream* [no dim]
y_i	*concentration of the gas i in the permeate stream* [no dim]
z	*direction of permeation* [m]

1

General Introduction

The work here presented is part of the area of the technology for future **fusion reactors**, whose tritium **self-sufficiency** shall be ensured by integrating a **Breeding Blanket** (BB) responsible to produce tritium inside the reactor. Therefore, the **extraction of the tritium** so produced requires a dedicated **Tritium Extraction System** (TES). The topic of this master thesis is related to a **membranes-based TES** concept, in which membrane's technology (a membranes pre-concentration stage followed by a membrane catalytic reactor) is proposed to separate the tritium from the helium gas flow purging the BB.

Despite non-conventional and imature technology, zeolite membranes have been identified as the most promising membranes to use upstream the catalytic reactor. However, experiments on the separation performances of that membranes are needed. Therefore, a facility was specifically built at the Tritum Laboratory Karlsruhe (TLK), in Karlsruhe Institute of Technology (KIT), Germany.

For the presented work, **four different inorganic (zeolite and carbon) membranes** from the Institut für Technologie und Keramische Systeme (IKTS) were initially available to perform experiments. In the **Zeolite Inorganic Membranes for Tritium (ZIMT) facility**, the membranes have been tested under relevant conditions for studying the transport properties for different gases of interest (helium, hydrogen and also water vapour). Initially, only single permeation tests could be done at ZIMT. Since the purpose of the study shall not be only limited to **single gases**, but also **binary and ternary mixtures gas experiments** should be achieved, the facility had to be gradually upgraded. Furthermore, the analysis has been extended by changing the operating conditions, such as different pressure differences across the membrane or temperatures. With these experiments, **insight towards the most promising membrane was gained**, and additional experiments were performed on it.

The aim of the present dissertation is to answer the following questions:

1. **Can the membranes be foreseen to process tritiated streams?**
2. **Which membranes are more suitable to employ in the pre-concentration stage of the future membrane-based TES concept?**

The master thesis here presented begins with a literature review starting from the basics of nuclear fusion up to the application of zeolite membranes for tritium processing in breeding blankets in **Chapter 2**. The principles underlying nuclear fusion and the production of energy in the future fusion reactors are discussed in section 2.1. The concepts proposed so far for the TES and the details concerning the membrane-based approach are explored in 2.2. The following sections present a general overview of the membranes properties (2.3) and the characteristics of the zeolites as materials and membranes as well as their transport mechanisms (2.4). The most promising zeolite membranes suitable for the membrane-based TES concept are presented in section 2.5. The ZIMT facility started to be developed in 2011 (ZIMT I), where single gas experiments were performed on a hollow-fiber type zeolite membrane, and in 2012 the ZIMT II opened the possibility to perform binary mixtures experiments on the same membrane. An upgrade towards experiments with water vapour (ternary mixtures) was accomplished in 2013 (ZIMT III). These previous results (status of the work) are discussed in section 2.6.

The **Chapter 3** aims to present the experimental setup and the comissioning of the ZIMT III facility. The ZIMT III has been (re-)built on a stage approach: initially prepared to perform only single gas experiments, it has been stepwise improved, extending its capacities to perform binary and ternary gas mixtures experiments. In section 3.1, the schematic overview and main features of the experimental rig are discussed, as well as the specific configurations that allow the realisation of experiments in the single, binary and ternary modes. In this section, the details concerning the main components of the facility are also presented. Safe procedures concerning the tightness of the facility, as well as proper operation of the measuring devices and careful introduction of the membranes into the system are issues that guarantee the quality of the measurements (section 3.2).

The experimental procedures concerning the experiments performed at ZIMT III are described in **Chapter 4**. The first section of this chapter (4.1) presents the specifications of the IKTS membranes for experiments at ZIMT III. After a brief explanation of the concept of steady-state measurements assumed in this work in section 4.2, the procedures and experimental conditions concerning the single gas experiments (section 4.3) as well as the binary (section 4.4) and ternary (section 4.5) mixtures experiments on the zeolite and carbon membranes are also discussed in this chapter.

The analysis and discussion of the results obtained in the experiments are presented in **Chapter 5**. It is intended to present a comprehensive analysis, where the different factors influencing the obtained results are systematically presented. Firstly, the equations used to calculate the most important parameters from the experimental data are presented in section 5.1. This section is followed by the discussion of the results obtained in the single (section

5.2), binary (section 5.3) and ternary (section 5.4) results. Finally, a summary of the results is presented in section 5.5.

A global discussion of the performed work and the achieved results are presented in **Chapter 6**. The more relevant conclusions that have to be retained about the developed work, as well as the perspectives for future experiments on membranes towards an understanding for application to the tritium process in the breeding blanket are presented.

2

Theoretical Introduction and Background

2.1 Nuclear fusion and fusion energy

Nuclear reactions produce changes in the basic structure of the nuclei of the atoms involved. Within the nuclear size range, the strong force dominates over the electromagnetic force. Therefore, comparing to the chemical reactions, governed by the electromagnetic force, the nuclear reactions can provide one million times more energy. In fact, 10^6 tons of oil burnt by chemical means is equivalent to 0.8 tons of uranium used in nuclear fission and 0.14 tons of deuterium used as fuel for nuclear fusion reactions [Fre07].

While fission reactions are due to the split of a heavy nucleus into two lighter nuclei, the fusion reactions are processes where two light nuclei are fused into a heavier one. Whichever is the case, the energy liberated ($\sim$ 1 MeV for fission and $\sim$ few MeV for fusion) in the nuclear reactions is explained by the difference of the binding energies of the nuclei between the final and initial state [Kra87, Har00]. In fusion reactions, the reactants are light nuclei (comparatively widely abundant) and the end reaction products are usually stable (non-radioactive) light nuclei. Therefore, fusion presents several advantages over fission, although one considerable disadvantage is the need to overcome the Coulomb repulsion between the nuclei when they are nuclear distances apart. This is accomplished by heating the fuels to energies ($\sim 10^5$ eV) far higher than the ionization energies ($\sim$ 10 eV) of the species involved, creating a plasma [Kra87, Fre07, Har00, BK13]. Several fusion reactions have been considered for energy production. These are briefly presented and discussed in 2.1.1 and 2.1.2.

In view of energy production, the fusion-based power has several advantages in comparison with its fission counterpart, namely in terms of (i) fuel reserves, (ii) environmental impact and (iii) safety [Fre07, BK13]:

i) Deuterium and lithium are the primary fuels of fusion reactions. Deuterium occurs naturally in oceans, with a proportion of 1/6700 relative to hydrogen, and can be easily extracted at a low cost; lithium exists in both Earth's crust and oceans. Taking into account the annual energy consumption, it can be estimated that enough deuterium exists to power fusion reactors for few billion years, and the lithium reserves will last for 10 million years;

ii) No greenhouse emissions, nor releases of harmful chemicals to the atmosphere occur in fusion reactions. However, the deuterium-based fusion reactions considered so far are characterised to have high-energy neutron(s) as by-products. Therefore, radioactive activation of the structural materials surrounding the core of the nuclear reactor is a problem that has to be considered;

iii) The very small mass of fuel in a fusion reactor at any time (no chain reactions) makes a reactor core meltdown impossible in a fusion reactor. Indeed, one of the safety strategies is to reduce all radioactive and energy inventories as far as possible.

However, the scientific and technological challenges of confining the plasma long enough to produce sufficient fusion power and finding low-activation materials capable of withstanding the neutron and heat loads generated by the plasma are serious drawbacks to overcome. In an economic perspective, the complexity of a fusion reactor likely raises its capital cost higher than that of a fission power plant [Fre07]. Above and beyond, the challenging issues concerning the design and realisation of the DT fuel cycle are of primary importance to surpass.

2.1.1 Deuterium-based fusion reactions

The deuterium (D) is virtually an unlimited fuel, due to its widespread existence in the oceans. Then, the fusion reaction involving two D atoms should be of primary interest. The DD fusion reaction has two branches of equal probability to occur:

$$\mathrm{D} + \mathrm{D} \rightarrow \begin{cases} {}^{3}\mathrm{He} + \mathrm{n} + 3.27 \text{ MeV } (0.82 \text{ MeV/nucleon}) \\ \\ \mathrm{T} + \mathrm{p} + 4.03 \text{ MeV } (1.01 \text{ MeV/nucleon}) \end{cases}$$

where T, n and p denote tritium (^{3}H), neutron and proton, respectively. The principal disadvantage of this reaction is the difficulty of initiating such reaction, in comparison to other fusion reactions.

Fusing deuterium with helium-3 is another possible fusion reaction from which alpha particles and protons are produced, with a large energy yield:

$$\mathrm{D} + {}^{3}\mathrm{He} \rightarrow \alpha + \mathrm{p} + 18.3 \text{ MeV } (3.66 \text{ MeV/nucleon})$$

This reaction is particularly interesting since the end-products are charged particles (helium nucleus and proton) which greatly reduces the problems associated with the activation of the structural materials. However, the inexistence of natural supplies of helium-3 combined with the difficulty to achieve such reaction makes it not desirable for fusion machines.

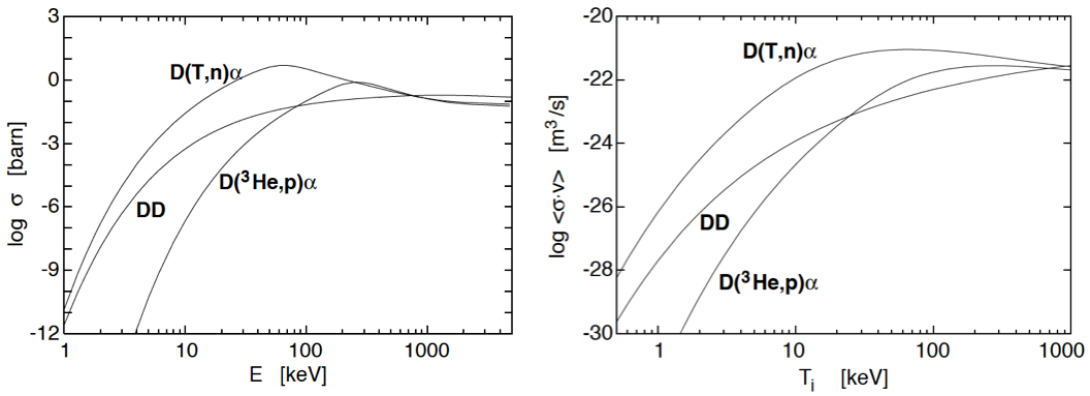

Figure 2.1: (Left) Measured cross-sections σ as a function of the center of mass energy E of the reactants for the DD, D^3He and DT fusion reactions. (Right) Reaction parameter $\langle\sigma v\rangle$ as a function of the ion temperature T_i for the DD, D^3He and DT fusion reactions [BK13].

The most attractive fusion reaction to use in reactor is the one that merges deuterium and tritium, producing a neutron (14.1 MeV) and an alpha particle (3.5 MeV):

$$\mathrm{D} + \mathrm{T} \rightarrow \alpha + \mathrm{n} + 17.6 \text{ MeV } (3.52 \text{ MeV/nucleon})$$

The use of tritium as fuel requires special attention since it is a radioactive isotope (with 4500 ± 8 days as half-life [LU00]) and only trace amounts exist on Earth. Nonetheless, this is the fusion reaction under consideration for fusion research around the world, mainly due to the relative ease of obtaining it. Also because the DT reaction cross-section for the temperatures of interest is higher than for the other reactions.

In figure 2.1 the measured cross-sections σ which are the probability of a given reaction to occur, are presented as a function of the center of mass kinetic energy E of the reactants. The DT reaction has cross-sections several order of magnitudes higher than that of the other reactions at low energies. For example, at 20 keV, $\sigma_{\mathrm{DT}} \sim 100\sigma_{\mathrm{DD}}$. Taking into account both the relative speed v of the reactants and the Maxwellian velocity distribution of the ionized species, the reaction parameter $\langle\sigma v\rangle$ (proportional to the reaction rate density) can be computed. The same figure shows the plot of $\langle\sigma v\rangle$ as a function of the ion temperature T_i; for temperatures of interest of around 10 keV, $\langle\sigma v\rangle_{\mathrm{DT}}$ is about 10 times higher than $\langle\sigma v\rangle_{\mathrm{DD}}$.

2.1.2 Self-sufficiency of a DT-based fusion reactor

The reaction involving the fusion between deuterium and tritium will be used for the first generation of fusion reactors [Har00]. Due to the rather short-living tritium no significant amount of such isotope exists in the nature. To ensure the self-sufficiency of a fusion reactor, tritium will have to be produced inside the machine. This could be accomplished by taking advantage of the nuclear reactions between the DT fusion neutrons and lithium [Kra87, Har00, BK13, Fre07]:

$$\mathrm{n\ (slow)} + {}^6\mathrm{Li}\ (7.4\%) \rightarrow {}^4\mathrm{He} + \mathrm{T} + 4.8 \text{ MeV}$$
$$\mathrm{n\ (fast)} + {}^7\mathrm{Li}\ (92.6\%) \rightarrow {}^4\mathrm{He} + \mathrm{T} + \mathrm{n}' - 2.5 \text{ MeV}$$

Indeed, the solution to the scarcity of tritium is to breed it using the neutrons from the DT reaction and Li-based material accomodated in the blanket surrounding the plasma. From these reactions, it is concluded that each fusion neutron produces at least one new tritium nucleus. Despite ^{7}Li exists more abundantly in the nature, the reaction that will dominate is the one involving ^{6}Li since it is easier to initiate [Fre07]. The tritium so produced shall be removed from the BB and then injected into the plasma as a fuel, ensuring the self-sufficiency of a future fusion device [Har00].

2.1.3 Fusion machines and reactors

The figure 2.2 presents a schematic diagram of a future tokamak-like[1] power plant. The plasma is heated by external heating power P_H and the fusion reactions in the core deliver a power output of P_F. The ratio of the fusion power output to the input heating is represented by Q. The breeding blanket ensures the tritium self-sufficiency of the reactor and also removes the generated heat for electricity production [MT13].

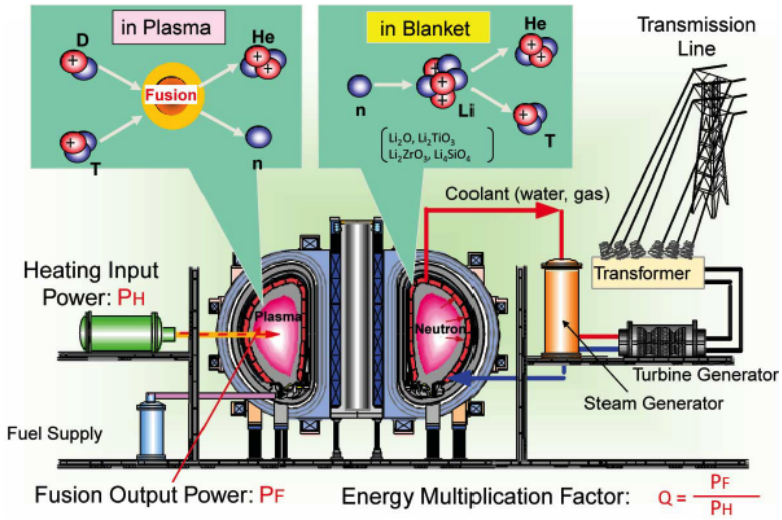

Figure 2.2: Tokamak-like future fusion power plant and definition of the Q-value [MT13].

The scientific and technological feasibility of fusion energy will firstly be tested in the International Thermonuclear Experimental Reactor (ITER), currently being built in Cadarache, France. In terms of plasma physics, the main goals of this fusion device are (i) to achieve inductive current operation lasting 300 - 500 s (pulsed mode) with $Q \geq 10$ and (ii) steady-state operation through non-inductive current with $Q \geq 5$. In parallel, the engineering performance and testing will be concerned to (i) demonstrate availability and integration of essential fusion technologies, (ii) test components for a fusion reactor, and (iii) test tritium breeding blanket modules that would lead in a future reactor to tritium self-sufficiency, to the extraction of high grade heat and to the production of electricity [ITE01]. Since the international fusion energy program is reactor-oriented, there is the need to construct an intermediate step reactor that

[1]Tokamak is a special configuration of the magnetic fields confining the plasma in a torus. The other existing type is the stellerator. Due to the more challenging engineering design of the latter configuration, actual fusion research is more advanced in the tokamak-type reactors, and is the one being considered for the first experimental fusion reactor.

demonstrates the electricity production at a plant level. The DEMO reactor shall be the last R&D device before the first-generation commercial fusion reactors integrating all the plasma physics and component technologies needed for a power plant [MT13].

One key issue that differentiates ITER and DEMO is the tritium fuel supply. While the former will use fuel from external sources (e.g., CANDU canadian fission reactor) the latter will have to produce its own tritium, taking advantage from its breeding blanket. Furthermore, a test blanket module (TBM) program on ITER will start in which several breeding blanket concepts will be tested under neutron environment. However, since these test units are of limited scale, topics concerning tritium inventory control, self-sustainment of the fuel supply, minimization of environmental release and extraction of tritium from the BB can not be extrapolated from ITER experiments [KGH08]. Some of the key parameters concerning tritium production and consumption for both ITER and DEMO are presented in table 2.1.

	ITER	DEMO
Fusion power [MW]	500	2700
T consumption [g/d]	76	412
T burn-up fraction, %	0.3	1.5
T production [g/d]	< 0.4	450

Table 2.1: Comparison of the tritium related parameters between ITER and DEMO [DBG$^+$13]. The DEMO parameters are only indicative, subject to several changes along the design studies.

2.2 Tritium Extraction System (TES) from the breeding blanket

A schematic view of the fuel cycle of a future fusion reactor is depicted in figure 2.3. It can be subdivided into an "inner" fuel cycle whose the objective is to recycle and purify the un-burnt fraction of tritium since its burn-up fraction is typically rather low (table 2.1) and an "outer" one, that comprises the tritium extraction from both the breeding zone via the TES and the coolant[2] via the Coolant Purification System (CPS). [DBG$^+$13]. The Accountancy Stage provides the interface between the two sub-cycles. It is a main engineering goal for ITER to test different concepts of tritium breeding blankets throught the TBMs in view of the next reactors like DEMO [AH00]. Different TBM concepts based on lithium (either in liquid or solid state) as tritium breeding material and a given type of coolant have been proposed by the several ITER Parties [MT13, GCA$^+$06, GCA$^+$07].

In this work, focus will be given to the TES of the european Helium Cooled Pebble Bed (HCPB) TBM, whose main functions are [RC08]:

1. to extract tritium from the lithiated ceramic breeder by gas purging;
2. to extract tritium from the purge gas, delivering it in concentrated form to the ITER Tritium Plant Systems for tritium recovery;

[2]Tritium permeation from the breeding region of the blanket into the Helium Cooling System (HCS) through the structural materials is unavoidable and can be significant.

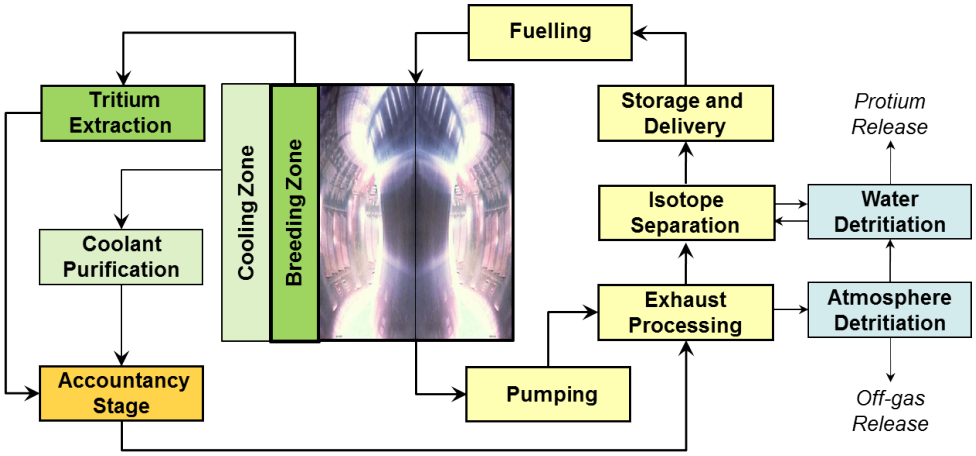

Figure 2.3: Schematic view of a fuel cycle of a future fusion machine [DBG+13].

3. to keep constant and control/adjust the He purge composition at the TBM inlet.

This TBM is constituted by lithium (Li_4SiO_4) and beryllium pebbles as tritium breeding and neutron multiplication materials, respectively. The extraction of the bred tritium is accomplished using helium as a low-pressure ($\sim$ 1 bar) purge gas containing up to 0.1% of hydrogen to facilitate its remotion by isotopic exchange [AH00]. The helium stream flowing out from the breeding material contains hydrogen isotopes (Q = H, D, T) in both molecular (Q_2) and oxidised (Q_2O) forms down to ppm amounts. For ITER, the helium stream flow shall range between 8 and 40 m^3/h, while for DEMO values as high as $\sim$ 10000 m^3/h are predicted [DBG+13]. The TES concepts proposed for the solid BB concept are presented in 2.2.1 and 2.2.2.

2.2.1 TES concepts based on conventional technology

In 2000, TLK formally proposed a two steps [AH00] process in which (i) Q_2O is frozen out in a cold trap (CT) operated at temperatures below 173 K and (ii) Q_2 and gaseous impurities (e.g., O_2 and N_2) are adsorbed on a zeolite 5A based molecular sieve bed (MSB) operated at LN_2 temperature. The cleaned helium is then sent to a unit where hydrogen can be added up until the H_2/He ratio of 1/1000 is again reached. At the end of an experimental ITER cycle (about one week) the water at room temperature (RT) colected in the CT is sent to the Water Detritiation System (WDS) while the hydrogen bound to the MSB is desorbed by electrically heating it up to 150 K. Periodically, total regeneration of the MSB at 600 K is required for complete impurities removal [BCNH03]. Despite the widely used technology, the need for using cryogenic temperature makes the process energy consuming. Furthermore, the adsorption (tritium removal from the helium purge) and recovery (extraction of the accumulated tritium) phases of the traps demands parallel processes for alternating operation [DBG+13, DSK11].

A revision (update) of TES in view of the TBM operation was proposed in 2008 [RCAB08], where a single adsorption column for Q_2O removal and two parallel getter beds for Q_2 extraction[3] both operated at RT are considered (figure 2.4). The Q_2O breakthrough is followed by

[3]The original concept proposed a two bed TSA (Temperature Swing Adsorption) operated at LN_2 temperature for this remotion process. This stage was later modified to the getter beds.

regeneration of the adsorption column at 573 K by counter-current He gas stream. In the regeneration line of this component, a reducing bed or a catalytic membrane reactor (PERMCAT) are also integrated to transform the Q_2O into Q_2 for easier handling in the Tritium Plant. Using ZrCo alloy, the getter beds will remove H_2 and release it at temperatures up to 573 K. The absence of cryogenic temperatures is an immediate advantage of this concept. However, likewise the previous approach, two parallel processes for each stage are needed for alternating operation in either adsorption or remotion mode.

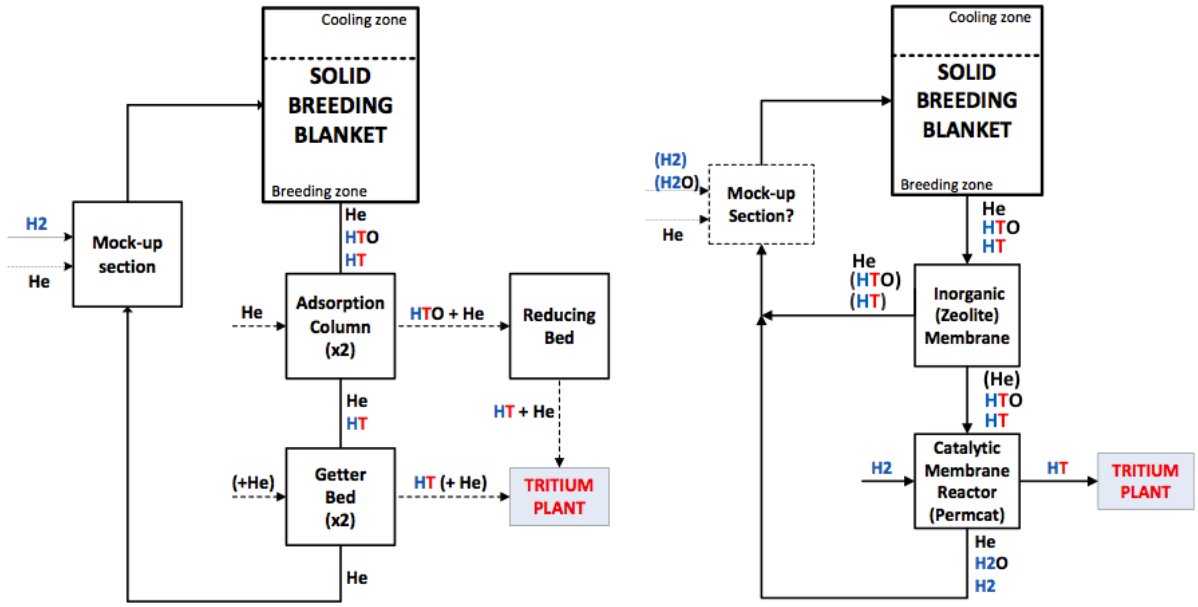

Figure 2.4: (Left) One of the TES concepts using conventional techniques, where a two-stage process considering an adsorption column and getter beds is considered. (Right) Advanced TES concept based on membranes technology.

2.2.2 Advanced TES concept based on membrane technology

A completely different approach also depicted in figure 2.4 was suggested by TLK in 2011 [DSK11]. In this proposal the Pd-base catalytic membrane reactor PERMCAT is used as a single step for simultaneously removing Q_2 and Q_2O from the helium purge stream. This stream is directed into the "impurity" side of the reactor while hydrogen is supplied in the "purge side" in counter-current. The permeation of H_2 into the catalyst bed promotes the tritium extraction in its molecular form, and tritium permeates back to the purge side. With this principle, only one step is needed for production of a continuous and pure Q_2 stream from the initial helium stream. Furthermore, PERMCAT ensures a clean and efficient tritium recovery without regeneration, as required for the technology suggested by the other two approaches. Thus, a continuous operation without cyclic operation is ensured. Moreover, in the present concept the tritium overall management (process and accountancy) is greatly improved, given that a pure Q_2 output stream can be maintained. In addition, this concept shall be easier to integrate to the DEMO scale in comparison with the conventional techniques.

Experiments concerning the PERMCAT performance have been performed in TLK [BGG+05, DSK11, DGG+08, DBG+13]. In order to optimize the PERMCAT stage, it seems advantageous

to introduce a pre-concentration stage upstream the reactor. Using membranes in this stage, the purge stream downstream the breeding zone from the ceramics is divided into one depleted in tritum further re-introduced in the helium loop and another one enriched in tritium which is directed to the catalytic reactor. This concept can even be more effective if water vapour is considered for the purge stream instead of H_2, since higher membrane separation performances are expected [DBG+13].

The tritium compatibility and the permeation and separation efficiency of the different tritiated species in the stream at low partial pressures are key features to be considered to choose the most suitable membrane for this concept. Organic (polymeric) membranes are widely used in several industrial applications (e.g., microfiltration, ultrafiltration, reverse osmosis or pervaporation), however they do not seem suitable for gas separation processes in general, due to fouling, compaction, chemical degradation and thermal instability [PC01]. Most importantly, they are not at all tritium compatible if high tritium levels are considered [DSK11]. Non-conventional membranes, such as dense-metallic membranes (particularly palladium), are exclusively permeable for hydrogen [Bak00] (Q_2 species) which makes them not suitable to use in TES. Furthermore, they are not also attractive for the low Q_2 partial pressures present in the purge streams. After a systematic literature research and numerical study performed by Stämmler at TLK [Stä10], it was concluded that high permeability and high separation factors could be achieved using newly developed inorganic membranes made of thin zeolite layers. Zeolite membranes are fully tritium compatible and able to handle at the same time tritium in both oxidised (Q_2O) and molecular (Q_2) forms. If a given membrane does not fulfill the requirements of separation for TES, a multi-stage configuration shall be used to overcome some problems and limitations demonstrated by single stage systems [BDKL13].

2.3 General Properties of Membranes

A membrane can be conveniently defined as a semipermeable active or passive barrier able to separate components in gaseous or liquid phase under a certain driving force. In other words, a membrane imposes preferential passage of one or more selected sepecies or components of a gaseous and/or liquid mixture or solution [Jar04, Hsi96]. Examples of driving forces are temperature, pressure, concentration or voltage gradients. Different driving forces give rise to different membrane processes as listed in table 2.2.

A schematic diagram of a membrane permeation is presented in figure 2.5. A feed stream for separation is directed into the membrane and two streams are then produced: one that is rejected by the membrane (retentate or solute) and another one that passes through the membrane (permeate or solvent).

Membranes can be primary divided into biological and artificial membranes, being the latter ones all those modified by man. Organic (made with polymers) and inorganic (made with alumina, metals, etc.) membranes are two sub-groups of the synthetic membranes. It is advantageous to classify the membranes according to their structural properties since they have direct impact on their performance as separators [Hsi96, BC96]. Thus the membranes are generally

Driving Potential	**Applications**
Pressure gradient	Reverse-Osmosis (RO), Ultra-filtration (UF), Micro-filtration (MF), Gas Separation (GS) and Pervaporation
Temperature gradient	Distillation
Concentration gradient	Dyalisis and Extraction
Voltage difference	Electrodyalisis

Table 2.2: Different membrane applications depending on the driving force used for the separation of the species [PC01].

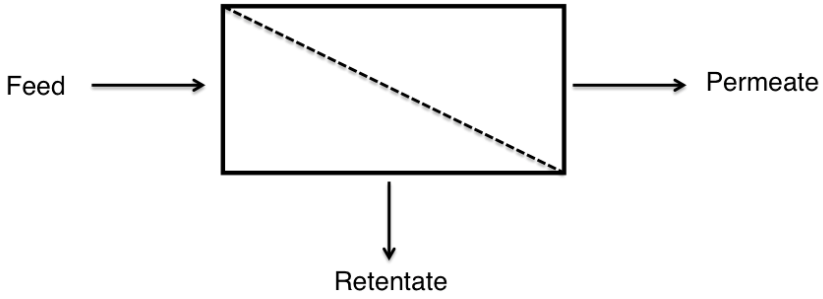

Figure 2.5: Schematic diagram of a membrane process.

divided into dense and porous membranes:

- **Dense Membranes**: free of discrete well-defined pores or voids. The separation of the various components of a fluid is based on the difference between their transport rates within the membrane, determined by the solubility and diffusivity. Therefore, for instance, dense membranes can separate species of similar sizes if their concentrations (i.e., solubility) on the membrane differ considerably.

- **Porous Membranes**: possess highly-voided structure with interconnected pores. The porous membranes are characterised to present a variety of transport mechanisms. These mechanisms greatly depend on the membranes pores size and pore-size distribution, and are influenced also by the chemical interaction between the transported species and the membrane material. According to their pore sizes, this type of membranes can be further differentiated into (1) microporous ($d_p < 2$ nm), (2) mesoporous ($2 < d_p < 50$ nm) and (3) macroporous ($d_p > 50$ nm).

When the membranes have an homogeneous structure they are also designated symmetric or isotropic. Since the flow rate through a membrane is inversely proportional to its thickness, it is desirable to make the homogeneous membrane as thin as possible. It is a common solution to add a supporting layer structurally different from the thinner one to ensure mechanical integrity, and these types of membranes are called asymmetric or anisotropic (if made of the same material) or composite (if made of different materials). In this class, the supporting layer has to be strong and

porous enough to ensure sufficiently low flow resistance. Indeed, all the resistance (or pressure drop) should be uniquely provided by the thin membrane layer [Hsi96, BC96, PC01, TD99].

2.3.1 Organic vs inorganic membranes

By the decade of 1990s, a limited value of performance of polymeric membranes for many applications was predicted, and since then only few new materials could cross this upper bound [PC01]. Furthermore, the decrease of efficiency of these membranes due to fouling (strong adsorption of the rejected component on the membrane surface that leads to deposition), mechanical, thermal and chemical instability limit their application in environments where for example hot reactive gases are present [PC01, NS95, Hsi96, BC96]. These drawbacks can be overcome by using inorganic membranes, which are sub-divided into ceramic[4] (such as γ-Al_2O_3), glass (made of silica, SiO_2), metallic (e.g, Pd or Pd-alloys) and carbon membranes. Inorganic porous membranes were primarily used for the enrichment of uranium by separating uranium isotopes in the form of UF_6 [Hsi96]. Because of their superior characteristics, inorganic membranes are also being used in the same applications as the polymeric membranes despite their higher capital cost [CNKS00].

The operable temperature limits of inorganic membranes (> 350 °C) are much higher than that of organic ($< 100 - 150$ °C) and inorganic polymers ($100 - 350$ °C). Around 100 °C most of the organic membranes become deteriotated. The susceptibility of organic membranes to microbial attacks during applications is another drawback not met in their inorganic counterparts. Moreover, inorganic membranes can withstand organic solvents and other chemicals better than the organic ones, which can lead to more effective cleaning procedures, by using corrosive chemicals. In addition, unlike the organic membranes, the porous support of inorganic membranes do not undergo compaction under high pressures, being mechanically stable (although the latter may present brittleness) [Hsi96, CNKS00]. In table 2.3, some examples of state of the art applications of inorganic membranes are provided.

2.3.2 Separation performance parameters

The differential rate of permeation (or differential flow) dF_i [mol s^{-1}] of a species i through a membrane of differential area dA [m^2] at any point is proportional to the partial pressure difference Δp_i [Pa] between the feed and permeate gas phases of that species. In addition, the rate of permeation is inversely proportional to the membrane thickness. The equation that relates all these quantities is given by

$$dF_i = \frac{P_i}{t_m} dA \Delta p_i \tag{2.1}$$

where t_m [m] is the thickness of the membrane and the constant of proportionality P_i [mol m^{-1} s^{-1} Pa^{-1}] is called the permeability, which shall be constant for a permeant-membrane combination but is function of the temperature [NS95]. Since the membrane thickness is usually

[4]Combination of a metal with a non-metal in the form of an oxide, nitride or carbide.

Membranes type	**Materials**	**Applications**	**References**
Dense	Pd-alloy (supported)	H_2 purification	[HGK$^+$10]
	$LaCoO_3$-based perovskite (ceramic flat or tubular standalone)	Commercial production of O_2 from air	[ZSS$^+$11]
Microporous ($d_p \sim 5$ nm)	Amorphous silica	Pervaporation	[CKV$^+$08]
	Zeolites MFI	p/o-xylene separation, Production of 95% pure H_2 gas turbine fuel from coal gas	[LKNA02, TDN09]
	Zeolite A (sodalite)	Removal of water from liquid mixtures (by pervaporation)	[GLELFdS02]
	SAPO-34	Separation of CO_2 from natural gas feeds	[LFN06]
Microporous ($d_p \sim 0.5$ - 2 nm)	Zeolite-Y	Capture of CO_2 from flue gas	[WDSV10]
Mesoporous	γ-alumina	^{235}U isotope enrichment	[Bha91]
	NaP1 zeolites	Remotion of nanosized pollutants for water purification	[SD05]
Macroporous	α-Al_2O_3	Gas separation	[MPM10]

Table 2.3: Examples of state of the art applications for inorganic membranes. The applications concerning the porous membranes are industrial in nature. Based on the reference [Ver12].

of difficult determination for composite (multilayer) membranes, the equation (2.1) should be re-written in terms of the permeance $\Pi_i \equiv P_i/t_m$ [mol m^{-2} s^{-1} Pa^{-1}]

$$dF_i = \Pi_i dA \Delta p_i \tag{2.2}$$

which in the integral form becomes

$$F_i = \Pi_i A \Delta p_i = \Pi_i A p_F (x_i - \gamma y_i) \tag{2.3}$$

The second equality holds if p_F (x_i) and p_P (y_i) are the absolute pressures [Pa] (concentrations of species i) in both feed and permeate sides of the membrane respectively, with $\gamma \equiv p_P/p_F$.

An immediate consequence of equation (2.3), in agreement of what was discussed in the beginning of this section, is that permeation only occurs if any driving force exists. Indeed, the condition $F_i > 0$ is fulfilled if there is a gradient of concentration of species i ($x_i \neq y_i$) and/or a pressure difference across the membrane (e.g., $\gamma < 1$). The relative permeation rate of two gases is given by

$$\frac{F_i}{F_j} = \frac{\Pi_i}{\Pi_j}\frac{\Delta p_i}{\Delta p_j} \equiv \alpha_{i/j}\frac{\Delta p_i}{\Delta p_j} \tag{2.4}$$

where $\alpha_{i/j} \equiv \Pi_i/\Pi_j$ is the ideal selectivity or permselectivity, which is a commonly used pa-

rameter to describe the separation performance of a given membrane for species i over species j. The higher this parameter, the better the separation capability of the membrane for these two species. The ideal selectivity is defined such that $\alpha_{i/j} > 1$ (with $\alpha_{i/j} = 1$ meaning no separation). When a binary mixture permeates a membrane, the transport of one gas can be influenced by the presence of the other, and the separation factor given by (2.5) to express the separation performance of a membrane has to be considered [YPF06].

$$\alpha^*_{i/j} = \frac{y_i/x_i}{y_j/x_j} \tag{2.5}$$

It can be shown that the relationship between $\alpha_{i/j}$ and $\alpha^*_{i/j}$ is given by [Hsi96]

$$\alpha^*_{i/j} = \alpha_{i/j}\frac{1-\gamma\frac{y_i}{x_i}}{1-\gamma\frac{y_j}{x_j}} \tag{2.6}$$

from which follows that $\alpha^*_{i/j} \leq \alpha_{i/j}$, with the equality holding when $\gamma \to 0$.

2.3.3 Transport mechanisms in membranes for gas separation processes

The transport mechanisms in membranes depend on the properties of the membranes themselves and on the properties of the permeant species, but also on the operating conditions (e.g, temperature and pressure). Specific single gas transport mechanisms in porous membranes arise depending on the ratio between the molecule-molecule and molecule-wall collisions number, given by the Knudsen number $K_n = l/d_p$, where l is the average mean-free path of the gas molecules and d_p the pores diameter [NS95, BC96, PC01, Hsi96, Bak00]:

- **Viscuous (Poiseuille) flow ($K_n << 1$)**: in this regime, the gas transport characteristics are determined by the much more frequent molecule-molecule collisions. The flow is proportional to the pressure gradient and to the square of the radius of the membrane porous and decreases with the temperature. Although it is important to take into account in mesoporous systems, the viscuous flow is inherently non-selective, since different gases will have the same permeation flow.

- **Knudsen flow ($K_n >> 1$)**: the Knudsen flow is obtained when the gas molecules thermalise (faster) with the pore walls. Each molecule is momentarily absorbed by the pore walls and then reflected again into a random direction. Since the molecules collide much fewer times with each other, they move independently and the separation of a gas mixture occurs because different species move at different molecular (mass-dependent) velocities. The Knudsen selectivity is determined by the root of the ratio between the inverse of the molecular weights of two gases i and j: $\alpha^{K_n}_{i/j} = \sqrt{\frac{M_j}{M_i}}$. As such, membranes where Knudsen diffusion dominates are poorly selective, specially for gases of similar molecular masses (e.g., $\alpha = 1.07$ for the O_2/N_2 pair); higher separation factors are thus predictable for separation of lightest and heaviest gas (e.g., hydrogen and buthane with $\alpha = 5.4$).

- **Transition flow** ($K_n \sim 1$): in this regime, both Knudsen and laminar flows play a role, and the transport equation becomes a linear combination of both contributions. It can be shown that the Knudsen permeability is independent of the average pressure between the inlet and outlet pressures, while the permeability in the viscuous regime increases linearly with it. This can be understood, realising that the higher the average pressure the lower the mean-free path of the molecules, thus decreasing K_n.

Generally stated, the Knudsen and viscuous flows are important for macroporous membranes, i.e., for $d_p > 50$ nm. Knudsen transport mechanism becomes dominant when the pore sizes are below 50 nm (at atmospheric pressure, the mean-free path of the gas molecules is in the range of 50 - 200 nm). In the interval $2 < d_p < 50$ nm, other two mechanisms play a role - surface diffusion and capillary condensation [NS95, BC96, PC01, Hsi96, Bak00]:

- **Surface diffusion**: occurs when the gas species permeating the membrane interact with the pore walls. The more strongly adsorbable molecules will then undergo surface diffusion due to a concentration gradient. In general, the diffusion coefficient of a surface adsorbed presents an Arrhenius type temperature dependency, i.e, is an activated diffusion process. Since heavier molecules show larger surface diffusion, this effect counteracts the effect of Knudsen separation, and this mechanism does not improve the overall separation efficiency.

- **Capillary condensation**: if the temperature is decreased and the pressure increased, a condensable component of a gas mixture undergoes a partial condensation, with exclusion of the others, followed by the transport of the condensed molecules through the pores. High selectivities are expected for this mechanism, but practical limitations concerning the removal of the condensed component exist. This mechanism is also observed for microporous membranes ($d_p < 2$ nm).

In order to obtain efficient high separation performances (high $\alpha^*_{i/j}$), the pores of the membranes shall be reduced. For $d_p < 2$ nm, surface diffusion becomes increasingly important, while the Knudsen flow contribution decreases. Membranes with molecular dimensions pores ($d_p \sim 0.5$ nm) provide another selective mechanism, based on the sizes of the molecules. If the membrane has pore sizes in between the largest and the smallest molecules, high separation factors are expected. In this regime, the molecular sieving mechanism and surface diffusion are the most important mechanisms for gas separation. Surface diffusion is specially important if condensable components are present in the gas mixture. Indeed, in a gas mixture consisting of condensable and non-condensable species, adsorption of the condensable components onto the pore walls can decrease or even vanish the permeation of the non-condensable components; the permeation of the condensable species are accomplished by surface diffusion, whereas the permeation of the non-condensable species is hindered by capillary condensation in the membranes pores. A pictorial comparison of the prevailing transport mechanisms through microporous membranes depending on the pore sizes and the species present in the gas mixture is presented in figure 2.6.

The transport of gases through dense membranes is usually described as a solution-diffusion mechanism. According to this theory, the gaseous species are firstly adsorbed or absorbed at the

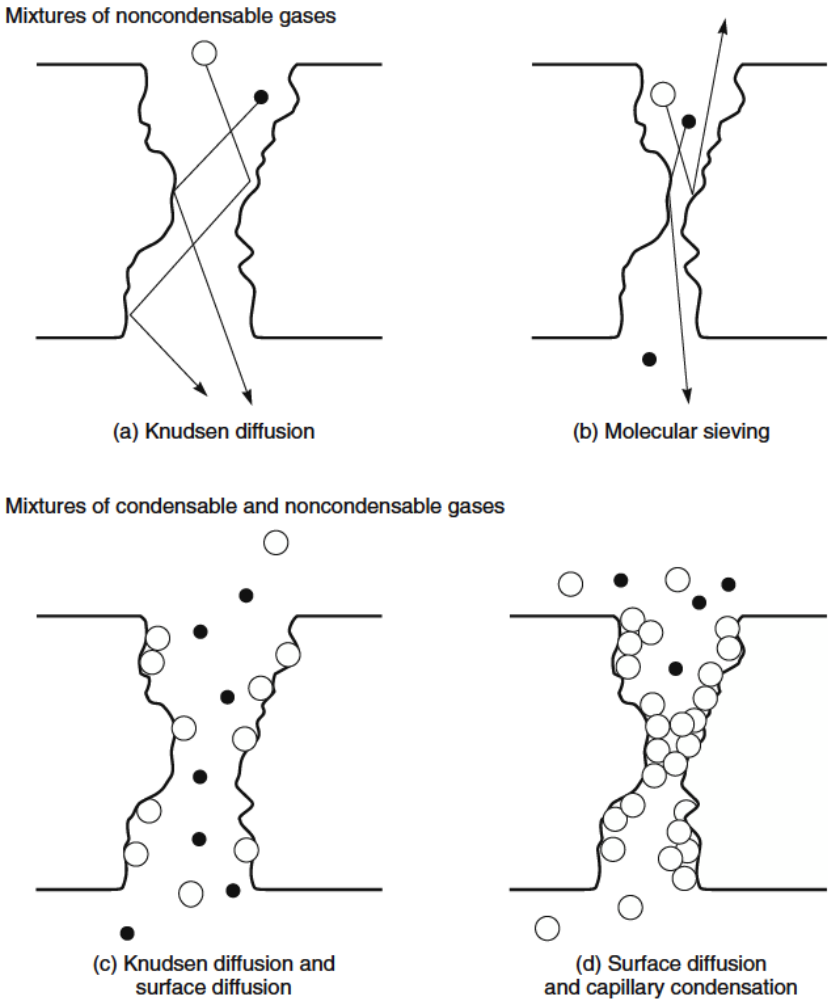

Figure 2.6: Permeation mechanisms through microporous membranes for gaseous mixtures containing condensable and non-condensable components. In the presence of non-condensable components, the decreasing of the pore sizes to molecular dimensions make the molecular sieving the prevailing mechanism. When condensable species are present, surface diffusion for those species increases with the decreasing of the pore dimensions and/or decreasing of temperature and increasing of pressure [Bak00].

upstream side of the membrane, followed by activated diffusion through the membrane, ending with desorption or evaporation on the downstream side. Separation in dense membranes is thus possible because of differences in the solubility and mobility of permeants in the membrane material. This solution-diffusion model assumes that the pressure across the membrane is constant, and the permeation is due to a concentration gradient. In general, the permeation behaviour of a gas through a dense membrane depends on the diffusion coefficent, nature of the gas, membrane material and vapour pressure (the last is applicable in the case of a permeating vapour: its permeation increases substiantially with increasing partial pressure when the pressure of the gas is near close to the saturation one).

2.4 Zeolite Materials, zeolite membranes and related transport mechanisms

In the beginning of 2000s, new application fields demanding membrane materials thermally and chemically stable, biocompatible or stelirizable, have appeared. To this end, research on inorganic membranes increased, since these requirements are hardly fulfilled by the widely used and developed organic membranes technology. In particular, supported zeolite layers, of main interest for the work here presented, have been intensively studied due to their wide range of potential applications: from separation technology (membranes and catalytic membrane reactors) to opto-electronics or nanotechnology [CNKS00, CN08].

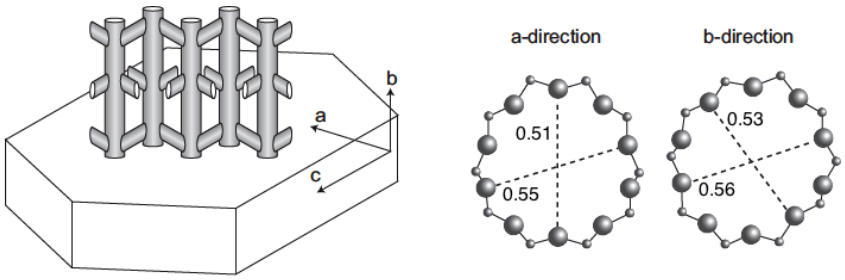

Figure 2.7: MFI material channel system. Crystallographic axes and pore dimensions (a and b directions) in nm. Adapted from [Jar04].

2.4.1 Zeolite materials

Zeolites are three-dimensional, microporous, crystalline solids formed by regular frameworks of aluminium, silicon and oxygen with well defined pores. Both Si and Al are tetrahedrally connected to each other through shared oxygen atoms (i.e., the building block of a zeolite is ZO_4, where Z = Si, Al). Since an oxygen atom is a bridge between two Z atoms, each SiO_4 unit is neutral. However, this is not the case for AlO_4 with a total charge of -1, so that the overall zeolite framework is charged. Charge balance of Al is achieved by adding extraframework cations [TD99]. As the Si/Al ratio of the framework increases, the hydrothermal stability as well as the hydrophobicity increases. Furthermore, the lower limit of Si/Al is one, since repulsive electrostatic forces between the negative charges arise with the placement of adjacent AlO_4^- [ACD03]. In general, the zeolite composition can be described as having three components [ACD03]:

$M_{n/m}^{m+}$	$[Si_{1-n}Al_nO_2]$	nH_2O
extraframework cations	**framework**	**sorbed phase**

Typically, water present during synthesis occupies the internal voids of the zeolites. Dehydration of the materials so produced is attained by thermal treatment, and in general the zeolites maintain their structural integrity upon loss of water [ACD03].

More than 190 distinct zeolite frameworks are known, being classified according to their frameworks symmetry with an identification code of three letters used by the International Zeo-

lite Association [TD99, YNF11]. One of the most studied framework is the MFI[5] ($Na_n(H_2O)_{16}$ $[Al_nSi_{96-n}O_{192}]$, $n < 27$) crystal, presented in figure 2.7. The thermally stable ($\geq$ 1175 K) silicalite and ZSM5 are two examples of zeolites with such structure. Moreover, both zeolites present good stability in strong acidic environments, are relative easy to prepare and have low affinity with water [BC96]. The MFI pore network consists of two interconnecting channel systems - sinusoidal channels (a direction) with dimensions 0.55 nm $\times$ 0.51 nm and straight oval channels (b direction) with 0.56 nm $\times$ 0.53 nm. At the intersection points, 0.9 nm size cavities are formed.

2.4.2 Zeolite membranes

Zeolite materials are characterised by the presence of uniform and well-defined, molecular-size pores (0.3 - 1.3 nm) and thermal, mechanical and chemical stability, which makes them suitable for membranes technology application. Due to their pore dimensions, zeolite membranes are capable of separating components in a mixture based on size and shape (molecular sieving mechanism). The different separation properties presented by the different zeolites are related to (i) the pore geometry and the connectivity of the network and (ii) the atom and ion arrangement on the pore surfaces. The adsorptive properties are primarily influenced by the extraframework cations and the hydroxyl groups (silanols), while the entire geometry of the pore system (in addition to the size of the channels) influences the adsorption as well as the mobility of the permeating molecules. To take advantage from the molecular-sieving and preferential adsorption properties in zeolite pores, the number and size of defects (intercrystalline spaces larger than the zeolite pores) has to be minimized. Presently less than 20 different zeolite membranes with significant separation selectivities are reported, which reflects the challenges of this process [YPF06, YNF11]. Several reviews of the state of the art of the zeolite membranes can be found in the references [TD99, CNKS00, CN08, CAD$^+$00].

MFI membranes are by far the most studied for gas separation, catalytic reactors and pervaporation applications, although other systems (e.g., LTA, FAU, MOR or FER) have also been synthesized. Improving synthesis control and reproducibility, control of the membrane quality (detection of defects) and clarification of transport mechanisms are examples of points still to be studied. Furthermore, the development of supported zeolite membranes is limited to large thicknesses ($\sim$ 20 μm) to ensure defect-free layers, and, as a consequence, rather low flows are obtained (see table 2.4 for comparison of the performances of MFI membranes with organic and other inorganic membranes in H_2 recovery applications). The low fluxes presented by the zeolite membranes make them economically not attractive, justifying their slow introduction in industrial processes. However, zeolitic membranes for specific applications with interesting results have been developed (e.g., DDR for H_2 and CO_2 separation, SAPO-34 for CO_2 separation or LTA for de-hydration).

H-SOD[6] and NaA are two zeolitic frameworks of special importance for this work, as it is described in section 2.5. Thus a brief description of those materials in view of membranes

[5] Mordenite Framework Inverted.
[6] Hydroxy Sodalite.

Membrane	**Temperature** [°C]	**Thickness** [μm]	**H_2 flow at $\Delta p = 1 - 2$ bar** [m^3/m^2h]
Organic Polymer	< 100	0.05 - 0.5	1 - 2
Thin-Pd alloy membrane	300 - 450	5	10 - 25
Molecular sieve silica	200	0.03	4.1 - 16.1
MFI	30 - 210	~ 40	0.97 - 0.83

Table 2.4: Typical performances of different H_2-selective membranes [CN08].

applications is now given [Kha10, KJK07, Szo92, CSARR$^+$13, AKM00]:

- **H-SOD**: the framework of the hydrophilic (Si/Al = 1) H-SOD is the same as sodalite (Na_8Cl_2 [$Al_6Si_6O_{24}$]), presenting a cubic array of β-cages (figure 2.8). Each cage is formed by four- and six- membered oxygen-rings linking the ZO_4 building blocks. The 0.265 nm kinetic window diameter of the largest oxygen rings make this material suitable for separation of small molecules. However, the cages are blocked by water, due to hydrogen bonding between the non-framework water and the framework oxygen. As a result, the permeation of other molecules is hindered. Dehydration of the structure leads to the destruction of such H bonds, resulting in the partial collapse of the framework. Therefore, these materials are suitable for processes where the water phase in the framework can be preserved, such as pervaporation (but not gas separation). The non-permeation of gases through the blocked framework is an experimental evidence of absence of defects [KJK07].

- **NaA**: as in the H-SOD, the LTA[7] ($(Na_{12}(H_2O)_{27}[Al_{12}Si_{12}O_{48}])_8$) framework of the NaA material consists in a cubic of β-cages. The void space between the β-cages are called α-cages and are connected by 8-membered ring windows. The extra framework sodium cations are initally colocated in the dehydrated structure at three different adsorption sites. This material is widely used as a membrane to separate polar from non-polar molecules by permeation, due to its hydrophilic nature (low Si/Al). Although the pore sizes are larger than the smallest molecules ($\sim 0.40 - 0.44$ nm), separation of such molecules is still possible due to differences in affinity to the pore walls. As an example, separation factors larger than 160 for 303 - 473 K were already attained for H_2O/H_2 [AKM00].

2.4.3 The transport mechanisms in zeolite membranes

The transport in zeolites follows an adsorption-diffusion mechanism, and thus the separation of mixtures is accomplished due to differences in adsorption and diffusion rates, but also by molecular sieving [YNF11]. With the decreasing of the pore walls, the permeating molecules are increasingly subjected to an attractive potential field. The sorption energy is thus larger than that on free surfaces[8], while the desorption energy decreases. As a consequence, the molecules move from an adsorption site to another adsorption site when a certain activation energy is

[7] Linde Type A.
[8] The molecules permeate free of any considerable wall potential.

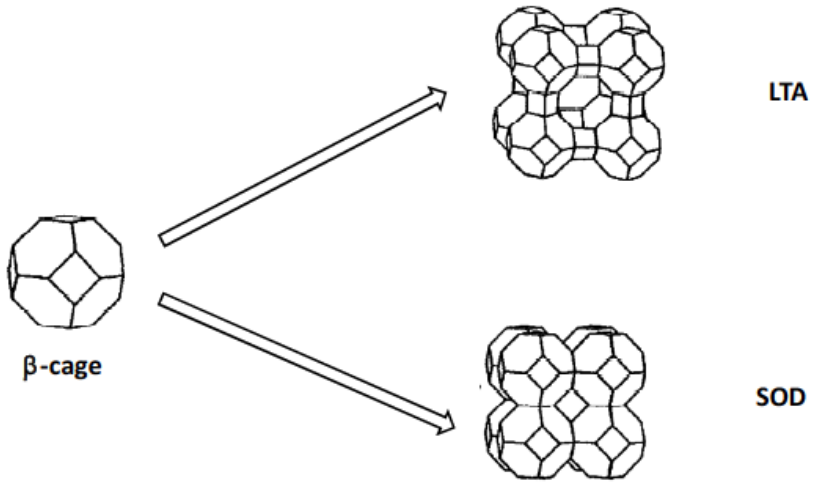

Figure 2.8: (Left) β-cage. (Right-Up) LTA structure. (Right-Down) Sodalite structure [Kha10].

overcome. This mechanism is a combination of molecules moving by gas translational (GT) diffusion and by surface diffusion. With further decrease of the pores dimensions, a stage in which a gaseous phase no longer exists is eventually reached. Depending on the ratio between molecule size and pore diameter, the sorption energy continues to increase. The transport mechanism is now purely based on diffusion[9], called configurational diffusion. When the ratio between the pore diameter and molecular diameter is less than unity, repulsive potentials arise, the sorption energy decreases, and the permeating molecule is excluded from the zeolite microporous system [Bur99].

The surface diffusion steady-state flux $J_{i,s}$ [mol m^{-2} s^{-1}] of a gaseous component i through a supported zeolite membrane can be described by[10] [Bur99, BVKV98, BC96, BVDBKM97]

$$J_{i,s} = \rho_z \widetilde{D}_{i,s} q_{sat} \frac{d\theta_i}{dz} = \frac{\rho_z \widetilde{D}_{i,s} q_{sat}}{t_m} \frac{K_i(p_{F,i} - p_{P,i})}{(1 + K_i p_{F,i})(1 + K_i p_{P,i})} \tag{2.7}$$

where z [m] is the direction of permeation, $\widetilde{D}_{i,s}$ [m^2 s^{-1}] is the chemical diffusion constant, q_{sat} [mol g^{-1}] the maximum sorption concentration compatible with the available surface adsorption sites, ρ_z the zeolite density [g m^{-3}], t_m [m] the effective layer thickness of the membrane, $p_{F,i}$ and $p_{P,i}$ [Pa] the partial pressures in feed and permeate respectively, and θ_i the fraction of occupied adsorption sites. Note that the Fick's law for concentration gradient as a driving force can be obtained from the first equality by using the relation $\theta_i = q_i/q_{sat}$. The underlying assumptions for derivation of equation (2.7) are (1) the steady state concentrations at both membrane/gas interfaces are equal to equilibrium concentrations and (2) the adsorption of the permeating species follows the Langmuir isotherm, in which the fraction of occupied adsorption sites depends on the gas phase pressure p [Pa] according to

[9] There are strong similarities between this permeation mechanism and those observe in solid state diffusion.
[10] Here a scalar relation between the flux and the concentration gradient is considered, and thus the minus signal is absent in the first equality.

$$\frac{q_i}{q_{sat}} = \frac{K_i p}{1 + K_i p} \tag{2.8}$$

where q_i [mol g^{-1}] is the amount of adsorbed species in the zeolite and K_i [Pa^{-1}] the Langmuir constant. K_i follows an Arrhenius-type temperature dependence, $K_i = K_{0_i} \exp\left(\frac{-\Delta H}{RT}\right)$, where $-\Delta H > 0$ [J mol^{-1}] is the enthalpy of adsorption (different for any adsorbate-adsorbent combination), R [J K^{-1} mol^{-1}] is the ideal gases constant and K_{0_i} [Pa^{-1}] a pre-exponential factor. The Langmuir parameter also depends on the entropy of adsorption ΔS [J mol^{-1} K^{-1}] through $K_i = \exp\left(\frac{\Delta S}{R} - \frac{\Delta H}{RT}\right)$. Similarly, the diffusion coefficient shows also the same dependence with the temperature: $\widetilde{D}_{i,s} = \widetilde{D}_{0_i,s} \exp\left(-E_{D_i,s}/RT\right)$, where $E_{D_i,s}$ [J mol^{-1}] is the activation energy for surface diffusion of the adsorbed species i.

If the GT activated diffusion mechanism (whose diffusion coefficient is $D_{i,\mathrm{GT}} = D_{0_i,\mathrm{GT}} \exp\left(-E_{D_i,\mathrm{GT}}/RT\right)$) is present, the total steady-state flux $J_{i,tot}$ [mol m^{-2} s^{-1}] through the membrane is a linear combination of both $J_{i,s}$ and $J_{i,\mathrm{GT}}$,

$$J_{i,tot} = \epsilon \left[\rho_z q_s D_{0_i,s} \frac{1}{1-\theta_i} \exp\left(-\frac{E_{D_i,s}}{RT}\right) \frac{d\theta_i}{dz} + \frac{\lambda}{\beta} \sqrt{\frac{8}{\pi M_i RT}} \exp\left(-\frac{E_{D_i,\mathrm{GT}}}{RT}\right) \frac{dp}{dz} \right] \tag{2.9}$$

where the relations $\widetilde{D}_{0_i,s} = D_{0_i,s}/(1-\theta_i)$ and $D_{i,GT} = (\lambda/\beta)\sqrt{8RT/\pi M_i}$ were used. ϵ is the porosity of the membrane's support (fraction of the total volume that is porous), λ [m] the distance between two adjacent sites, β the coordination number of the zeolite (inserted to take into account the probability of motion of the molecules to other directions other than the direction of diffusion under consideration [Xia90]) [BVDBKM97].

The description here given for the transport in zeolite membranes as a function of the temperature is pictorically presented in figure 2.9. Although in the AB region the transport is governed by adsorption (which continuously decreases with the temperature), the overal flow increases due to the increase in the mobility of the adsorbed molecules. At a certain temperature, the diffusion mechanism no longer compensates the decrease in adsorption leading to a decrease of the total flow (BC). When adsorption is not anymore the governing parameter (turning point C), the increase of the flow with the temperature is due to configurational diffusion. It should be noted that concerning adsorption, any changes on surface characteristics of the material (e.g., acido-basicity or composition) dramatically affect the shape and position of the ABCD curve [CAD$^+$00].

In the presence of a mixture, the selective adsorption has an important role on the permeation of the permeating species. In fact, the more adsorbable species can pass easily through the pores, blocking the passage of the others (weaker adsorbable) species. As mentioned before, the existence of defects in the crystalline structure has a direct influence on the permeation of the gas species, being an additional contribution to the total flow through the membrane, while lowering the separation performance of the membrane [ABG$^+$03].

With gas permeation measurements, e.g. by a gradient pressure driven process, the permeation of a certain species through a given membrane as a function of temperature and pressure

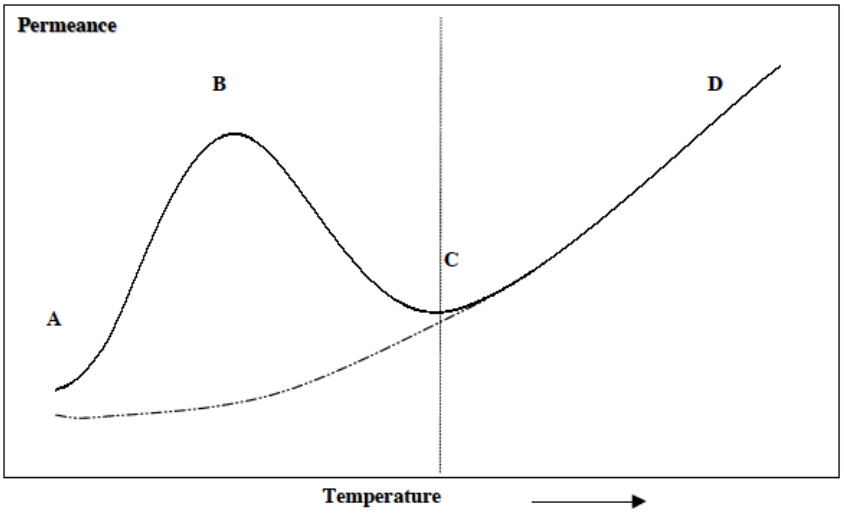

Figure 2.9: Permeance of a single gas through a defect-free zeolite membrane as a function of the temperature [ABG+03]. The transport in the AB region is governed by the thermal increase of the mobility of the molecules with increasing temperature. In the turning point B, the diffusion mechanism no longer compensates the decrease of adsorption, and a decrease of the total flow in the BC region results. From the point C on, the adsorption is not anymore the governing parameter, and the overall flow increases due to configurational diffusion.

can be studied. Such dependencies reveal which mechanism(s) is(are) governing the permeation process. Also, from the experimental permeation results, the presence of defects can also be inferred. Indeed, consider for instance a given gaseous mixture permeating through a membrane for which high separation factors are expected due to molecular sieving mechanism. If however lower separation factors are obtained, along with higher flows, larger pores (defects) have to be present, also suggesting that other transport mechanisms (e.g., Knudsen flow) are present. It should be emphasized that the separation efficiency of a zeolite membrane depends greatly on the operating conditions - the same membrane may enable a highly selective separation for a given separation under certain conditions, and show no selectivity in other cases [BCMS02].

2.5 Zeolite membranes for tritium process in the breeding blanket

As discussed in 2.2.2, zeolite membranes gather the most interesting features to be used for the pre-concentration stage of the TES. The membranes have to handle a He stream gas that transports hydrogen isotopes species in both molecular (Q_2) and oxidized (Q_2O) form, from which two streams are produced: one depleted and another concentrated in tritium. The very similar kinetic diameters of the molecules of interest (d_k(He) = 0.260 nm, d_k(Q_2O) = 0.265 nm and d_k(Q_2) = 0.289 nm [YPF06]) might be a difficulty to promote the molecular-sieving mechanism.

Different zeolitic membranes has been identified to use as a pre-concentration stage. LTA (NaA), with $\sim$ 0.4 nm pore size, and MFI (ZSM-5), with $\sim$ 0.5 nm pore size, membranes have shown promising performances for the tritium processing applications. H_2O/H_2 perm-selectivities between 10 and 500 at $\sim$ 350 and 100 °C, respectively, for the MFI-ZSM5 membrane

have been published [RSK+08]. Furthermore, the $\sim 0.27 - 0.29$ nm pore size H-SOD defect-free membrane might exhibit high-selectivity since Q_2 molecules are larger than the pore dimensions. Moreover, carbon membranes (< 0.5 nm pore size) promoting surface diffusion with polarizable molecules have been produced [Kan00].

Since there is too scarced published experimental data of permeation of the gases of interest through those membranes, dedicated experiments must be performed in order to conclude which membrane(s) is(are) more suitable for the pre-concentration stage of the TES.

2.6 Status of the work at TLK – ZIMT

2.6.1 The ZIMT facility

The lack of experimental data for $He/H_2/H_2O$ mixtures on zeolite membranes has motivated the design and the development of the ZIMT (Zeolite Inorganic Membranes for Tritium) facility at TLK, gradually upgraded to perform single (ZIMT I), binary (ZIMT II) and ternary (ZIMT III) mixtures on candidate membranes.

The facility started to be built in 2010, and the first setup (figure 2.10) was designed to perform only single gas experiments. In 2012, binary mixtures experiments, where a mixture of two gases (H_2/He) flows through the membrane, could be performed due to an upgrade to ZIMT II (figure 2.10). One year later, the facility was finally upgraded to perform ternary mixtures gas experiments, where moisture could be added to the previous binary mixture.

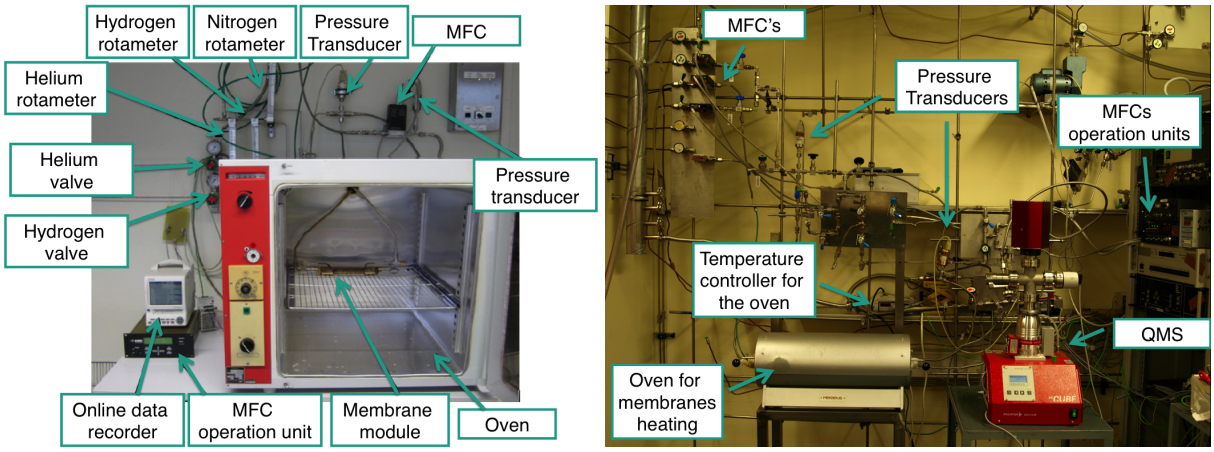

Figure 2.10: Experimental apparatus of ZIMT I (left) and ZIMT II (right). MFC - Mass Flow Controller, QMS - Quadrupole Mass Spectrometer.

2.6.2 Previous results on a MFI hollow fiber membrane

Only one membrane was available for tests in ZIMT (both ZIMT I and ZIMT II). It is a very thin selective layer (< 1 μm) nanocomposite hollow-fiber MFI membrane (MFI-HF) produced by IRCELYON (France) and presented in figure 2.11.

At ZIMT I, permeation experiments on the MFI-HF membrane were performed at different temperatures (RT - 400 °C) by heating the membrane module in an oven [Par11]. The influence of the temperature on the permeance of both helium and hydrogen is depicted in black rhombus

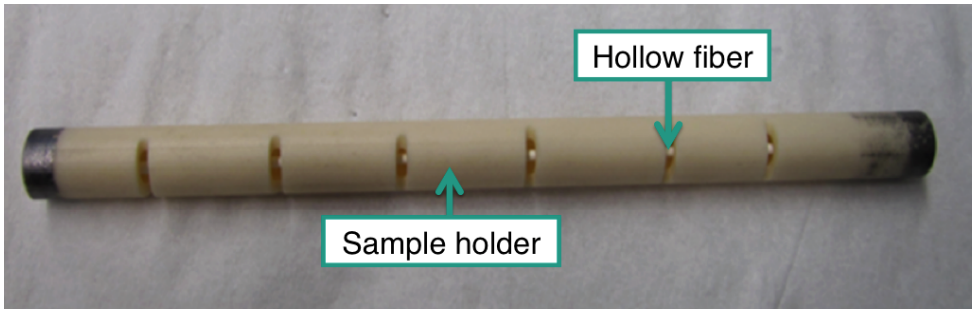

Figure 2.11: Hollow fiber membrane from IRCELYON inserted in the sample holder tested at ZIMT I and ZIMT II.

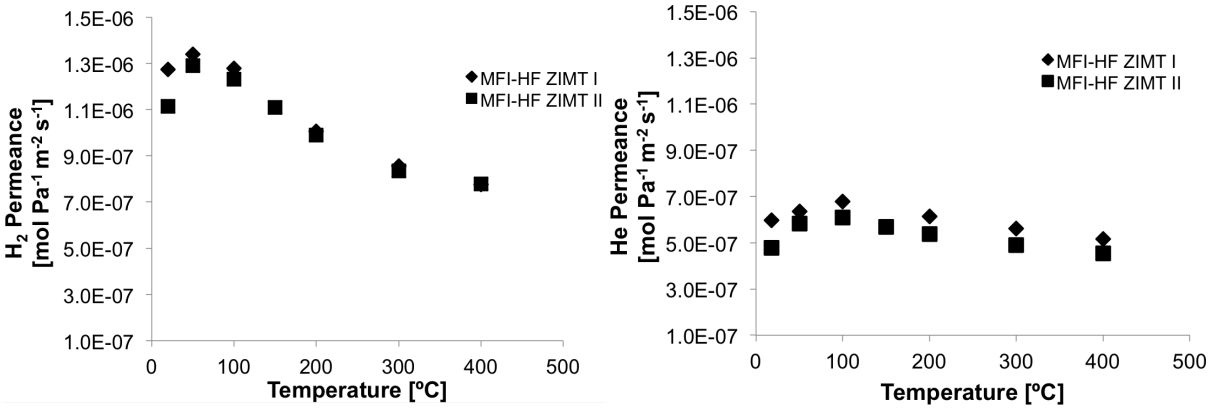

Figure 2.12: Permeance as function of temperature for H_2 (left) and He (right) for the MFI hollow fiber (MFI-HF) membrane tested in ZIMT I (black rhombus) and ZIMT II (black squares).

in the plots of figure 2.12. The observed dependence resembles the BC path of figure 2.9. These results evidence the transition between the contribution of the mobility to the increase of the permeance ($\sim$ 20 - 50 °C) and the dominating decreasing effect of adsorption on the overall permeance ($\sim$ 100 - 400 °C). Furthermore, it was observed that H_2 is the most permeable gas, with the highest permeance being 1.34×10^{-6} mol m^{-2} s^{-1} Pa^{-1} at 50 °C, while the highest value for He was 6.77×10^{-7} mol m^{-2} s^{-1} Pa^{-1} at 100 °C. From these results, it can be concluded that the H_2/He permselectivity is rather limited, not exceeding 2.2. On the other hand, the permeance is rather high. For instance, the H_2 permeance at RT is two orders of magnitude higher than the permeance obtained from the data presented in table 2.4 for the MFI at 30 °C (around 6×10^{-8} mol m^{-2} s^{-1} Pa^{-1}). The reason for this is the difference of about two orders of magnitude in the membranes thickness.

A repetition of the helium and hydrogen single gas permeation experiments with the same MFI-HF membrane and also H_2/He binary mixtures experiments were performed at ZIMT II [Sim12, SAB$^+$14, DBG$^+$13]. As shown in black squares on figure 2.12, the single mode results are consistent with the previous ones (obtained at ZIMT I). In the binary mixture gas experiments, a study of the effect of varying the concentration of H_2 in the H_2/He stream on the separation efficiency of the membrane was performed. The observed results showed that the H_2/He separation factor is not particularly affected by changing the hydrogen concentration down to 1%. Indeed, the performance of the membrane for low H_2 partial pressures (of interest to the breeding blanket conditions) shows to be as efficient as concluded from the single experiments.

In 2013, after the final upgrade integrating the water vapor system (ZIMT III, figure 2.13), ternary mixtures experiments (1% H_2, 1% H_2O and 98% He) were performed on the MFI-HF membrane. At room temperature only the water vapor was permeating through the MFI membrane (corresponding to selectivities of about 91 to H_2O/H_2 and 87 to H_2O/He), in contrast with what was observed at 100 °C where no separation existed.

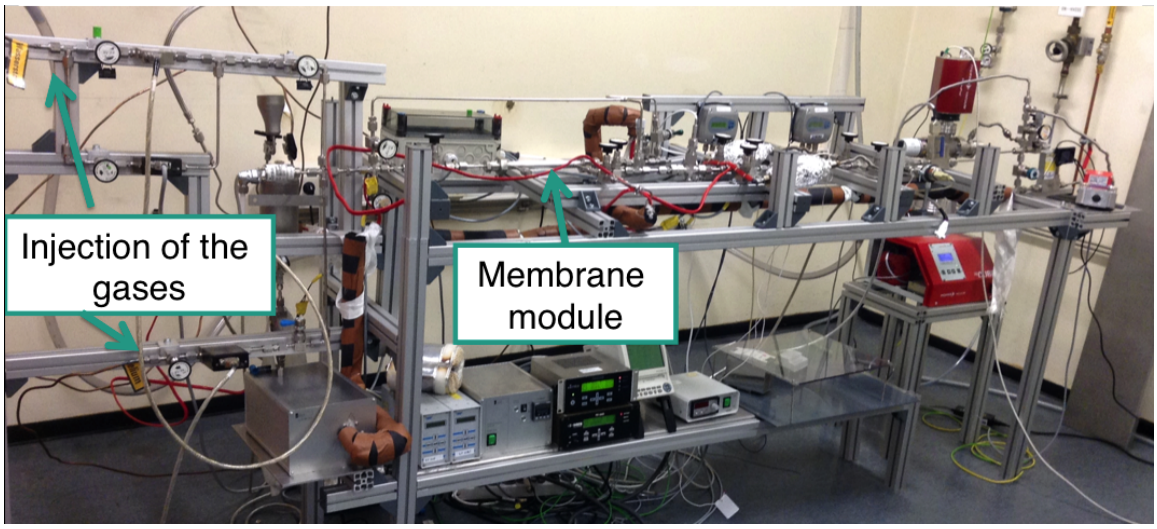

Figure 2.13: Picture of the ZIMT III facility.

3

Experimental Setup and Comissioning of the ZIMT III Facility

3.1 ZIMT III overview and details of the main components

3.1.1 Overview of the ZIMT III apparatus

In figure 3.1, a schematic overview of the final configuration of the ZIMT III facility is presented. This final setup was achieved after gradual improvements on the initially existing configuration at the beginning of this work, where the facility was only prepared to perform single gas experiments[1].

One of the most important features of the configuration presented in figure 3.1 is its flexibility, since single, binary and ternary gas experiments can be performed. Furthermore, using a by-pass connection between the feed and permeate sides of the membranes (dark grey dashed line), it is possible to perform calibration of the measuring devices. In addition, this facility allows continuous mode measurements.

The facility is consisted of several measuring and controlling devices. With the mass flow controllers (MFC's) a certain set flow can be imposed. A MFC can also be used in the measurement mode, by setting the flow to its full scale (here designated MFR - Mass Flow Register). Therefore, the device is totally "opened" to the gas stream. The pressure controller (PC) associated with a vacuum pump keeps a certain pressure of interest, whereas the pressure registers (PR) are pressure transducers from which the pressures are measured. When wet streams are flowing throughout the pipes, the humidity sensors (HS's) are used to measure humidity (both

[1]Since the membrane module of the newly developed tubular membranes from IKTS has different size compared the one used to accomodate the hollow-fiber, the design of the ZIMT III facility had to be modified. As a consequence only single gas experiments could be performed at the beginning of this work.

relative and absolute) values. The Quadrupole Mass Spectrometer (QMS) is used to analyse the process streams in both permeate and retentate lines.

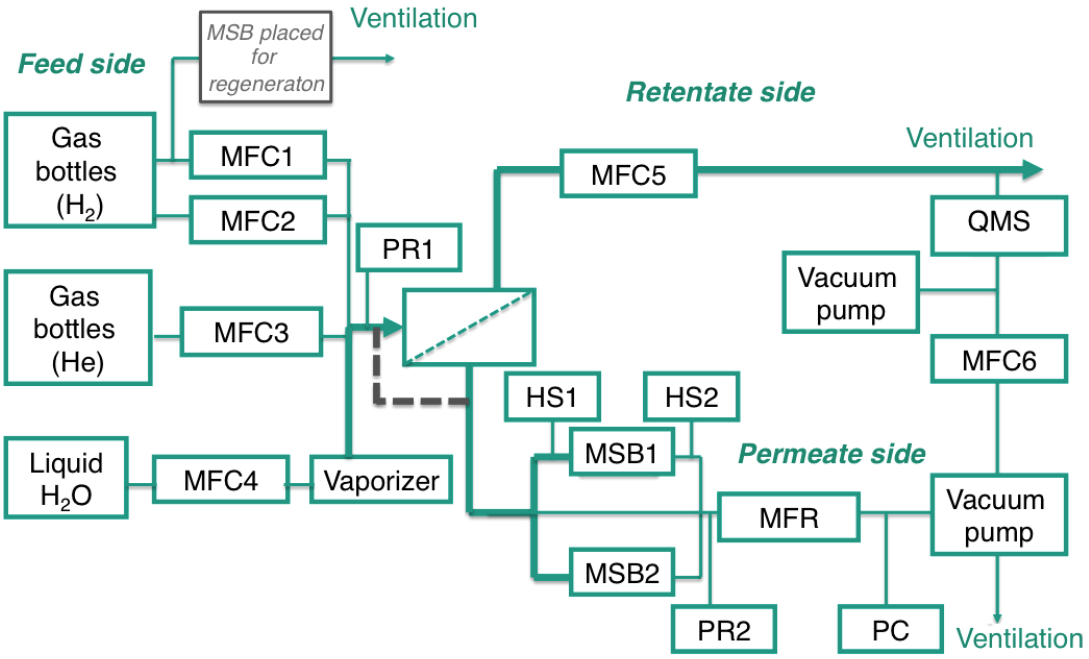

Figure 3.1: Block diagram of the ZIMT III facility featured to perform single, binary and ternary gas experiments. Bold lines indicate the heated pipes, and the dark grey dashed line indicates the by-pass line. MFC - Mass Flow Controller; MFR - Mass Flow Register; PR - Pressure Register; PC - Pressure Controller; MSB - Molecular Sieved Bed; HS - Humidity Sensor; QMS - Quadrupole Mass Spectrometer. MFC calibrated for H_2: MFC1 (500 ml/min) and MFC2 (10 ml/min). MFC calibrated for He: MFC3, MFC5 (10^4 ml/min) and MFC6 (10^3 ml/min). MFC4 calibrated for H_2O. MFR calibrated for He (10^4 ml/min).

By opening/closing valves it is straightforward to change the configuration of the facility to start a specific study. The details and properties of the configuration for each mode are presented below.

3.1.2 Different configurations of the experimental setup

3.1.2.1 Setup for single gas experiments

The block diagram of the facility on the single mode is presented in figure 3.2. The single gas experiments are performed using the dead-end mode (retentate closed), where the entire helium, hydrogen or nitrogen feed stream imposed by MFC6 (10^3 ml/min MFC calibrated for He) is forced to permeate through the membrane. The permeate pressure is imposed either using the PC associated to the vacuum pump or directly connecting this side to the ventilation where an atmospheric pressure is kept. These imposed pressures are measured/verified by PR2. The imposed feed flow leads to a pressure difference across the membrane, determined by measuring the pressure on the feed side with PR1.

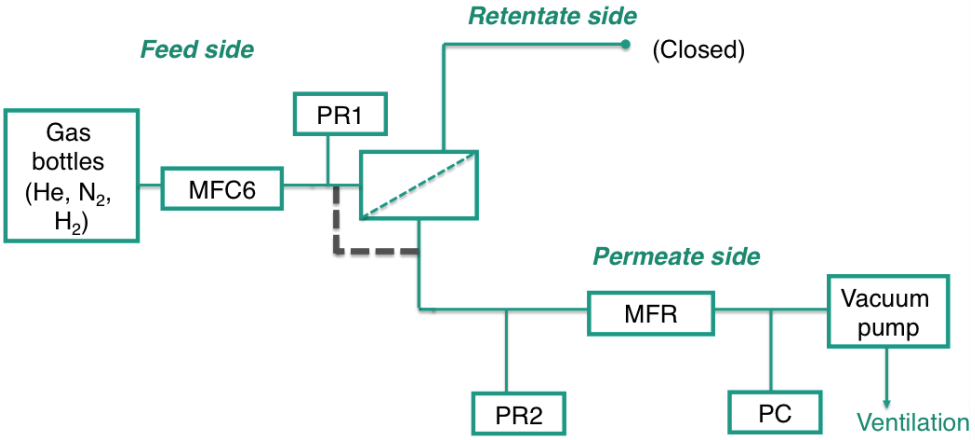

Figure 3.2: Block diagram of the experimental setup for single gas experiments. MFC - Mass Flow Controller; MFR - Mass Flow Register; PR - Pressure Register; PC - Pressure Controller. MFC6 calibrated for He (10^3 ml/min). MFR calibrated for He (10^4 ml/min).

3.1.2.2 Setup for binary mixtures gas experiments

The initial single gas apparatus was upgraded to the one presented in figure 3.3. In this configuration, the feed flow of helium is imposed with a 10^4 ml/min MFC calibrated for He (MFC3 in the figure) and the feed flow of hydrogen is controlled with either a 10 or 500 ml/min MFC calibrated for H_2 (MFC2 and MFC1, respectively, in the figure). Therefore, a dynamic mixing of both species is achieved. The selected flows give rise to the concentration of each gas in the total stream. For instance, setting 50 ml/min flow for H_2 and 1000 ml/min for He, a H_2/He concentration of 5% is obtained.

In this setup, the retentate line is opened. A 10^4 ml/min MFC calibrated for He (MFC5 in the figure) is used on the retentate side at atmospheric pressure to maintain a desired flow. As a consequence, the permeate flow is also controlled (on the permeate side a 10^4 ml/min MFR calibrated for He is used). The permeate pressure is maintained constant (at around 300 hPa) using the PC and the associated vacuum pump. Due to those imposed pressures, a higher pressure in feed exists, enabling the permeation/rejection of the gaseous species. The analysis of the permeate and retentate streams is then accomplished by using the QMS.

The by-pass measurements for the calibration of the QMS demonstrated that this setup provides no reliable calibrations and the steady-state measurements are reached after very long time (around two hours). The injection system by the QMS has been modified, and the resulting configuration is in figure 3.4. In this setup, the flow in the injection line of the QMS is kept constant using MFC6. Moreover, another stronger vacuum pump was introduced in the system. With the new configuration the efficiency and reliability of the QMS meauserements is improved, and the steady-state values are obtained in around 20 min.

3.1.2.3 Setup for ternary mixtures gas experiments

The schematic diagram presented in figure 3.1 presents the configuration used for the H_2/H_2O/He ternary and H_2O/He binary mixtures gas experiments. The water vapour is injected into the

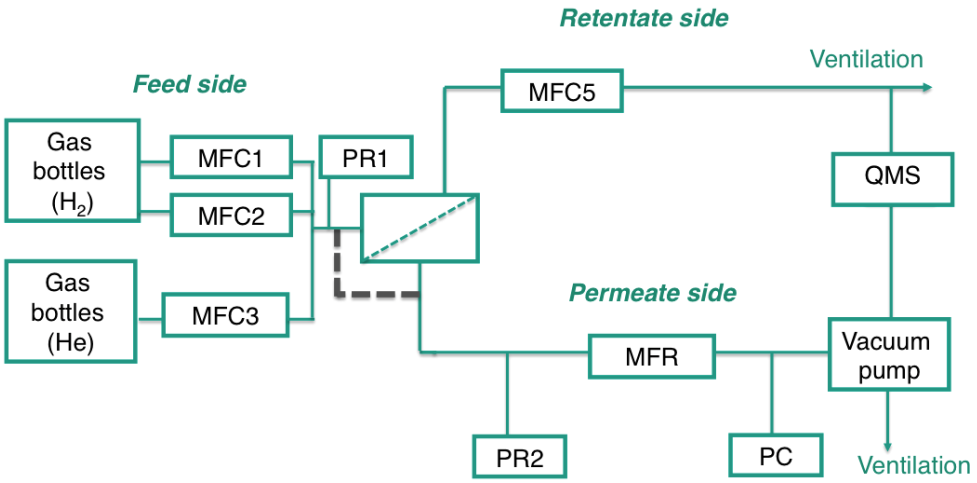

Figure 3.3: Block diagram of the inital experimental setup for H_2/He binary gas experiments. MFC - Mass Flow Controller; MFR - Mass Flow Register; PR - Pressure Register; PC - Pressure Controller; QMS - Quadrupole Mass Spectrometer. MFC calibrated for H_2: MFC1 (500 ml/min) and MFC2 (10 ml/min). MFC calibrated for He: MFC3 and MFC5 (10^4 ml/min). MFR calibrated for He (10^4 ml/min).

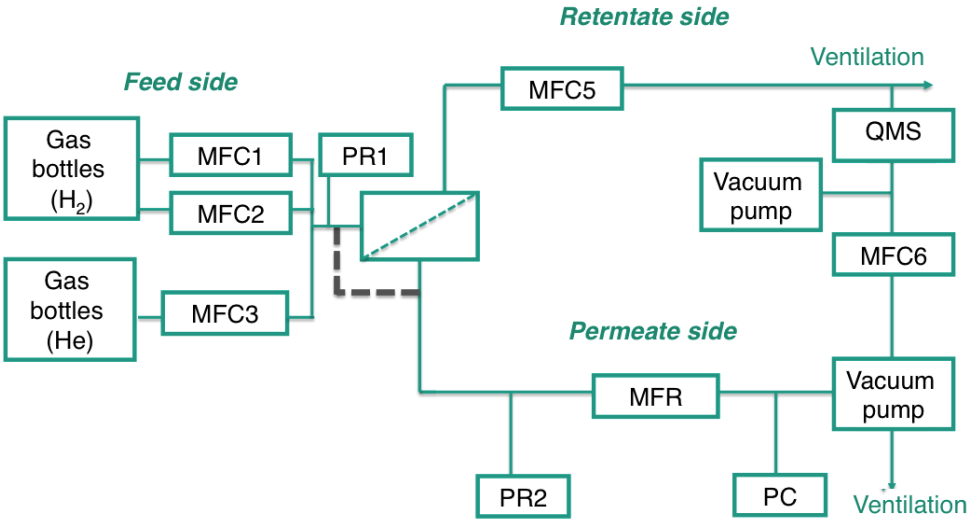

Figure 3.4: Block diagram of the final experimental setup for H_2/He binary gas experiments. MFC - Mass Flow Controller; MFR - Mass Flow Register; PR - Pressure Register; PC - Pressure Controller; QMS - Quadrupole Mass Spectrometer. MFC calibrated for H_2: MFC1 (500 ml/min) and MFC2 (10 ml/min). MFC calibrated for He: MFC3, MFC5 (10^4 ml/min) and MFC6 (10^3 ml/min). MFR calibrated for He (10^4 ml/min).

system through a 10 - 200 ml/min liquid water MFC[2] (MFC4 in the figure) followed by a vaporizer with which the temperature of the steam can be set up to 200 °C. The presence of moisture in the stream requires a proper heating of the pipes all along its pathway. This was accomplished by wrapping electrical heating cables to the pipes, while ensuring a proper insulation with fiberglass and flexible elastomeric foam. This configuration allows the dynamic mixing of helium, hydrogen and water vapour whose concentrations in the total stream are determined by the set flows.

[2]The range of flows 10 - 200 ml/min comprises the minimum and maximum values that can be imposed with this MFC.

On the permeate side, the two parallel lines containing each a MSB (MSB1 and MSB2 in the figure) for drying the carrier gas are used. In addition, two humidity sensors are placed before (HS1) and after (HS2) the MSB's, with which relative (RH) and absolute (AH) humidity values and also temperature measurements inside the pipes can be measured. HS1 is used to obtain online measurements of the actual humidity, and HS2 is used to check the saturation of the MSB in use: if the MSB is saturated, no more H_2O molecules are adsorbed and thus detected in that sensor. It should be noted that after the MSB's, the lines are not heated and then condensation of non-adsorbed water must be avoided. When the MSB's are saturated, regeneration at 400 °C with He as a sweeping gas has to be done. To perform experiments while one of the MSB is regenerating, an additional connection before one of the MFC's on the feed side exists where the MSB is placed. The total regeneration of each MSB lasts between three and four hours, being the first hour needed to achieve the desired temperature in the MSB.

3.1.3 Details of the main components

The principal components integrating ZIMT III that enable single, binary and ternary mixtures gas experiments are listed below and some of them are also presented in the figures 3.5 - 3.8.

- He, N_2, and H_2 6.0 purity level gas bottles (Air Liquide);
- Stainless membrane module (IKTS);
- Valves, pipes and pipes sealings (Swagelok);
- Connections to the ventilation for exhaust;

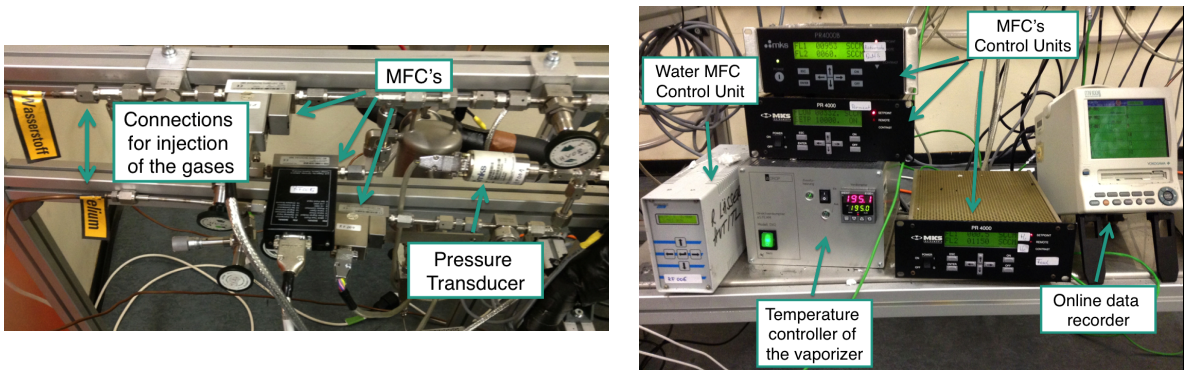

Figure 3.5: (Left) Components upstream of the membrane module: connections for the injection of the gases, MFC's and pressure transducer. (Right) Gas and water MFC control units, temperature controller for the vaporizer, and online data recorder for the temperature of the module and pressures.

- Pressure sensors (750 B series, MKS Instruments);
- Mass flow controllers (MFC's) 10 and 500 ml/min range calibrated for H_2 and 10^3 and 10^4 ml/min range MFC's calibrated for He (MF1 series, MKS Instruments);
- Operation unit for readouts of the flows (PR 4000, MKS Instruments);

- Online data recorder for readouts of the pressure transducers and temperature in the module (MobileCorder MV100, YOKOGAWA);
- Membrane module heating jacket, with associated thermoregulator (HORST);

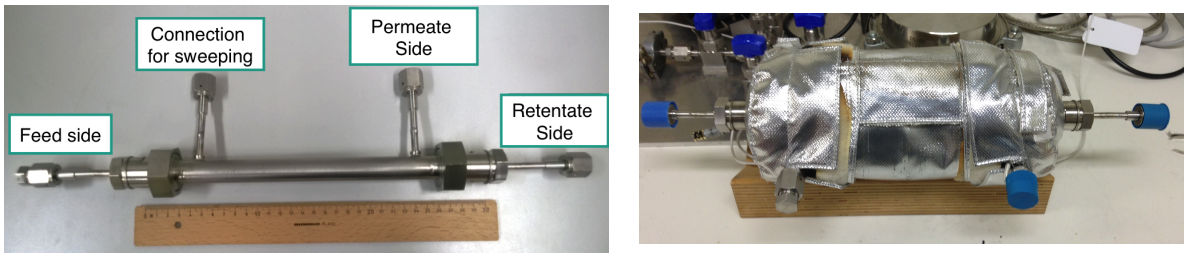

Figure 3.6: (Left) Membrane module. (Right) Membrane module inside the heating jacket.

- Thermocouples;
- Vacuum pump S(N_2) = 0.288 m^3/h (MVP 006-4, Pfeiffer-Vacuum);
- Vacuum pump S(N_2) = 0.77 m^3/h (DIVAC 0.8 T, Oerlikon Leybold-Vacuum);
- Pressure sensor and controller with an associated Readout/Control module (EL-Press series, Bronkhorst High Tech);
- Quadrupole Mass Spectrometer (Prisma-Plus QMG 220 F, Pfeiffer-Vacuum) with associated software (QUADERA);

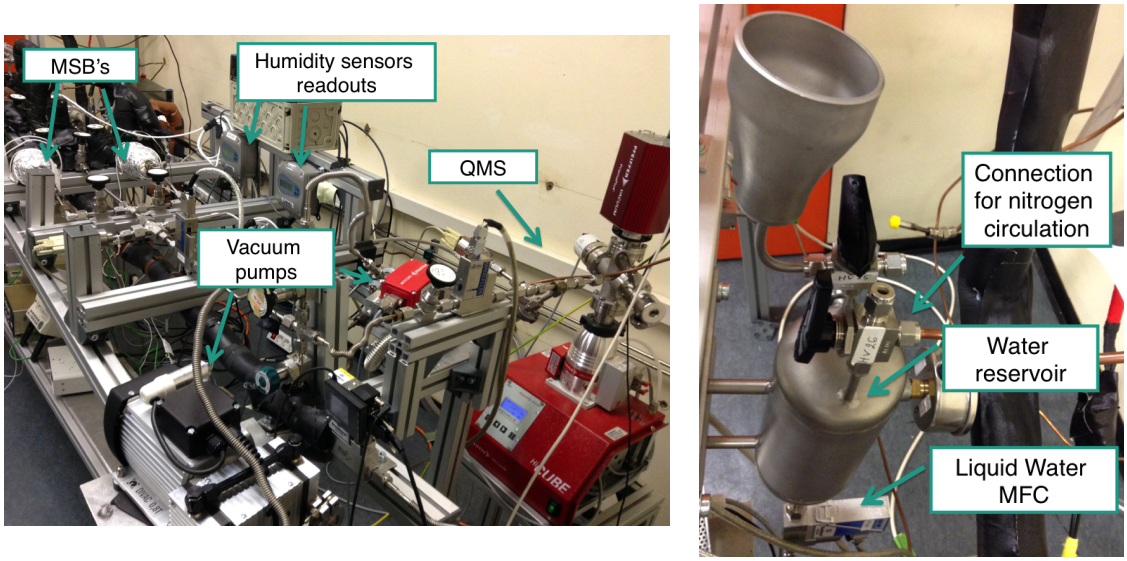

Figure 3.7: (Left) Components downstream the membrane module. (Right) Water reservoir and respective MFC for injection of the water into the system (via the vaporizer).

- H_2O mass flow controller (LIQUI-FLOW L13, Bronkhorst High Tech);
- Vaporiser (aSTEAM DV2, Adrop);
- Digital relative humidty and temperature transmitter (WR-293, Michell Instruments);
- Two 5A-zeolites molecular sieve beds;

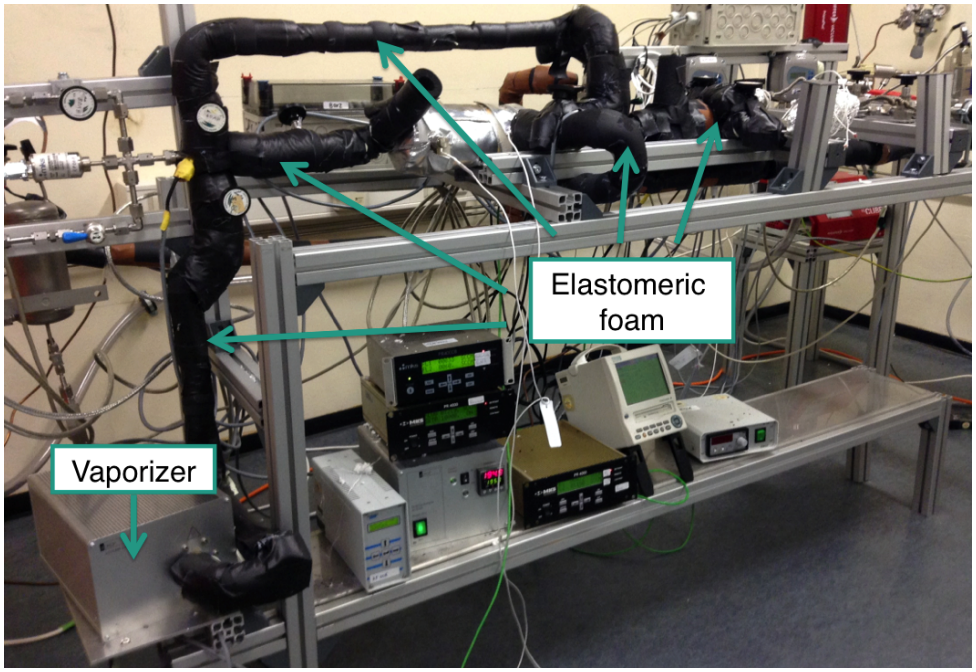

Figure 3.8: Vaporizer and elastomeric foam used for insulation of the pipes to perform ternary mixtures gas experiments.

- Thermoregulator (Heraeus);
- Pipes heating system (HSB60, BARTEC);
- Fiber glass and flexible elastomeric foam;
- 5 g - 5000 g Balance (Sartorius);
- 0.1 mg precision balance (Sartorius).

3.2 Comissioning of the facility

3.2.1 Leak tests

The ZIMT III facility consists mainly of connected stainless pipes (through VCR connections) inside which the gases flow. It is therefore important to ensure tightness between these connections for several reasons: (1) to avoid leaks of highly reactive and explosive gases such as hydrogen, (2) not to pollute the system and the high purity gas bottles and thus (3) to ensure the quality of the measurements. To this end, pipes sealings between each VCR connection are used and systematic leak tightness tests throughout the system must be performed.

The leak tests are performed using the helium leak detector presented in figure 3.9, and the tightness of the facility is analysed by measureing the He leak rate given by the detector. This device can be used in two distinct modes: (1) sniffing mode and (2) vacuum mode. The first one consists on pressurising the entire system with He, and using the sniff probe to check each connection. In this mode, the He background leak rate is around 4×10^{-6} hPa l s^{-1}. The second mode is accomplished by first evacuating all the system, reaching the smallest (background) helium leak rate of around 2×10^{-8} hPa l s^{-1}. Then, by spraying each connection

with helium, its tightness can be analysed. The vacuum mode is a more sensitive and delicate technique and it was used after subjecting the facility to considerable changes (e.g., upgrading it from the single gas configuration to the binary mixtures one). The sniffing mode was used in a more regular basis since in one hand is accurate enough to check the tightness of some connections and in another hand is more practical (less time consuming) comparing to the other method. Whichever technique is used, it was considered that a leaky connection exists when the measured He flow rate is at least between two and three times higher than the background signals.

The tightness of the connections of the system can also be investigated by pressure tests. In fact, if the pressure of a certain section of the system is steadily increasing, it means that there are leaky connections within that section.

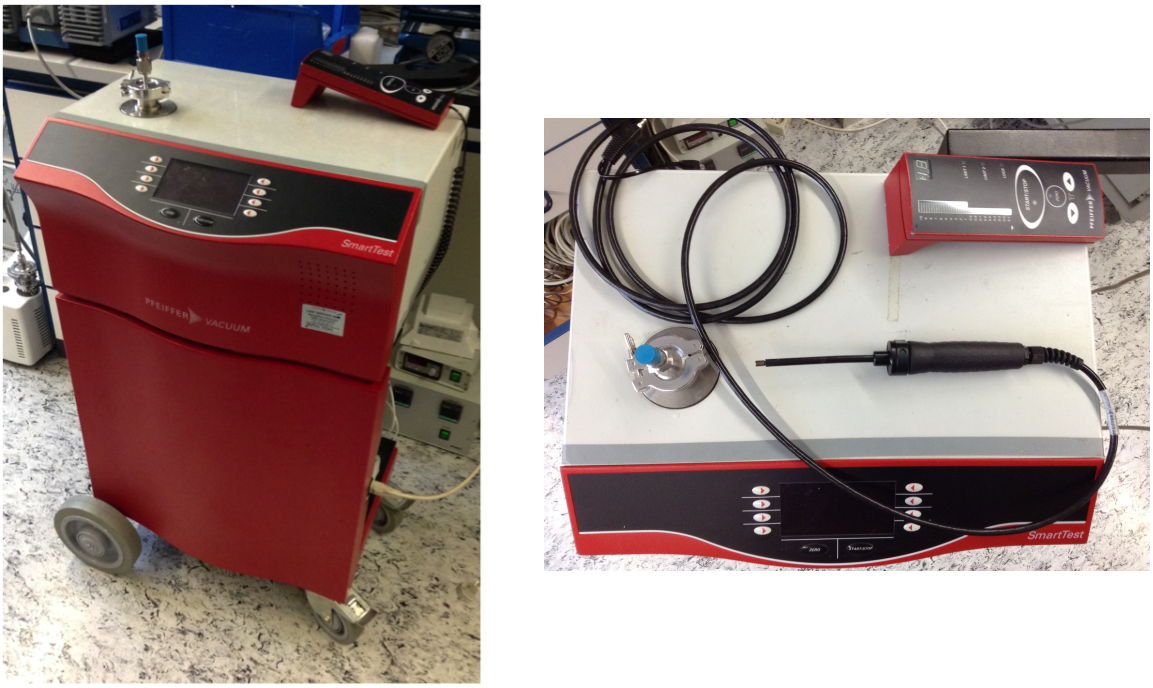

Figure 3.9: (Left) Helium leak detector, Pfeiffer Smart Test HLT 570. (Right) Probe for operation in the sniffing mode.

3.2.2 Calibration of the measuring devices

3.2.2.1 Mass Flow Controllers

It is important to note that the mass flow controllers are calibrated at the manufacturers for a specific gas. If the flow of a gas j has to be measured with a MFC calibrated for a gas i, gas corrections provided by the manufacturer have to be used to find the true values. However, experimental calibrations were performed to find the actual relationship between those quantities and the resulting calibration equations were used instead. These calibrations were performed by imposing distinct flows of gas j with a MFC calibrated for that gas, and measuring it with another MFC calibrated for other gas i, using the by-pass line. Furthermore, the MFC operation units were regularly zeroed, to cancel eventual electonic drifts. In Appendix A, the results of the calibration of the 10^3 MFC (calibrated for helium) for hydrogen and nitrogen, useful for the

single gas experiments, are presented.

3.2.2.2 Pressure Transducers

The pressure transducers had also to be periodically calibrated by first pumping down the unit and adjusting the zero of the transducer and then adjusting the span setting to a given calibration standard (for example, the atmospheric pressure of the ventilation). The pressure values are quantified by using the data acquisiton unit.

3.2.2.3 Quadrupole Mass Spectrometer

The QMS in this work was calibrated only for the H_2/He mixture. Using the by-pass connection pumped down[3] to 300 hPa, the QMS can be calibrated for a H_2/He concentration range of interest. For proper operation of this device, a certain vacuum pressure below 10^{-2} Pa inside its chamber must be kept. By using the QMS associated software Quadera (see Appendix B), the electrical current signals respective of each gas can be measured. Therefore, the steady-state ratio between the electrical signals of H_2 and He is proportional to the concentration of H_2 in the H_2/He stream. Plotting the H_2/He signal ratio as a function of the hydrogen concentration, a calibration curve is obtained.

The range of calibration of the QMS was conveniently established from 0.050% to 15%, with a constant QMS pressure of 4.0×10^{-5} Pa. However, for more accurate measurements at low concentrations (0.050% up to 0.50%) the QMS pressure was increased by one order of magnitude. The reason for this is the sensibility of the mass spectrometer: the lowest attained pressure was 6.3×10^{-6} Pa (without any gas entering into the system), and thus the electrical current values for 4.0×10^{-5} Pa at low concentrations are close to the background levels. The QMS background electrical current signals for both He and H_2 for the three pressures in the chamber are presented in the table 3.1. These values shall be compared for instance with the ones obtained at 0.10% H_2/He, where the H_2 flow is 0.63 ml/min: 5.14×10^{-12} A for 4.0×10^{-5} Pa and 2.30×10^{-11} A for 4.0×10^{-4} Pa. A total flow[4] of 2500 ml/min was used for the range 1.0% – 15%, while a total flow of 1250 ml/min was used for 0.050% – 0.50%, whose plot is in figure 3.10. Some points of the calibrations were checked periodically in order to detect some possible deviations.

$\mathbf{p}_{\mathbf{QMS}}$ [Pa]	6.3×10^{-6}	4.0×10^{-5}	4.0×10^{-4}
He	$< 10^{-14}$	$< 10^{-14}$	2.6×10^{-13}
H_2	2.73×10^{-12}	3.27×10^{-12}	5.35×10^{-12}

Table 3.1: QMS background electrical current signals (in A) for He and H_2 for three different pressures of interest inside the QMS chamber.

The a and b parameters of the QMS calibration equation $y = ax + b$, where y is the signal

[3]Note that the by-pass connection links the permeate side to the feed side, and as a consequence the pressure inside the pipes is the one imposed by the pressure controller associated to the vacuum pump.

[4]Since the same flow is being imposed into the QMS (60 ml/min), the ratio of the signals (and thus the calibration) is independent of the total feed flow.

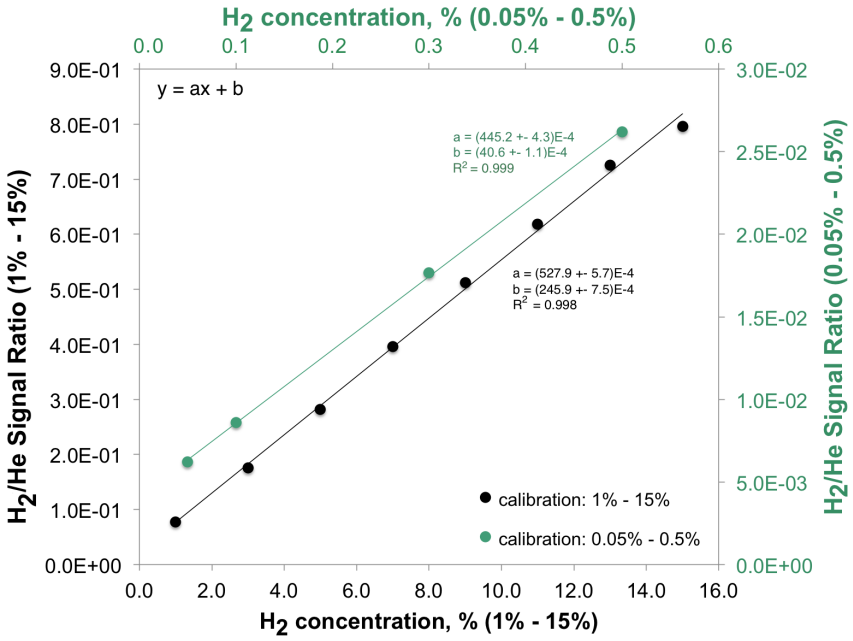

Figure 3.10: Calibration of the QMS for 0.050% - 15% H_2/He concentrations. In black, the 1.0% - 15% concentration range and in green the 0.050% - 0.50% range are presented. The coefficients of determination R^2 indicate how well the data fits the linear regression.

ratio and x the concentration in percentage, are presented in table 3.2, and these values were used to calculate the hydrogen concentrations in the helium stream.

Range, %	a $\times 10^{-4}$	b $\times 10^{-4}$
0.05 - 0.50	445.2 $\pm$ 4.3	40.6 $\pm$ 1.1
1 - 15	527.9 $\pm$ 5.7	249.5 $\pm$ 7.5

Table 3.2: $y = ax + b$ QMS calibration a and b parameters, where y is the signal ratio and x the concentration in percentage.

3.2.3 Integration of the membranes into the system and heating of the module

The membrane to be tested is carefully placed inside the specifically designed stainless tubular module (presented in figure 3.6). Two rubber sealings between the membrane's ends and the module are used to ensure tightness (figure 3.11). The module is then accomodated inside the experimental setup.

The heating of the module was firstly accomplished by the heating jacket that guarantees uniform heating. The way of heating the module had to be however changed along the work because the electrical connections associated with the heating jacket failed. Flexible heating cables have been wrapped around the module (figure 3.12), and the previous jacket was further used to provide thermal insulation. The temperature of the module is measured by using the thermocouple onto its surface, whose values are registered using the data acquisiton unit.

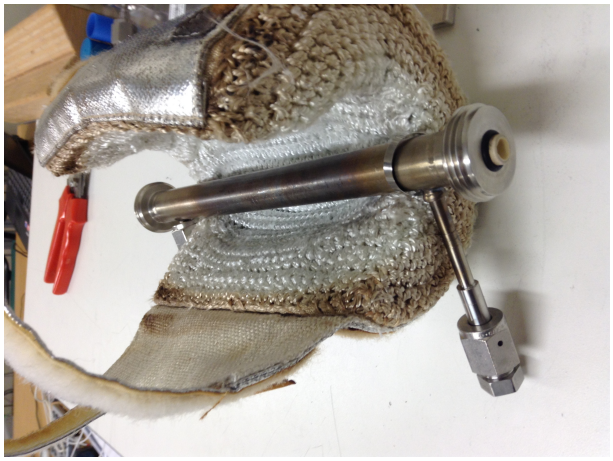

Figure 3.11: Membrane inside the module with the rubber sealings ensuring tightness.

Figure 3.12: New heating system used for the membrane module.

4

Membranes to be Tested at ZIMT III and Experimental Procedures

4.1 Zeolite and carbon membranes for experiments at ZIMT III

The MFI-HF membrane produced by IRCELYON was the first tested under single, binary and ternary mixtures in ZIMT. The need for study other membranes of interest for tritium processing led to the search of other manufacturers, and contact was established with IKTS (Institut für Keramische Technologien und Systeme) in Germany.

Newly developed tubular (length = 250 mm, inner/outer diameter = 7/10 mm, comprising a total surface area of $\sim 5.5\times10^{-3}$ m^2) microporous zeolite and carbon membranes have been purchased from IKTS (see figure 4.1). While the carbon membrane has a graphitic crystalline structure, the zeolite membranes are made of three different frameworks: MFI-ZSM5, NaA and SOD. The sodalite IKTS membrane has a H-SOD framework although doped with sulfur (S-SOD), added in the synthesis process to increase its hydrothermal stability. Although the H-SOD membranes might not be stable for temperatures higher than 150 °C, the S-SOD membranes can be used up to at least 300 °C [GRV13]. In total, two membranes of each type were available for experiments[1]. All the membranes are synthesized on the inner side of ceramic (alumina or titania) tubes to ensure mechanical integrity. The structural characteristics of the four membranes are presented in table 4.1. Some of the parameters can be found in papers published by the manufacturers and other ones were provided by the manufacturers themselves.

[1]The membranes can easily get broken by handling it, and then it was preferred to have two of each type. In addition, another aspect is to check quality/reproducibility of the membranes comparing the results from two different samples.

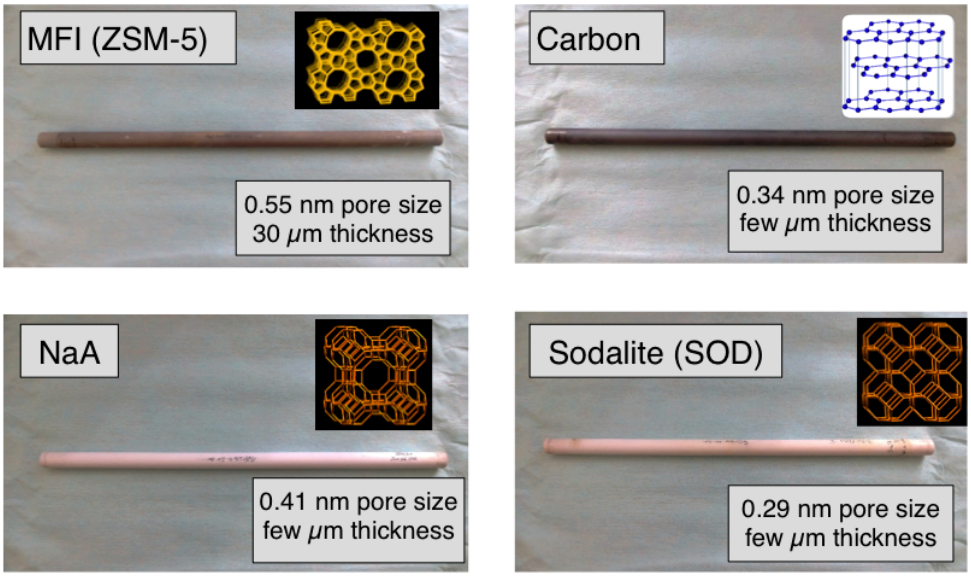

Figure 4.1: Zeolite and carbon membranes from IKTS to be tested at ZIMT III.

Active layer material	t_m [μm]	d_p [nm]	**Support**	**References**
MFI (ZSM-5)	30 - 60	0.55	TiO_2	[RVFP03, RVV$^+$10]
NaA	< 10	0.41	Al_2O_3	[RVK06]
S-SOD	< 10	0.29	TiO_2	[GRV13]
Carbon	< 1	0.34	TiO_2	[WBK$^+$12]

Table 4.1: Structural characteristics of the zeolite and carbon membranes manufactured by IKTS to be tested in ZIMT III.

4.2 Steady-state measurements

The measurements of flows, pressure differences, QMS electrical current ratios, RH/AH values, etc., are considered in steady-state when they are constant (within an acceptable error margin) during an empirical time interval corresponding to the reality of the involved processes, for which transients no longer exist. Since different processes and quantities are measured in each configuration, the steady-state values are reached in different times.

4.3 Procedure for Single Gas Experiments

The single gas experiments allow estimating, using a simple setup (figure 3.2) and an easy procedure, important parameters such permeances and ideal selectivities, at different pressure differences and temperatures. Furthermore, with these simple experiments the quality of a membrane can also be inferred.

In the single gas experiments the gas flows of helium, hydrogen and nitrogen were imposed such that pressure differences of 500, 1000 and 1500 hPa across the membrane were obtained with the permeate side connected to the ventilation. For each pair of flow and pressure difference, several measurements were done until steady-state (i.e., stable pressure in feed) was reached (around 20 min for the MFI-ZSM5 membrane). Using the permeate flows and pres-

sure differences, the permeances of each gas are calculated using the equation 2.3. Dividing the permeances of two different gases the ideal selectivity is then determined, according to the equation 2.4. Using the heating jacket, the experiments were performed in a temperature range from RT up to 130 °C, which allows a study of the variation of the flows, permeances and ideal selectivities with the temperature.

Since the 10^3 ml/min MFC calibrated for He was used to impose the flow of the three gases, previous calibrations for hydrogen and nitrogen were done. The calibration curves were fitted with $y = ax$, where y represents the imposed flow and x is the flow measured by the helium MFC. The a parameters obtained for each gas are presented in table 4.2 (see Appendix A).

	$a \times 10^{-3}$
H_2	674.6 ± 3.2
N_2	663.8 ± 3.8

Table 4.2: a parameters obtained in the calibration of the 10^3 He MFC for the single gas experiments using a linear regression with the equation $y = ax$.

A summary of the experimental conditions concerning the single gas experiments is presented in table 4.3.

F_F [ml/min]	p_F [hPa]	p_P [hPa]	T [°C]
Maximum for H_2: 700 at RT on MFI-ZSM5	1500 – 2500	1000	RT - 130

Table 4.3: Summary of the experimental conditions used for the single gas experiments. For simplicity, only the nominal values are presented.

4.4 Procedure for Binary Mixtures Gas Experiments

Binary mixtures gas experiments are accomplished by mixing dynamically two different gases into the membrane module, with the retentate side opened. In this configuration, the influence of species i on the permeation of species j (and vice-versa) can be determined (e.g., permeance and separation factor). The partial pressures of each component (i.e., concentration) upstream the membrane might have an influence on the permeation of both species. In addition, the fraction of the feed flow that is recoverd in the permeate (i.e., the cut, ν) also affects the separation performance of the membrane. Indeed, if the flow on the permeate is zero ($\nu = 0$) or if it is equal to the feed flow ($\nu = 1$) no separation exists, and as a consequence the separation factor will have a maximum between these two limiting cases. In general, the higher is the cut, the lower is the driving force for the fastest permeating species, and thus the molar fraction of that species and the separation factor both decrease. In contrast, at low cut, since the partial pressure in the permeate side is low, the driving force is high as well as the selectivity [NS95].

At ZIMT III, the hydrogen/helium and vapour/helium binary mixtures experiments were performed on different membranes, using the apparatus presented in figures 3.4 and 3.1, respec-

tively. The details of each experiment are described in 4.4.1 and 4.4.2.

4.4.1 H_2/He

The H_2/He binary experiments were performed for 0.10%, 1.0%, 10% H_2/He concentrations with a total feed flow of 1250 ml/min and with a constant permeate pressure of 300 hPa at RT. Using the MFC on the retentate side (MFC5 in figure 3.4), the influence of the cut between 0.1 and 0.7 on the separation performance of the membrane was also studied.

The permeate and retentate process streams are separately analysed with the QMS until a H_2/He steady-state signal ratio is reached. This steady-state was observed to be reached between 15 and 30 min. Using the data from table 3.2, the concentration of hydrogen in both permeate and retentate lines is then determined. These concentrations are used to determine the separation factor given by equation 2.5. The measurements of the feed pressure and permeation flow allow the determination of the permeances of the gases. This calculation is achieved by taking into account the partial permeation flow and partial pressure difference of each species: $\Pi_i = F_i y_i/[(p_F x_i - p_P y_i)A]$.

In addition to the periodic measurements of the pressure in feed and permeate flow (as performed to the single gas experiments), the retentate flow and the electrical current values given by QMS respective to each gas have also to be controlled and measured. Therefore, the procedure of these binary experiments is more complex than in the single mode and involves the control and measurement of more parameters.

The H_2/He binary mixtures experiments were mostly performed on the MFI-ZSM5 since it was the one providing the most reliable results for single gas experiments. Few experiments were also performed with the S-SOD membrane.

In table 4.4, a summary of the experimental conditions for the tests on the MFI-ZSM5 and SOD membranes is presented. The total flow in feed is the sum of the flows of both hydrogen and helium.

	F_F [ml/min]	p_F [hPa]	p_P [hPa]	T [°C]	H_2/He %
MFI-ZSM5	1250	1000 – 4000	300	RT	0.10 - 10
S-SOD	1250	1000	300	RT	1.0

Table 4.4: Summary of the experimental conditions used for the H_2/He binary mixtures gas experiments. The experiments were mostly performed on MFI-ZSM5 and few experiments were performed on the S-SOD membrane. For simplicity, only the nominal values are presented.

4.4.2 H_2O/He

4.4.2.1 By-pass measurements

Prior to the experiments on the membranes using wet streams, by-pass measurements at 300 hPa were performed to ensure that a given moisture concentration can be maintained constant. The temperature of the heated pipes was measured to be in all sections above 100 °C after about

one hour[2]. The temperature of the vaporizer was set up to 195 °C. Under these conditions, a proper handling of humid gases all over the experiments is possible.

The liquid water flow was kept constant with 3.5 ± 0.2 g/h (∼ 73 ml/min). This value was found to be convenient concerning the concentrations to achieve and also the adsorption capacity of the MSB's. Preliminary by-pass measurements to determine the actual moisture content in the H_2O/He streams measuring the flow of water vapour were performed. The flow of water vapour was measured by weighing the MSB's before and after a period of adsorption. This method turned out however not to be reliable to obtain the water flows neither to determine the actual moisture content. An alternative method to do it in view of a future upgrade of the ZIMT facility could be the integration of cold traps at LN_2 temperature. This is a technique widely used for drying streams with condensable species with boiling points higher than −196 °C and accurate measurements of the flow of that species can be obtained [WL12, AMSZ12, Hir02].

The most reliable method of determining the actual concentration of water vapour with the configuration presented in figure 3.1 consists of using the humidity values given by the sensors. The water concentration in a stream can be determined using for example the volume mixing ratio, defined by the ratio of number of moles of water vapour to the number of moles of the gaseous mixture. Equivalently, the volume mixing ratio is given by [Cor]

$$c_{H_2O}(\%) = \frac{RT}{p_T}\frac{\mathrm{AH}}{M_{H_2O}} \times 100 \tag{4.1}$$

where R is the ideal gas constant in m^3 Pa K^{-1} mol^{-1}, T is the temperature in K, p_T the absolute pressure in Pa, AH the absolute humidity in g/m^3 and M_{H_2O} the molar mass of water in g/mol.

Mixing the water vapour with different helium flows, reliable and reproducible by-pass measurements of the concentration of water vapour were obtained. From these results, two different concentrations of water vapour were used for experiments: (5.57 ± 0.36)% for 650 ml/min He flow and (1.09 ± 0.10)% for 1150 ml/min (table 4.5). To simplify the notation, these concentrations are referred as 6% and 1% along the text.

F_{He} [ml/min]	c_{H_2O} %
650 ± 32	5.57 ± 0.36
1150 ± 36	1.09 ± 0.10

Table 4.5: Water vapour concentrations used for the experiments.

Systematically, before injecting the H_2O/He mixture into the MM, by-pass measurements were performed until the concentration of vapour in H_2O/He is observed to be constant. These steady-state values were reached after at least one hour.

[2]The temperature provided by the humidity sensor before the MSB's was used as an indicator to determine when the temperature of the pipes reached its maximum.

4.4.2.2 Membranes measurements

By mixing water vapour with helium, binary gas/vapour experiments were performed on the MFI-ZMS5, S-SOD and NaA membranes. Similarly to the binary dry experiments, the permeate pressure was maintained constant at 300 hPa. In these experiments with wet streams, the cut is a parameter difficult to control for two reasons: (1) the MFC on the retentate side[3] (MFC5 in figure 3.1) is not conceived to handle wet streams and thus non-feasible flow measurements are obtained[4] and (2) the permeation process of vapour across the membrane itself influences the cut.

The H_2O/He concentration (equation 4.1) is determined using the AH and T values measured by the HS1 and also the absolute pressure on the permeate side (given by PR2). The experiments are performed analysing separately the permeate and retentate lines until steady-state H_2O/He concentrations are measured. The steady-state measurements were achieved on average after one hour. Using the concentrations of vapour and helium on both feed (that are considered to be either 6% or 1%) and permeate sides in equation 2.5, the separation factor is determined. The membranes are weighed before and after the experiments to investigate possible increase in weight due to water adsorption in the zeolitic framework.

Comparatively to the single and H_2/He gas experiments, the experimental procedure concerning the wet experiments is more complex, delicate and more time consuming. In fact, by-pass measurements are firstly performed until a constant c_{H_2O} is reached. In the membrane experiments, the permeate and feed pressures, the flow in permeate and the AH and T values given by HS1 have to be periodically measured. Furthermore, the RH/AH values of HS2 must also be tracked to know when a MSB is saturated. In addition, before each experiment the MSB's are weighed to determine how close they are from the saturation capacity (the used MSB's have an adsorption capacity of around 20 g).

The first experiments were performed at 6% H_2O/He on the MFI-ZSM5 membrane at RT and also at 100 °C. The influence of temperature and moisture content on the H_2O/He separation factor of the MFI-ZSM5 membrane was studied by performing experiments at 100 and 70 °C and at 6% and 1% of vapour concentrations. Furthermore, systematic experiments for all the three membranes were done to determine the evolution of the H_2O/He separation factor with the decrease of temperature, starting at around 100 °C.

In table 4.6, a summary of the experimental conditions concerning the moisture binary experiments for the three membranes is presented. The feed flow F_F is the flow of helium.

4.5 Procedure for Ternary Mixture Gas Experiments

4.5.1 H_2O/H_2/He

A single set of 1%/1% H_2O/H_2/He measurements on MFI-ZSM5 was obtained. This H_2O/H_2/He experiment consisted on adding 1% H_2 to a 1% H_2O/He binary mixture permeating through

[3] Actually, all the MFC's used in this facility are not suitable for water vapour.

[4] An improvement to consider for future upgrades is the introduction of a MSB between the module and the MFC on the retentate.

	F_F [ml/min]	p_F [hPa]	p_P [hPa]	T [°C]	c_{H_2O} %
MFI-ZSM5	650	1000 – 4500	300	77 and 100	6
MFI-ZSM5, NaA, SOD	1150	1000 – 4500	300	RT – 100	1

Table 4.6: Summary of the experimental conditions used for the H_2O/He binary mixtures gas experiments. The 6% experiments were only performed on the MFI-ZSM5 membrane. The feed flow F_F is the flow of helium. For simplicity, only the nominal values are presented.

the MFI-ZSM5 at around 32 °C. The experimental procedure is similar to the one presented in 4.4.2.2, however additional measurements of the QMS electrical signals of both helium and hydrogen have also to be done. Therefore, H_2O/He and H_2/He separation factors can be determined.

After this experiment, the MFI-ZSM5 was removed out from the module to weigh it. When re-integrating it into the system, the membrane was accidentally broken (figure 4.2), and no more experiments were performed on it. Moreover, no ternary experiments were performed on the other membranes.

Figure 4.2: MFI-ZSM5 accidentally broken after removal from the module.

5

Results and Discussion

5.1 Uncertainties of the experimental results

The explicit and generic calculation of the uncertainties of the several measured and calculated quantities presented in the next sections is provided in Appendix C.

5.2 Single Gas Experiments

5.2.1 MFI-ZSM5

The He, H_2 and N_2 permeation flows are plotted as a function of the pressure difference[1] at RT and at 130 °C in figure 5.1. Since flows higher than 1000 ml/min for H_2 were obtained for 1500 hPa of pressure difference, the maximum Δp_{H_2} measured was 1240 hPa.

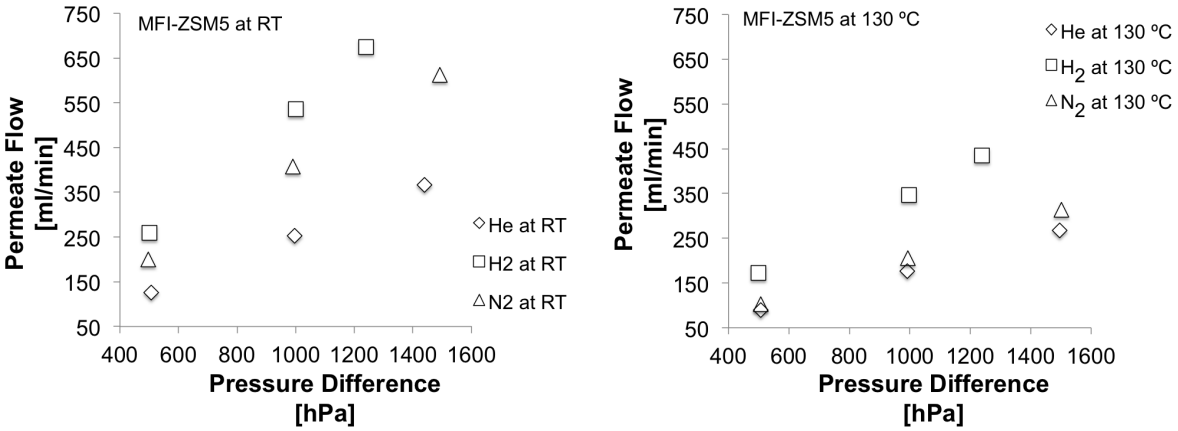

Figure 5.1: Permeation flow as a function of the pressure difference for He (rhombus), H_2 (squares) and N_2 (triangles) in MFI-ZSM5 at RT (left) and at 130 °C (right).

[1]The data concerning these experiments for all five temperatures are presented in the table D.1 in Appendix D.

As observed, a linear dependency ($R^2 > 0.99$) between both quantities exists, regardless of the gas and temperature. This means that the ratio between the flow and pressure difference is constant, and thus the permeance is constant for each temperature. Hydrogen is the most permeable gas reaching a maximum of permeation flow of 674 ml/min at RT, while helium with 366 ml/min at RT is the less one. These observations can be explained based on the adsorption properties and kinetic diameters of the involved species, in comparison with the pore sizes of the MFI. In contrast to hydrogen and nitrogen, the enthalpy and entropy of adsorption for helium is zero [BVDBKM97]. Although nitrogen is more adsorbable than hydrogen[2], the latter has lower kinetic diameter[3] and therefore is the most permeable. This is in agreement with the published data where the permeance of H_2 is increasingly higher than that of N_2 for temperatures above RT [BVDBKM97].

The permeance as a function of the temperature for the three gases is presented in figure 5.2 (see table D.2 in Appendix D for details of the plotted data). The obtained uncertainties are below 9%. Comparing this plot with the generic variation of the permeance as a function of the temperature for zeolites presented in figure 2.9 (section 2.4.3), it can be concluded that adsorption dominates the transport in the MFI-ZSM5 membrane between RT and 130 °C.

Hydrogen exhibits the highest permeance with $(7.22 \pm 0.27) \times 10^{-7}$ mol m^{-2} s^{-1} Pa^{-1} at RT while the permeance obtained for helium is $(3.41 \pm 0.10) \times 10^{-7}$ mol m^{-2} s^{-1} Pa^{-1} at the same temperature.

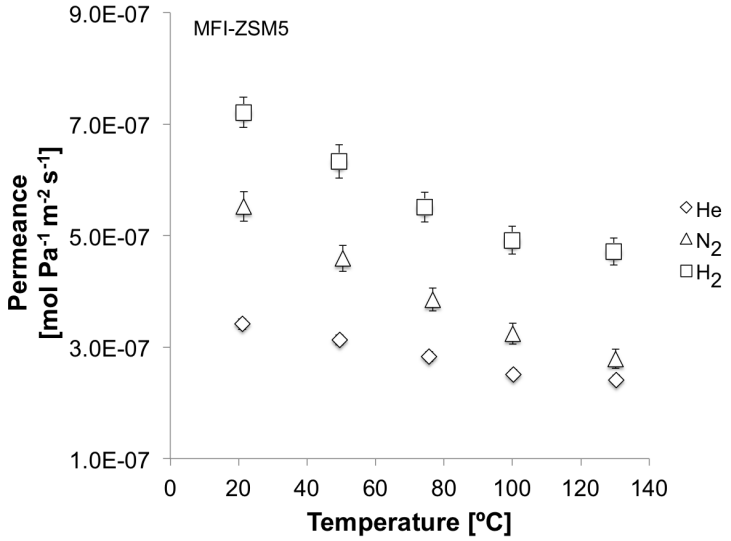

Figure 5.2: Pemeance as a function of the MFI-ZSM5 temperature for He (rhombus), N_2 (triangles) and H_2 (squares) in MFI-ZSM5.

It is instructive to analyse the figure 5.3, where the experimental H_2 permeance as a function of the temperature is compared with a numerical fit using the equation[4] 2.9, where the porosity ϵ and thickness of the active layer t_m are given as fit parameters (all the other coefficients are given in Appendix E). These structural parameters are not exactly known for the titania-

[2]The enthalpy of adsorption is $-\Delta H = 5.9$ kJ mol^{-1} for H_2 and $-\Delta H = 13.8$ kJ mol^{-1} for N_2 [BVDBKM97].
[3]The kinetic diameter of nitrogen is 0.364 nm.
[4]Since the equation 2.9 gives the flux, this expression shall be divided by the pressure difference across the membrane to calculate the permeance.

supported MFI-ZSM5 used in the experiments, and a value of 0.13 for the porosity (used for an allumina-supported MFI [PTAN$^+$09]) and a thickness of $t_m = 30$ μm (see table 4.1) were used.

The dashed line represents the adsorption contribution of equation 2.9 ($J_{i,s}$) and in the dashed-point line the total flux $J_{i,s} + J_{i,\mathrm{GT}}$ is used. As can be observed, the expected permeance for H_2 is one order of magnitude lower than the one experimentally obtained. On one hand this shows that the used MFI-ZSM5 has not a defect-free structure, while on the other hand these differences also suggest that the thickness used for fitting is higher than the real one. In fact, a better fitting with the adsorption curve is obtained for membrane thicknesses below 10 μm, even if the porosity is raised up to 0.5. This simple analysis evidences the difficulty to predict performances of a given membrane, if its exact structure is not well known. In addition, it should be noted that the shape of the experimental permeance curve suggests that the hydrogen transport through the MFI-ZSM5 is mainly due to surface diffusion.

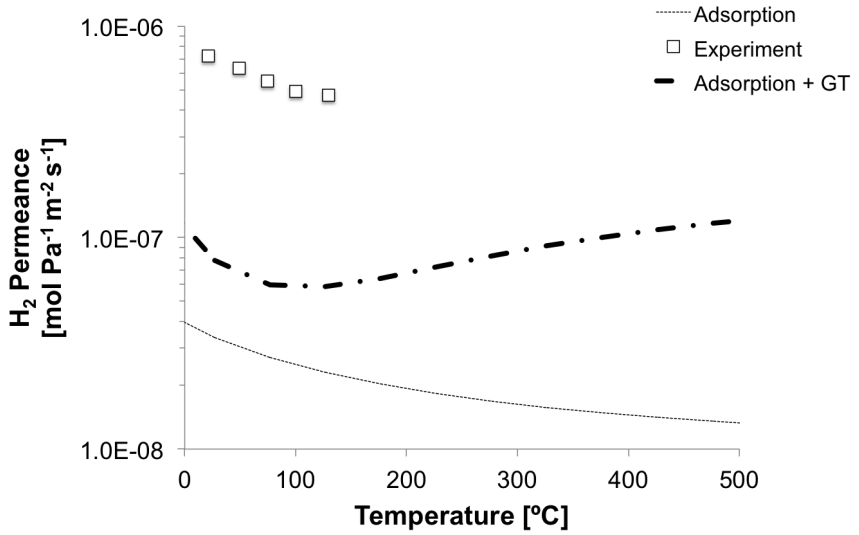

Figure 5.3: Comparison of the H_2 permeances as a function of the MFI-ZSM5 temperature with a numerical fit using the equation 2.9. The dashed line is obtained considering only the adsorption term $J_{i,s}$, while the dashed-point line considers both surface and GT contributions. The fit was obtained for $\epsilon = 0.13$ and $t_m = 30$ μm.

In figure 5.4, the He and H_2 permeances as a function of the temperature obtained for the hollow fiber (ZIMT I and II) and for the MFI-ZSM5 are compared. Due to the lower thickness of the HF membrane, higher permeances were measured. In addition to the adsorption regime between $50 - 400$ °C ($100 - 400$ °C) for hydrogen (helium), the increasing in permeance due to the contribution of thermal diffusion is also observed.

The H_2/He, N_2/He and H_2/N_2 permselectivities as a function of the temperature for the MFI-ZSM5 are plotted in figure 5.5 (in table D.3 of Appendix D the values of the plotted data are presented). The ideal selectivity is higher for the combination hydrogen/helium and is almost independent of the temperature, with an average value of 1.99 ± 0.11. The highest ideal selectivity obtained for H_2/N_2 is 1.69 ± 0.14 while the highest for N_2/He is 1.62 ± 0.10.

The Knudsen selectivites for these three combinations are $\alpha^{K_n}_{\mathrm{H_2/He}} = 1.41$, $\alpha^{K_n}_{\mathrm{H_2/N_2}} = 3.74$ and $\alpha^{K_n}_{\mathrm{N_2/He}} = 0.38$. A higher permselectivity is obtained for H_2/He, which implies that adsorption plays a role to increase the efficiency of separation. The fact that a lower ideal selectivity than

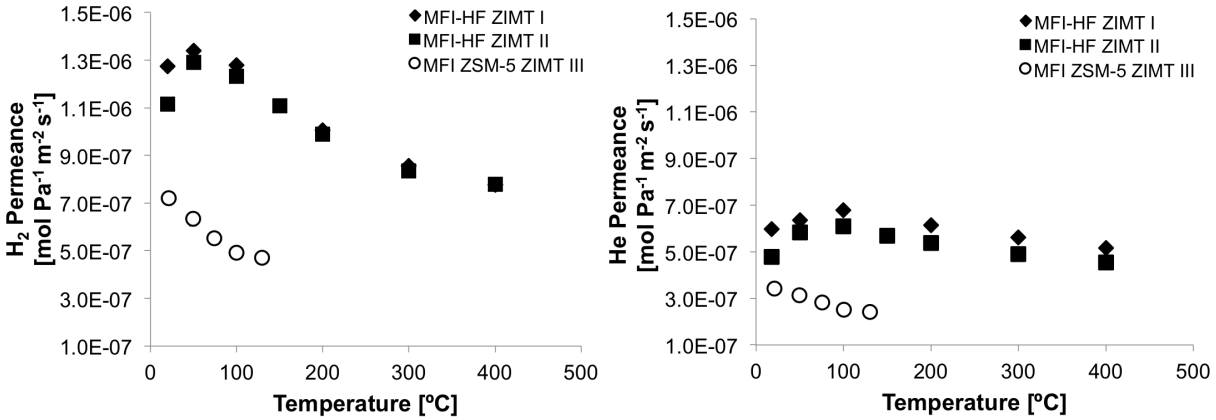

Figure 5.4: Comparison of the permeance as function of the membrane temperature for hydrogen (left) and helium (right) obtained with ZIMT I (black filled rhombus), II (black filled squares) and III (empty circles).

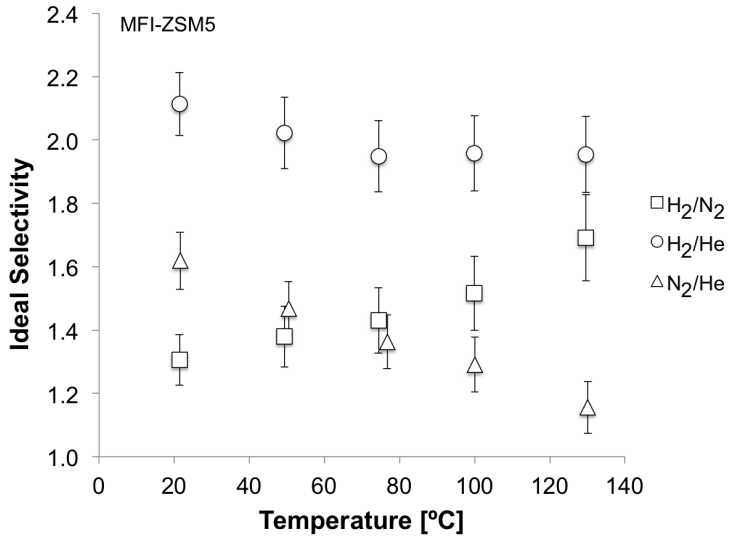

Figure 5.5: H_2/N_2 (squares), H_2/He (circles) and N_2/He (triangles) ideal selectivity as function of the MFI-ZSM5 temperature.

$\alpha^{K_n}_{H_2/N_2}$ is obtained might be related with the existence of defects within the membrane (and thus Poiseuille flow is a non-neglecting transporting mechanism). The Knudsen diffusion mechanism is based on the differences on kinetic mobilities of species of different molecular masses and since N_2 is heavier than He, a ideal Knudsen selectivity towards the latter is expected (i.e., $\alpha^{K_n}_{N_2/He} < 1$). Since however higher values of N_2/He permselectivity higher than unity are observed, it means that preferential adsorption of nitrogen on the membrane surface exists, supporting what is discussed above.

The comparison of the H_2/He ideal selectivity as a function of temperature between the ZIMT I, II and III is presented in figure 5.6. For the MFI membranes, both perm-selectivity values and temperature dependence are consistent. At RT, 2.11 ± 0.10 was obtained for the tubular membrane, while 2.14 and 2.33 were obtained with ZIMT I and II, respectively. The MFI-ZSM5 membrane shows the same separation performance as the MFI-HF. It can be thus concluded that the results obtained here are characteristic of the MFI material itself.

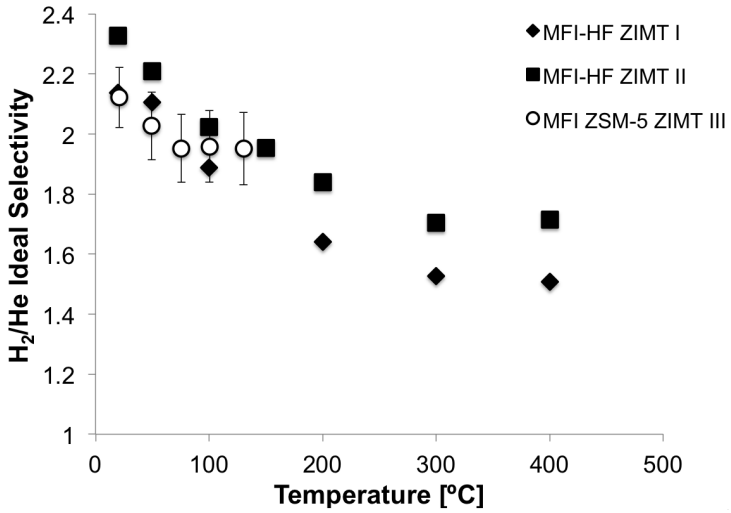

Figure 5.6: H_2/He ideal selectivity as function of the membrane temperature obtained with ZIMT I (black filled rhombus), II (black filled squares) and III (empty circles).

5.2.2 S-SOD

The helium and hydrogen permeate flow as a function of the pressure obtained for the S-SOD membrane at RT is plotted in figure 5.7. Similarly to the MFI-ZSM5, the linear regression fits apparently well the data. However, the plot of the permeance of both gases in the same figure evidences that the permeance is not independent of the pressure difference. Of major importance, the obtained permeances ($\sim 10^{-6}$ mol m^{-2} s^{-1} Pa^{-1}) are three orders of magnitude higher than the reported by the membrane's manufacturers for the same gases ($\sim 10^{-9}$ mol m^{-2} s^{-1} Pa^{-1}) [GRV13]. All the possible sources of experimental errors that could explain such results were excluded (e.g., not tightness of the module). Therefore, it could be concluded that the high permeances strongly suggest the presence of defects[5], which make the membrane not suitable to perform experiments.

5.2.3 NaA

The obtained He permeate flow as a function of the time is plotted in figure 5.8, where a 1150 ml/min feed feed is imposed. After about one hour the flow increased suddenly and dramatically from 4 ml/min up to 28 ml/min. This flow increased continuously up to a value equal to the feed flow, giving a permeance of 2.5×10^{-6} mol m^{-2} s^{-1} Pa^{-1}. These results suggest that condensed water phase exists in the high hydrophilic zeolite framework, but is gradually released from the pores due to the permeation of the gas.

The membrane was also tested for two different flows of H_2 at RT. First, a feed stream of 400 ml/min was imposed. After 30 min, the flow was decreased to half of it and after the same period of time, the initial flow was injected again into the membrane. The permeate flow as a

[5]The quality of the H-SOD type membranes is usually verified by the very low permeance values of light gases. Indeed, He permeances of $\sim 10^{-11}$ mol m^{-2} s^{-1} Pa^{-1} and no N_2 detected permeance was already observed [Kha10]. After feedback from the IKTS manufacturers, it was informed that all the S-SOD IKTS produced membranes are considerably defective and these results are also obtained by them. In fact, permeation of molecules as large as SF_6 (kinetic diameter of 0.49 nm) was already observed. As a conclusion, these S-SOD membranes shall not be used for gas separation.

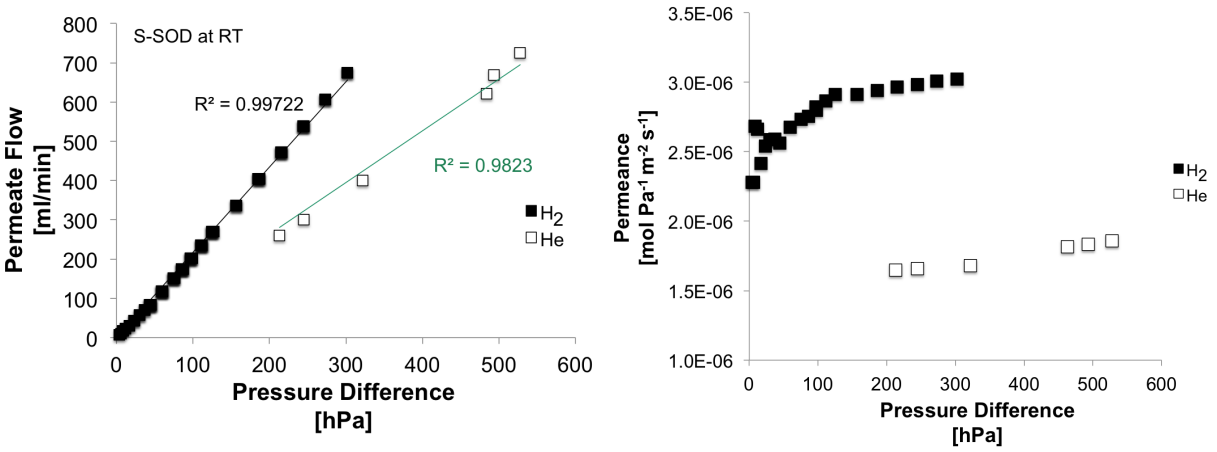

Figure 5.7: (Left)H_2 (black filled squares) and He (empty squares) permeation flow as a function of the pressure difference obtained for the S-SOD membrane at RT. The correlation coefficients R^2 are presented to quantify the degree of linearity between both quantities. (Right) Permeance as function of the pressure difference for hydrogen (black filled squares) and helium (empty squares) obtained for the S-SOD membrane at RT.

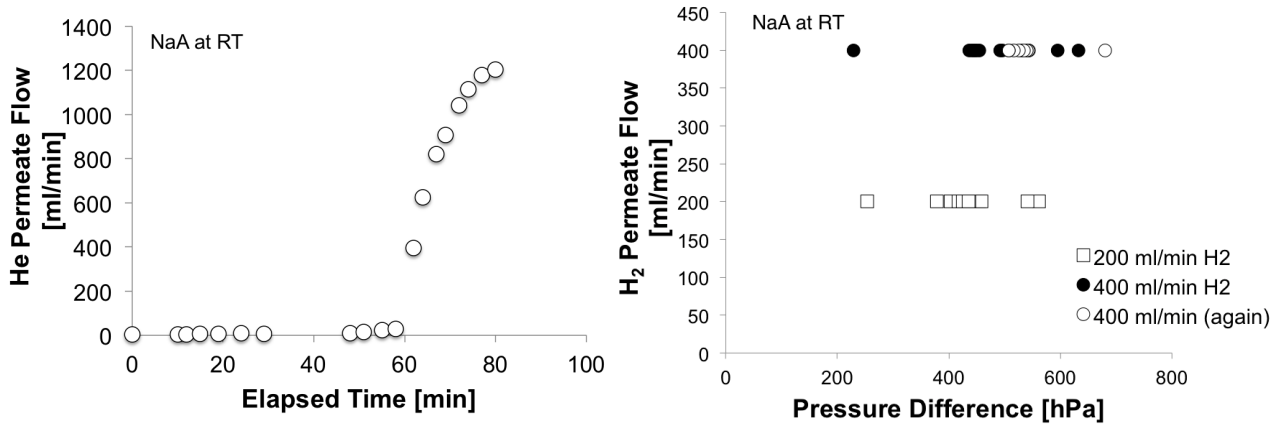

Figure 5.8: (Left) He permeation flow as function of the elapsed time obtained for the NaA membrane at RT for a feed flow of 1150 ml/min. (Right) H_2 permeate flow as a function of the pressure difference obtained for the NaA membrane at RT for two feed flows: 400 (circles) and 200 (squares) ml/min.

function of the obtained pressure difference is presented in the figure 5.8. During the three series of measurements, no constant pressure difference could be achieved, that might be justified by the continuous releasing of the condensed water molecules. Furthermore, the two different flow values lead almost to the same pressure difference across the membrane. Therefore, for the 400 ml/min flow a permeance of 1.1×10^{-6} mol m^{-2} s^{-1} Pa^{-1} and for half of it the permeance decreases down to 6.4×10^{-7} mol m^{-2} s^{-1} Pa^{-1}. No gas permeance values for these IKTS membranes are published. It was however found some results reporting that high quality NaA membranes exhibit 10^{-7} mol m^{-2} s^{-1} Pa^{-1} of hydrogen permeance [XBS+05]. Although this value was here obtained, further experiments should be performed to evaluate the membrane quality. These experiments shall be performed after complete regeneration of the membrane, to eliminate any influence of the release of the water.

Due to lack of time, this membrane was not fully studied for single gas experiments as the MFI-ZSM5. It should also be noted that this membrane has large pores which means that no

significant gas separation performance (for light gases) should be expected. However, separation of wet streams might be of relevant interest to study due to its superior hydrophilicity.

5.2.4 Carbon

For the carbon membrane, high H_2 and He flows ($\sim$ 800 ml/min) for pressure differences of $\sim$ 40 hPa were obtained, leading to a permeance of 10^{-5} mol m^{-2} s^{-1} Pa^{-1}. The expected permeance of He and H_2 should be at least one order of magnitude lower for these IKTS carbon membranes, and a N_2 single gas permeance of 1.4×10^{-7} mol m^{-2} s^{-1} Pa^{-1} is reported for this IKTS membrane [WBK$^+$12]. Such very low pressure differences across the membrane suggests defects, compromising the separation efficiency of the membrane. The obtained results can in principle be attributed to the internal structure of the carbon membrane, which might be defective[6]. Although carbon membranes are the ones produced with the highest quality in IKTS, the two carbon membranes for experiments at ZIMT evidenced to be not suitable for gas separation.

5.3 Binary Mixture Gas Experiments

5.3.1 MFI-ZSM5

5.3.1.1 H_2/He

The mesured and determined quantities (cut, concentrations, pressure differences and flows on the permeate and retentate sides) are presented in Appendix F. The quality of the measurements can primarily be inferred by calculating the mass balance, i.e., the sum of the flows in the permeate and retentate side must be equal to the total feed flow. In the figure 5.9 the mass balance determined for the three 0.10%, 1.0% and 10% H_2/He concentrations as function of the cut is presented; for reference the total 1250 ml/min feed flow is also presented[7]. From the graphic, it can be concluded that consistency concerning the mass balance exists.

In figure 5.10, the variation of the separation factor with the cut for the three hydrogen concentrations at RT is plotted. As expected, for all concentrations, $\alpha^*_{H_2/He}$ increases first with the increasing of ν, with a maximum of 1.68 $\pm$ 0.10 for 0.10% H_2/He at around 0.3, and then a continuous decrease is observed, reaching a value of 1.21 $\pm$ 0.10 for the same concentration at ν = 0.7. This higher performance for this cut is in agreement with a numerical study made in TLK [BDKL13]. The justification for the large error bars concerning the 1.0% concentration is related to the relatively high uncertainty (12.3%) by imposing a flow of 12.5 ml/min with the 500 ml/min MFC; for 0.10% (1.25 ml/min with the 10 ml/min MFC) and 10 % (125 ml/min with the 500 ml/min) concentrations, low relative errors of 2.6% and 1.6% are obtained. These uncertainties are considered for the determination of the experimental error of the feed concentration and thus influence the errors associated with the separation factor.

[6] In fact, discussing these results with the manufactures, it was argued that these permeance values are far higher (at least one order of magnitude) than the ones obtained in IKTS.

[7] The feed flow here presented is for the 10% case, as a result of the sum between 125 ml/min of H_2 and 1125 ml/min of He. This graphical comparison is however still valid since the obtained uncertainties are almost the same ($\sim$ 34 ml/min) for the three concentrations.

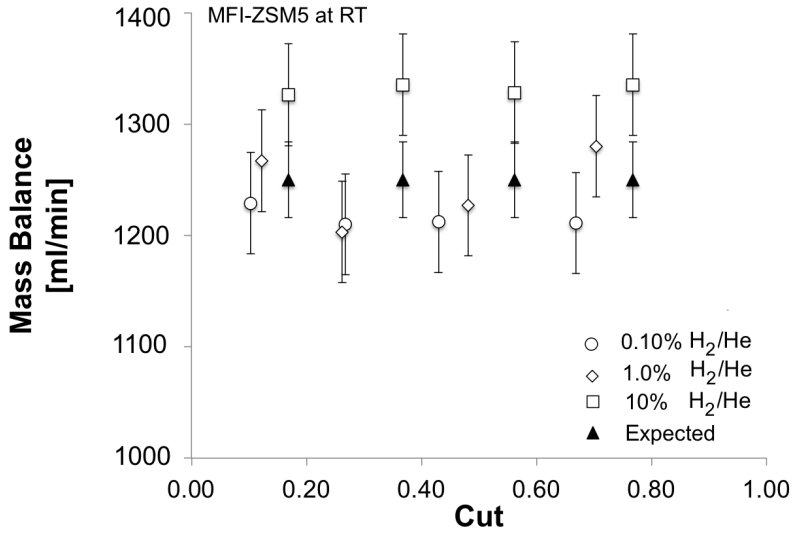

Figure 5.9: H_2/He mass balance as function of the cut for different H_2 concentrations in He. The empty symbols represent the mass balance computed from the sum of the flows on both permeate and retentate sides for the three hydrogen concentrations (circles for 0.10%, rhombus for 1.0% and squares for 10%) and the filled triangles show the mass balance obtained from the sum of the flows in feed.

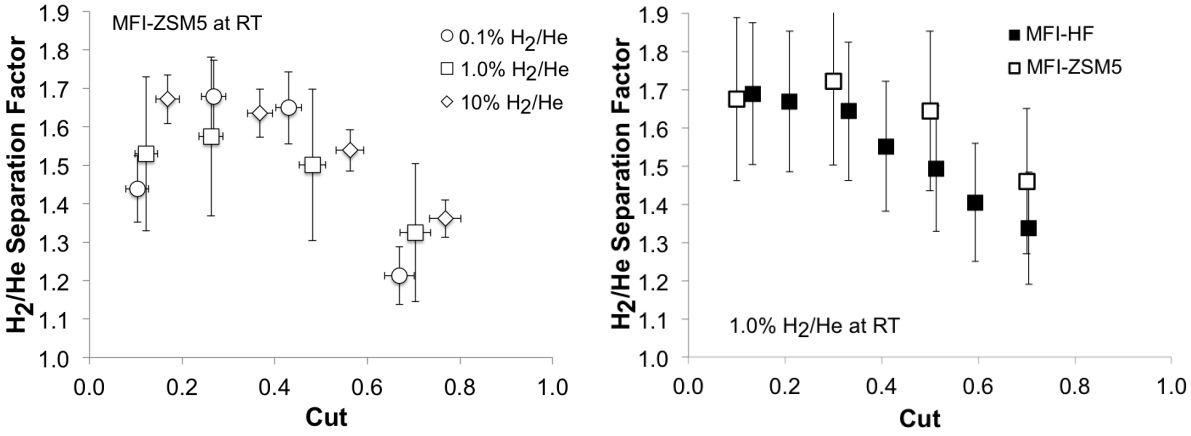

Figure 5.10: (Left) H_2/He separation factor as a function of the cut for 0.10%, 1.0% and 10% H_2/He concentrations. (Right) Comparison of the H_2/He separation factor as function of the cut for 1.0% H_2/He concentration obtained for the MFI-HF (black filled squares) and the MFI-ZSM5 (empty squares).

Only for $\nu \geq 0.7$ separation factors lower than the Knudsen one are found. On the other side, in the entire range of cut experimentally explored, all values are below the ideal selectivity. In addition, the H_2/He separation factor seems to be independent of the concentration. These results shall be compared to the ones obtained for ZIMT II, whose the same behaviour is observed for 1.0% H_2/He concentration (figure 5.10).

For completeness, it is interesting to compute the permeances from the binary experiments data as function of the cut (figure 5.11). While the helium permeance remains rather constant for all the four ν at a given concentration, the permeance of hydrogen slightly decreases with the increase of ν, although still the more permeable. This might be related to a mutual competition of the permeating species, but more probably due to a depletion of the most permeating species across the membrane. The fact that the He permeance values do not change with the cut is to

be expected, since the cut only changes the partial pressure difference across the membrane, and if the flow varies linearly with it, the permeance shall be independent of the cut. Instead of what is observed in the single gas experiments, the permeation flow of hydrogen shows a non-linear dependency with the partial pressure difference specially at the lowest concentration. For this concentration, to reach the 0.1 cut the permeate pressure had to be increased up to 700 hPa and a higher value of permeance at this conditions was obtained. As evidenced in the plots of the figures F.1 – F.3 presented in Appendix F, the linearity of the hydrogen flow as a function of the pressure difference is higher for higher concentrations.

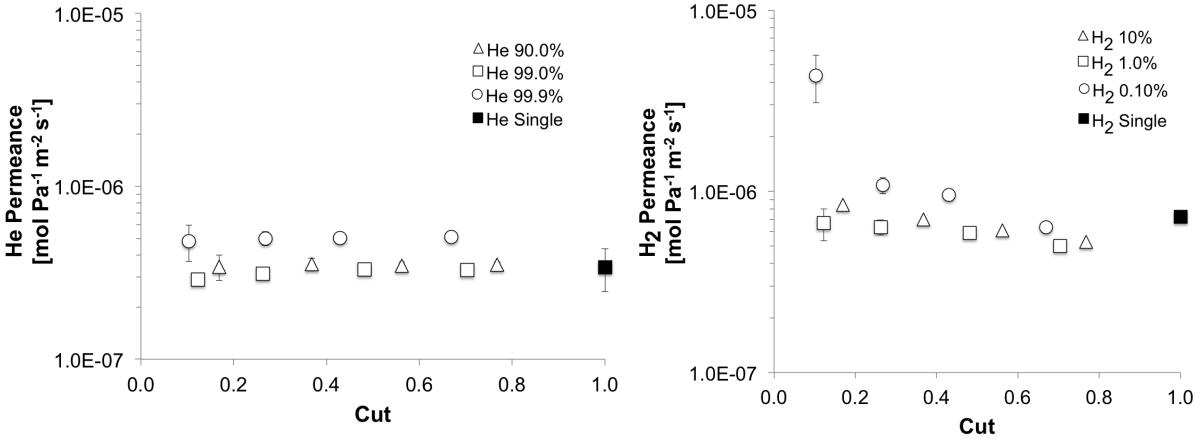

Figure 5.11: Permeance of helium (left) and hydrogen (right) as function of the cut, determined from the binary experiments data for 0.10% (circles), 1.0% (squares) and 10% (triangles). In black squares the single gas permeances of helium (left) and hydrogen (right) at RT are also plotted for comparison.

Despite the discussion above, the values obtained for the permeance are well in agreement to the values obtained in the single gas experiments (black squares[8] in figure 5.11). At RT, the helium permeance obtained in the single gas experiments was $(3.41 \pm 0.10) \times 10^{-7}$ mol m^{-2} s^{-1} Pa^{-1}, which is very similar to the permeances obtained at 1.0% and 10%; for instance for the latter case, the average permeance is $(3.49 \pm 0.26) \times 10^{-7}$ mol m^{-2} s^{-1} Pa^{-1}. For hydrogen, the value obtained in the single permeation tests was $(7.22 \pm 0.27) \times 10^{-7}$ mol m^{-2} s^{-1} Pa^{-1}, which is again similar to the permeances at the two higher hydrogen concentrations: at 10% the determined average permeance is $(6.68 \pm 0.55) \times 10^{-7}$ mol m^{-2} s^{-1} Pa^{-1}.

5.3.1.2 H_2O/He

- **Experiment at RT for 6% H_2O/He**

The first binary wet mixture experiment on the MFI-ZSM5 was performed at RT for 6% H_2O/He. The feed pressure as a function of the time is plotted in figure 5.12. As observed, the pressure on the feed side of the membrane was steadily increasing until a sudden and drastic raise after 90 minutes from 1.5 bar up to 4.5 bar was observed. This pressure built could be an indication of water condensation inside the pipes on the feed side, condensation within the module or saturation of the membrane. After removing the membrane from the module,

[8]The experimental points were placed at $\nu = 1$ since the single gas experiments are by definition at $\nu = 1$.

considerable amounts of water (above 60 g) were present inside the module and its flanges. In addition, the weight of the membrane was measured, and an increase of approximately 3 g in comparison with the initial weight (around 29 g) was observed. This result is interesting since by using the ratio of the thickness of the active layer (around 30 μm) to that of the whole membrane ($\sim$ 3 mm), it can be estimated that 1% of the weight (0.29 g) is zeolite. Using the density of silicalite ($\rho = 1.76$ g/cm^3 [BVDBKM97]) as the densitiy of the ZSM5 membrane, the mass of zeolite presented in the membrane is about 0.18 g, i.e., 6% of the amount of adsorbed water. This means that most of the water was adsorbed on the hydrophilic titania support.

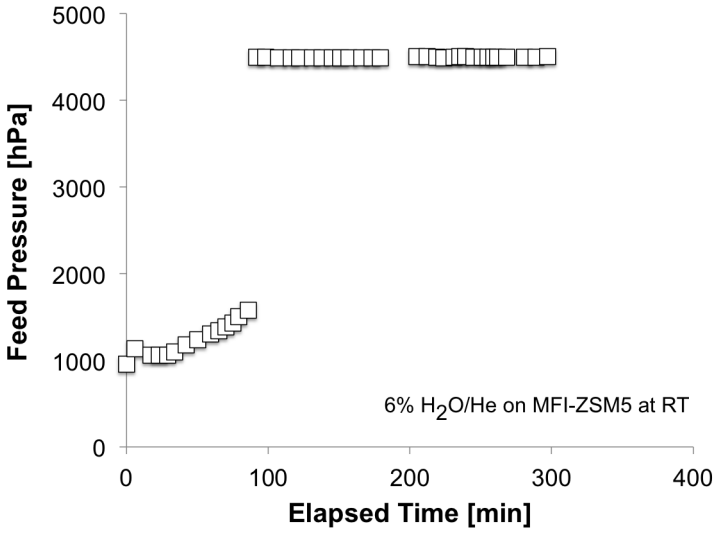

Figure 5.12: Feed pressure as a function of the elapsed time for the 6% H_2O/He experiments on the MFI-ZSM5 membrane at RT.

The reason of the condensation of water is explained considering the dew point, which is the temperature T_{D_p} of the gaseous mixture at a certain absolute pressure at which the water vapour phase condensates at the same rate the liquid phase evaporates. Using the August-Roche-Magnus formula, which relates the equilibrium saturation vapour pressure p_s in hPa and the temperature T in °C through the equation $p_s(T) = 6.1094 \exp\left(\frac{17.625T}{T+243.30}\right)$, the T_{D_p} can be calculated for a certain partial pressure of the moisture. For 6% H_2O/He at 1000 hPa (initial pressure in feed) the temperature of the module should be no less than 35 °C to avoid condensation. Since the membrane was operated at RT (< 30 °C) condensation occured obviously as observed in this test.

- **Influence of the cut on the separation factor**

The first experiments with vapour content on the MFI-ZSM5 membrane comprised to study the influence of the cut on the separation factor. In figure 5.13, three different $\alpha^*_{\mathrm{H_2O/He}}$ values for three different cuts obtained at around 76 °C for 6% H_2O/He are plotted.

The expected effect of the cut on the separation factor is observed, where the decrease of the former results in an increase of the later. No further $\alpha^*_{\mathrm{H_2O/He}}$ vs ν experiments were performed because the control of the cut is particularly difficult due to the presence of a wet stream. In fact, since no MSB is placed between the module and the MFC on the retentate side (figure

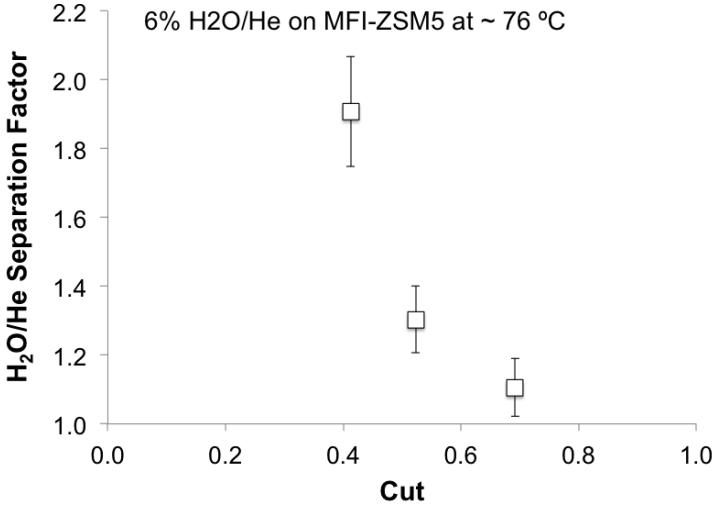

Figure 5.13: H_2O/He separation factor as function of the cut for 6% H_2O concentration with the MFI-ZSM5 membrane at 76 °C.

3.1), the corresponding measured/imposed flow values are strongly influenced by the presence of water molecules, providing erratic measurements.

- **Influence of the temperature and concentration on the separation factor**

At two different temperatures (103 °C and 77 °C) and two different concentrations (6% and 1%) the H_2O/He separation factor was investigated. The table 5.1 presents the results and it can be concluded that the separation factor increases with the decrease of both temperature and moisture content. The thermal dependence is justified by the fact that the higher is the temperature of the membrane the less is the number of condensed water molecules within the framework of the zeolite. That is, the preferential adsorption of water into the zeolitic pores is stronger at lower temperatures. As a consequence, the higher is the temperature the more helium can permeate through the membrane, decreasing the separation factor.

H_2O/He, %	77 °C	103 °C
6	1.91 ± 0.16	1.09 ± 0.10
1	3.68 ± 0.32	1.81 ± 0.34

Table 5.1: H_2O/He separation factor obtained for two different vapour concentrations (6 % and 1 %) and two different MFI-ZSM5 temperatures (77 °C and 103 °C). The uncertainties of the measured temperatures of the module are below 2%.

The increase of the separation factor with the decrease of concentration is of difficult analysis due to the pressure and cut conditions that each separation factor value was obtained. In table 5.2 the partial pressure differences of water vapour and the cuts (ratio $F_{P,\mathrm{He}}/F_{F,\mathrm{He}}$) relative to those results in table 5.1 are presented. The different obtained cuts are related to the difficulties of imposing the cut mentioned above; different cuts are obtained even though equal set (pressure and flow) values are maintained.

Considering for instance $T \simeq 103$ °C, a higher driving force (higher partial pressure dif-

ference) is measured for the highest concentration, although with a considerable higher cut. Therefore, from the results at this temperature is not clear that the higher $\alpha^*_{H_2O/He}$ for 1% is due to the decrease of concentration or the decrease of the cut. For $T \simeq 77$ °C, a similar cut is obtained for both concentrations whereas the driving force is higher for the highest concentration, which does not explain the increase of $\alpha^*_{H_2O/He}$ with the lowering of the vapour concentration.

H_2O/He %	T [°C]	ν	Δp_{H_2O} [hPa]
6	103	0.78 ± 0.06	89.0 ± 7.0
1	103	0.22 ± 0.03	4.5 ± 1.3
6	77	0.41 ± 0.05	23.0 ± 3.9
1	77	0.39 ± 0.03	3.9 ± 1.3

Table 5.2: Vapour partial pressure differences Δp_{H_2O} and cut ν values obtained in the experiments of the influence of the moisture content and temperature on the H_2O/He separation factor performed on the MFI-ZSM5 (from the data presented in table 5.1). The uncertainties of the measured temperatures of the module are below 2%.

The influence of the partial pressure (concentration) of water in the feed stream on the permeation of a given species is not totally understood and/or studied in the literature. Indeed, in [CY91] it is described that the surface diffusivity increases with the fractional surface coverage, although the opposite (decreasing tendency of the surface diffusivity with the concentration) can also be observed if the sorbate-sorbate bond is stronger than the sorbate-surface bond. It was recently reported the influence of moisture on the permeances of the binary mixture H_2/CO_2 on a ZSM5 membrane [WL12]. A supression effect of the vapour on the permeances of that gases was observed, due to the hydrophilicity of the zeolitic material. At a fixed temperature, the permeances of both H_2 and CO_2 decreased with the increase of the partial pressure of H_2O in the mixture $H_2O/H_2/CO_2$, since more water zeolitic pores are blocked by water at higher partial pressures. No published data reporting results similar to the ones presented in tables 5.1 and 5.2 was found.

- **Influence of the temperature on the separation factor at 1% H_2O/He**

In the plot of figure 5.14, the results concerning the influence of the temperature (keeping all the other parameters constant) on the H_2O/He separation factor at 1% H_2O/He are presented. As indicated, these experiments were not all performed in the same day. In the first day, the temperature was decreased from 106 °C down to 68 °C. In the second day, the temperature was further decreased from 51 °C down to 36 °C, while in the last day only one experiment at 32 °C was performed. In these experiments, all the obtained cut lie in the interval $\nu = 0.25 \pm 0.03$ (the He permeate flow is also presented in the plot and it remains almost constant for all the temperatures).

A continuous increase of the separation factor from 1.81 ± 0.34 up to 5.61 ± 0.46 with the decrease of the temperature is encountered, in agreement with what is expected and with what was obtained in previous experiments (table 5.1). However, it was also expected that the

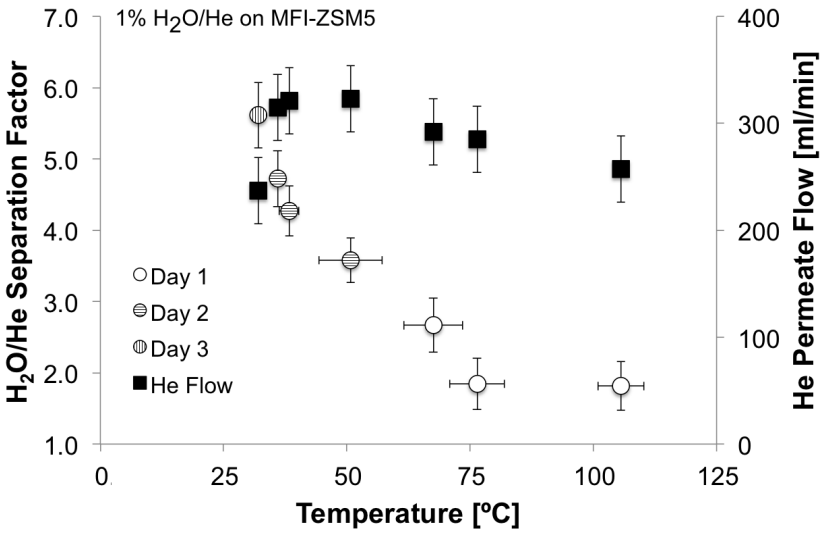

Figure 5.14: H_2O/He separation factor as function of the MFI-ZSM5 temperature. In empty, horizontal-striped and vertical-striped circles are the separation factors obtained in the days 1, 2 and 3 respectively. The He permeate flow is also plotted in black filled squares.

$\alpha^*_{H_2O/He}$ values could reach higher values. In fact, H_2O/H_2 ideal selectivities around 500 with the MFI-ZSM5 at 100 °C were already reported [RSK+08]. Although obtained for the ternary experiments, the H_2O/He separation factor obtained for the MFI-HF membrane was as high as 87 at around 30 °C. This high separation factor is explained by the high blockage of the zeolite pores due to condensed water preventing the permeation of helium. The rather constancy of the He permeation flow through the MFI-ZSM5 might be related with the existence of defects in the zeolite crystalline structure. The increase of the separation factor with the decrease of the temperature is thus mainly due to the stronger adsorption of water in the zeolitic matrix.

A further increase of the separation factor might be achieved if the driving force of water is increased. Since it is not of interest to increase its concentration (the aim of the experiments is to dilute the water down to 0.10% that is the typical value considered for the He stream purging the BB), the feed pressure shall be increased or the permeate pressure decreased.

5.3.2 S-SOD

5.3.2.1 H_2/He

A set of H_2/He experiments were performed on the two S-SOD membranes, that have a different sulfur content in the matrix: 0.5% and 1.5% in weight. The total permeate flow measured in the 1% H_2/He experiments at RT on those membranes is presented in figure 5.15. For reference, the 1150 ml/min (11.5 ml/min H_2 and 1139 ml/min He) total imposed flow is also showed.

As can be observed, the permeate flow is continuously increasing independently of the flow set in the MFC on the retentate side. This means that the membrane is not able to separate the feed in two constant streams, confirming that the membrane is not properly working, as already concluded for the single gas experiments (section 5.2.2).

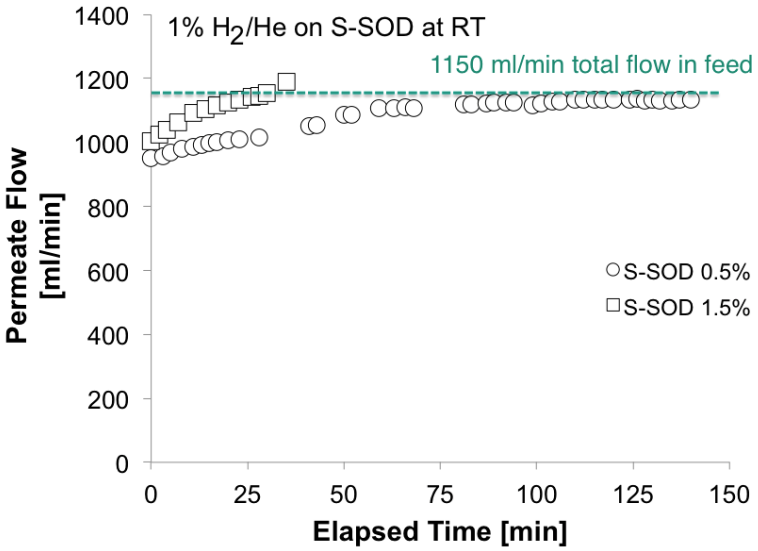

Figure 5.15: Permeate flow as a function of the elasped time of the experiment obtained in the 1% H_2/He binary mixtures experiments on the 0.5% (circles) and 1.5% (squares) S-SOD membranes at RT.

5.3.2.2 H_2O/He

Despite the unsatisfactory results obtained in the single and binary dry mixtures, a systematic study of the separation efficiency of the S-SOD membrane of 1% H_2O/He as a function of the membrane temperature similar to the one accomplished to the MFI-ZSM5 was performed. Since the vapour is a condensable gas, and the SOD framework is considerably hydrophilic it could be that some interesting separation performance of the membrane towards water could be achieved.

This study was performed in two days on the S-SOD 0.5%, in which in the first one the temperature was decreased from 85 °C down to 62 °C and in the second day the decrease was from 58 °C down to 44 °C. The observed behaviour was completely different from what could be expected. In fact, the retentate was enriched in water, while a wet stream in the permeate was hardly seen, which makes the membrane selective towards helium. Furthermore, the plotted He/H_2O separation factor in figure 5.16 shows no tendency with the temperature even within the results obtained during the same day. These results show that these SOD membranes are not also suitable to separate wet streams.

5.3.3 NaA

5.3.3.1 H_2O/He

A single wet 1% H_2O/He binary mixture experiment was performed on the NaA membrane to study the influence of the temperature on the separation factor. The results are plotted in figure 5.17; the separation factor is represented in empty circles and the helium permeate flow is shown in green. The separation factor shows an initial tendency of fast increase with the decrease of the temperature (from 1.95 ± 0.35 at 102 °C up to 7.02 ± 0.56 at 65 °C) but a decrease at around 55 °C is observed. No real explaination can be advanced and more experiments are required. Since the NaA is highly hydrophilic (is the most hydrophilic of the four membranes) these results show

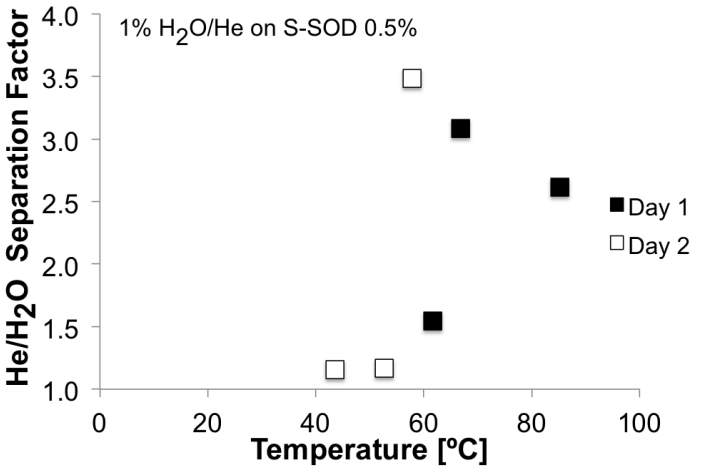

Figure 5.16: He/H_2O separation factor as function of the S-SOD 0.5% temperature for 1% H_2O/He in feed.

rather poor performances. These membranes are usually tested in pervaporation (separation of vapours) experiments, and IKTS published results of dewatering of ethanol with a separation factor of 30000 [RVK06]. Moreover, no water/gas separation results in the literature were found.

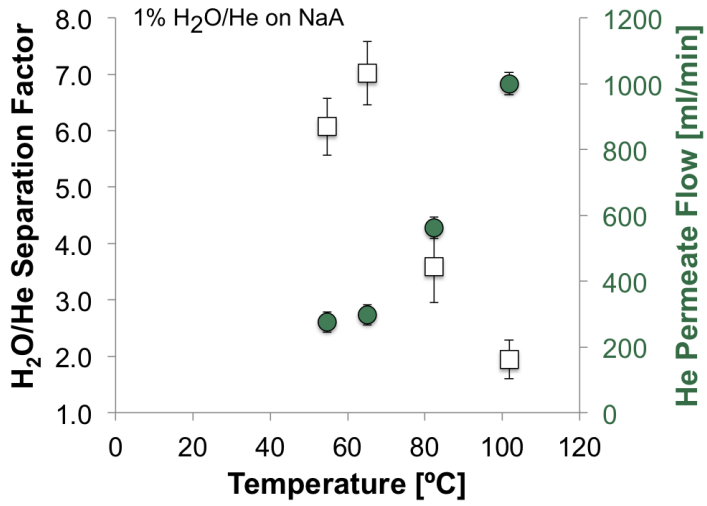

Figure 5.17: He/H_2O separation factor as function of the NaA temperature for 1% H_2O/He in feed. In green circles the He permeate flow is also present. The uncertainties of the measured temperatures of the module are below 2%.

As discussed for the MFI-ZSM5, the analysis of the results is difficult since different cuts and partial pressure differences are obtained for each point, as presented in the table 5.3. Despite the differences in the cut, the low driving forces might explain the low separation factors. A rather interesting phenomena is observed since separation occurs even with a negative partial pressure difference. This effect might be a result of the considerable decrease of the helium flow, leading to higher measured concentrations of vapour in the permeate stream. Weighing the membrane in the end of the experiments, it was observed no measurable adsorbed water. The improvement of the separation factor could be obtained by increasing the pressure difference, but no time was left to extend the experimental program.

T [°C]	ν	Δp_{H_2O} [hPa]
102	0.87 ± 0.04	4.0 ± 1.3
82	0.49 ± 0.03	-1.2 ± 0.8
65	0.26 ± 0.03	-5.7 ± 1.4
55	0.240 ± 0.003	0.5 ± 0.3

Table 5.3: Vapour partial pressure differences Δp_{H_2O} and cut ν values obtained in the study of the influence of the temperature on the H_2O/He separation factor performed on the NaA. The uncertainties of the measured temperatures of the module are below 2%.

5.4 Ternary Mixture Gas Experiments

5.4.1 MFI-ZSM5

The ternary experiment performed on the MFI-ZSM5 was accomplished by adding 1% H_2 to the binary mixture 1% H_2O/He in the "Day 3" of the binary experiments on this membrane (plot of figure 5.14), at around 32 °C. The evolution of the feed pressure and H_2O/He separation factor with the time is plotted in figure 5.18. The average of the rather constant $\alpha^*_{H_2O/He} = 5.61 \pm 0.46$ values at a pressure of 1000 hPa (until the minute 70) is the separation factor plotted in figure 5.14.

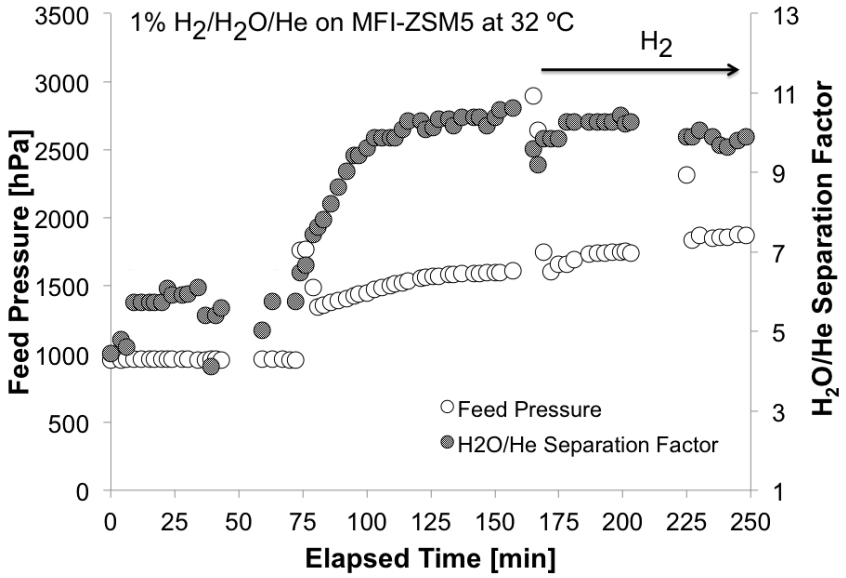

Figure 5.18: Feed pressure (empty circles) and separation factor (patterned circles) as a function of the elapsed time of the 1% H_2O/He and 1%/1% H_2/H_2O/He binary and ternary experiments on the MFI-ZSM5 membrane at RT. The instant of injection of H_2 is also indicated.

After more than one hour, the feed pressure suddenly starts to increase corresponding to a increase of the water/helium separation factor along with a decrease of the helium permeate flow (not showed). The transient lasts during approximately one hour, within which $\alpha^*_{H_2O/He}$ increases 1.4% up to 10.4, as well as the pressure in feed increases 1.2 %. In this period, the He feed flow decreases from 157 to 104 ml/min (at 0 min, the He flow was 439 ml/min). The

enhancement of the separation factor might be related with the increase of the driving force, since the same absolute pressure is maintained on the permeate side. Around the minute 165, 11.5 ml/min of H_2 is added to the permeating binary wet mixture. Its introduction evidences to not influence both the previous increase tendency of the pressure in feed and the $\alpha^*_{H_2O/He}$ plateau around 10.

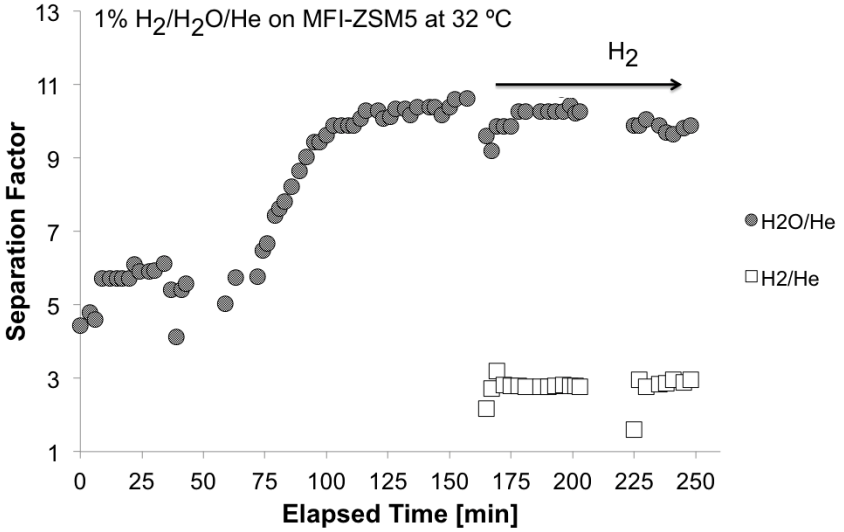

Figure 5.19: H_2O/He (empty circles) and H_2/He (empty squares) separation factors as a function of the elapsed time of the 1% H_2O/He and 1%/1% $H_2/H_2O/He$ ternary experiment on the MFI-ZSM5 membrane at RT.

In figure 5.19, the H_2O/He and H_2/He separation factors as a function of the elapsed time are presented. Averaging the experimentally obtained $\alpha^*_{H_2O/He}$ and $\alpha^*_{H_2/He}$ it is obtained 9.82 $\pm$ 0.76 and 3.05 $\pm$ 0.31, respectively. The latter result is surprising since in the binary mixtures experiments the highest separation factor obtained for 1% H_2/He was 1.58 $\pm$ 0.21. Thus these results show that the partly blocked pores in the zeolite enhance the H_2/He separation factor towards hydrogen. H_2O/H_2 and CH_4/H_2O experiments on this membrane were performed by IKTS, and a completely blockage of the ZSM5 pores led to a rejection of CH_4 while H_2 permeation was observed. This behaviour has not been yet understood and more experiments on this membrane shall be performed to test reproducibility and to investigate how the performance varies with variating important parameters such as partial pressures.

As observed for the very first H_2O/He binary experiments on the MFI-ZSM5 membrane, an increase of approximately 2 g of weight of the membrane was observed after these binary – ternary experiments, although without any condensation within the module and its flanges[9].

5.5 Summary of the experimental results

The figure 5.20 gives an overview of the He and H_2 permeances across the membranes. For reference, dashed green lines represent the order of magnitude of the permeances expected from the pulished data. In line with what was discussed before, only the experiments with the

[9]To exist condensation at RT ($\sim$ 30 °C) for a 1% H_2O/He stream, the absolute pressure should be as high as 4000 hPa. For pressures around 1000 hPa the dew point is approximately 7 °C.

MFI-ZSM5 membrane provided gas permeances in agreement with the expected ones. The ideal selectivity towards H_2 in hydrogen/helium at RT is 2.21 ± 0.10. The permeances obtained for the NaA show also agreement with the published data, although consolidation of these experiments after regeneration of the membrane shall be done. The diagram evidences the gap (one order of magnitude different) for the carbon membrane and a even larger one for the S-SOD membrane (three orders of magnitude).

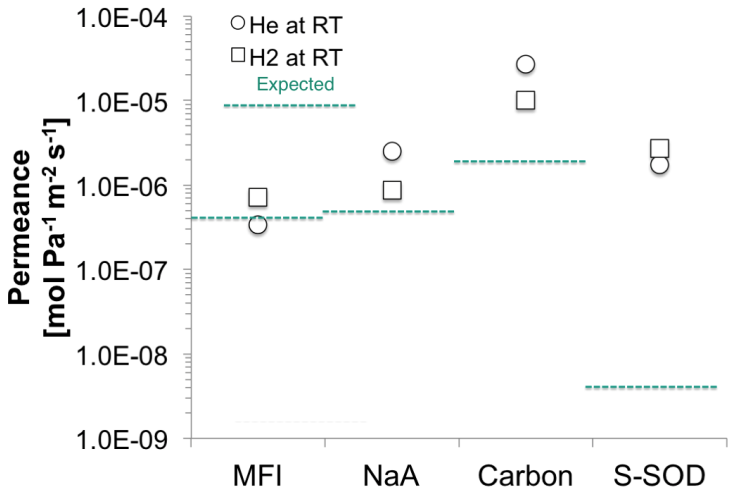

Figure 5.20: Comparison of the performances of the four membranes from the results obtained from the single gas experiments at RT.

The separation performance of the MFI membrane concerning the dry H_2/He stream depends largely on the cut and to a less extent on the hydrogen concentration. The ideal selectivity and the three highest separation factors obtained for each concentration at RT are presented in table 5.4. As expected, the separation factors are lower than the rather low ideal value due to a mutual influence of the permeating species across the membrane.

$\alpha_{H_2/He}$	$\alpha^*_{H_2/He}$		
	0.10% H_2/He	1.0% H_2/He	10% H_2/He
2.11 ± 0.10	1.68 ± 0.10	1.58 ± 0.21	1.64 ± 0.10

Table 5.4: Comparison of the hydrogen/helium ideal selectivity and separation factors obtained for the MFI-ZSM5 at RT. The here presented separation factors are the highest obtained (i.e., $\nu \simeq 0.3$).

In figure 5.21, it is plotted the variation of the separation factor with the concentration of the vapour/helium feed stream and temperature obtained for the MFI-ZSM5. The effect of temperature on the separation factor is expected and is coherent with the transport mechanism. The enhancement of $\alpha^*_{H_2/He}$ for lower concentrations is not yet really understood.

Concerning the performance of the membranes separating the 1% H_2O/He feed stream, the separation factor as function of the temperature obtained for the MFI and NaA membranes is plotted in figure 5.22. Although the driving forces obtained for the NaA were comparitevely low to the ones obtained for the MFI, the H_2O/He separation factor is larger for the NaA at each temperature. This might be related to the higher hydrophilicity of the NaA.

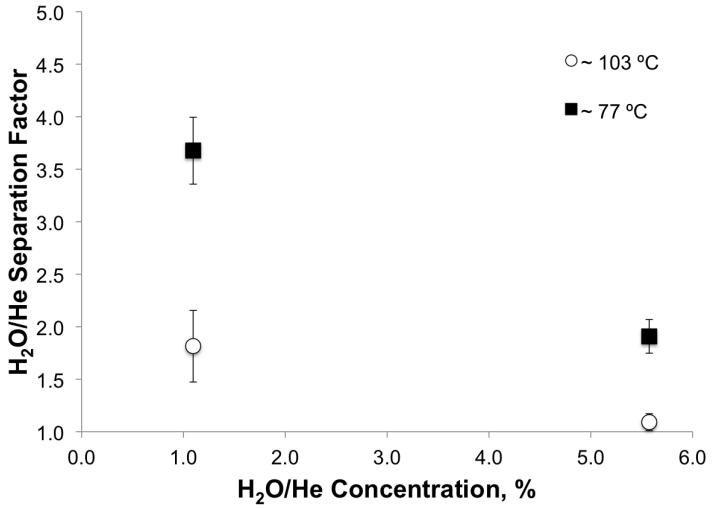

Figure 5.21: Separation factor as a function of the temperature and H_2O/He concentration obtained for the MFI-ZSM5 membrane.

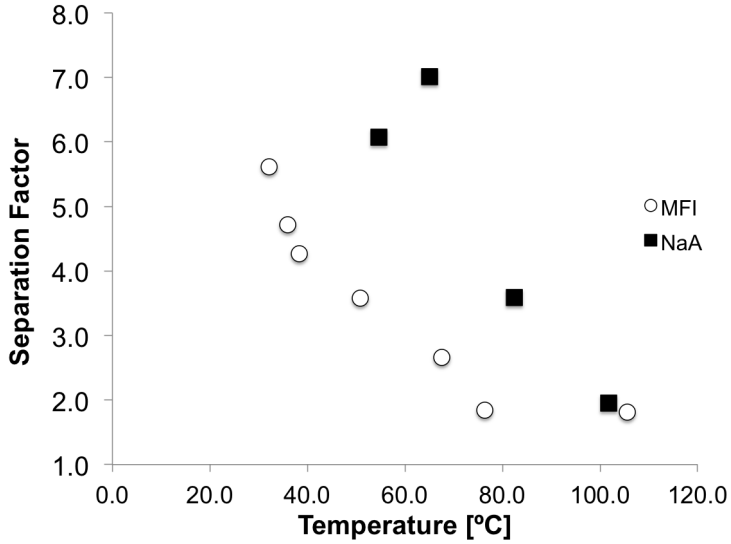

Figure 5.22: Comparison of the performances of the NaA and MFI membranes on the separation of the 1% H_2O/He as a function of the temperature.

The 1%/1% H_2/H_2O/He ternary experiment at 32 °C performed on the MFI-ZSM5 provided interesting results. A separation of that stream towards water vapour and hydrogen was obtained, with a H_2/He separation factor higher than the ones computed in the single and binary experiments. A bar plot is presented in figure 5.23, where these separation factors are showed. No ternary experiments on the other membranes for comparison were performed.

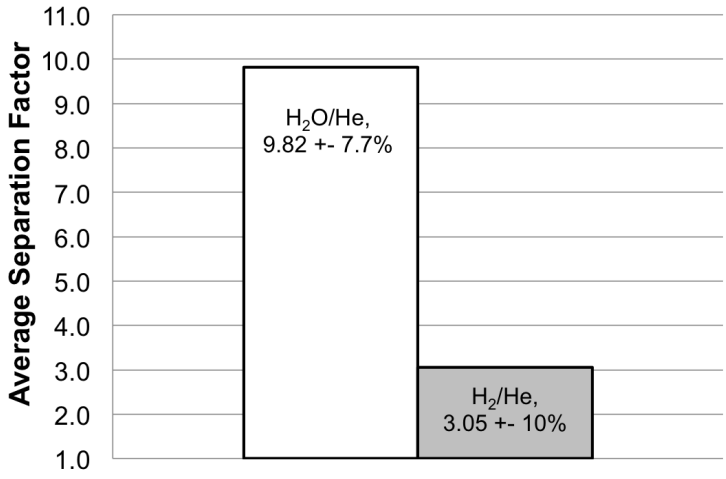

Figure 5.23: H_2O/He (white filled bar) and H_2/He (grey filled bar) separation factors obtained in the 1%/1% H_2/H_2O/He ternary experiment at 32 °C on the MFI-ZSM5 membrane.

6

Conclusions and Perspectives

The experiments performed at TLK – ZIMT aimed to investigate the separation efficiency of four different inorganic membranes by performing gas experiments in the single, binary and ternary mode towards the search for the most promising membrane to the application for the tritium process in the breeding blanket of future fusion reactors. In these experiments, hydrogen and water vapour replaced their radioactive counterparts, tritium and tritiated water, respectively.

The IKTS produced zeolite (MFI-ZSM5, SOD and NaA) and carbon membranes were characterized in terms of permeation and separation perfomances using the ZIMT III facility gradually upgraded during the work to provide single (He, H_2, N_2 and H_2O), binary (H_2/He and H_2O/He) and ternary (H_2/H_2O/He) mixtures experiments. The performances of the membranes were studied by controlling fundamental parameters such as temperature, pressures and concentrations of the mixtures. The experiments with wet streams were very delicate to perform due to the presence of the condensable water vapour. Indeed, several primary by-pass experiments were performed to understand the behaviour of the mixing with helium and to determine the exact concentration of water in the stream.

The main results obtained from the experiments are listed below:

- H_2 is the fastest permeating species through the MFI-ZSM5, while He is the less permeating one. At RT, a H_2/He ideal selectivity of 2.11 ± 0.10 and a separation factor of 1.68 ± 0.10 for 0.10% H_2/He were achieved on the MFI-ZSM5. There was no evidence of a dependence of the separation factor with the hydrogen concentration within the range 0.10% – 10%;
- the SOD and carbon membranes evidenced to have a considerably defected internal structure, which make them not suitable for further experiments;
- a steep increase of $\alpha^*_{H_2O/He}$ with the decreasing of the temperature at 1% H_2O/He in the MFI-ZSM5 and NaA membranes was observed. The separation factor of 5.61 ± 0.46 for the MFI-ZSM5 at 32 °C and 7.02 ± 0.56 for the NaA at 65 °C confirm the higher hydrophilicity of NaA. At 32 °C, the H_2O/He separation factor on the MFI-ZSM5 increased up to 9.82 ± 0.77 due to a progressively higher blocking of the zeolite pores.;
- an increase of $\alpha^*_{H_2O/He}$ at two different temperatures with the decrease of the moisture content in the H_2O/He stream was measured. However, from the experimental data, it is not clear that the lowering of $c_{H_2O/He}$ is the only source of such increase;
- the ternary 1%/1% H_2/H_2O/He experiments performed on the MFI-ZSM5 at RT showed that interestingly the H_2/He separation factor is enhanced (3.05 ± 0.31) in comparison to what was measured for the single and H_2/He binary mixtures.

The experiments here performed open a series of questions that have to be answered by performing more experiments on the membranes. Concerning the MFI-ZSM5 and NaA membranes, binary and ternary experiments containing water vapour at room temperature with an

increasing dillution of H_2O and H_2 in He shall be performed. These experiments might clarify the role of the moisture content on the separation efficiency of the membranes and shall also investigate the optimal driving force that provides the highest separation performances. Single, binary and ternary mixtures tests on a new IKTS carbon membrane should be also performed. Due to its smaller pores (in comparison with MFI-ZSM5 and NaA) superior separation factors can be expected. In view of future testing with tritium, several aspects concerning the experimental apparatus might be revised for a better control and measurement (e.g., to use of cold traps to dry the wet streams).

From the experience acquired during the experiments on these inorganic membranes the questions addressed in the General Introduction (chapter 1) can be answered as follows:

1. Tritium is an isotope of hydrogen which means that its chemistry is not different from the hydrogen one, and thus no isotopic effects on the separation performances of a membrane are expected. Therefore, these inorganic membranes might be suitable to perform experiments with tritium in both molecular and oxidised form;

2. Both MFI-ZSM5 and NaA membranes demonstrated superior and promising performances for H_2O/He separation in comparison with H_2/He. Therefore, the recovery of tritium in oxidised form seems to be more efficient than the process with tritium in the molecular form. To use these membranes in TES, the 0.1% H_2O/He stream purging the BB shall be considered. For TES, enrichment factors[1] of 20 and recovery factors[2] of 90% are used as minimum parameters for the processing of the 0.1% H_2/He purge stream. [BDKL13]. Since low performances of the tested membranes towards H_2/He separation are observed, a multi-stage cascade shall be implemented to efficiently process that stream. If a 0.1% H_2O/He stream is used instead, the single-stage configuration using these membranes might be sufficient to achieve the separation requirements.

[1]The enrichment factor is defined by the ratio of the concentration of a species in the permeate to the concentration of that species in the feed.

[2]The recovery factor is the fraction of the feed flow of a certain species i that is in the permeate.

Bibliography

[ABG+03] C Algieri, P Bernardo, G Golemme, G Barbieri, and E Drioli. Permeation properties of a thin silicalite-1 (MFI) membrane. *Journal of Membrane Science*, 222:181–190, 2003.

[ACD03] S M Auerbach, K A Carrado, and Prabir K Dutta. *Handbook of Zeolite Science and Technology*. CRC press, 2003.

[AH00] H Albrecht and E Hutter. Tritium recovery from an ITER ceramic test blanket module—process options and critical R&D issues. *Fusion Engineering and Design*, 49:769–773, 2000.

[AKM00] K Aoki, K Kusakabe, and S Morooka. Separation of gases with an A-type zeolite membrane. *Industrial & Engineering Chemistry Research*, 39:2245–2251, 2000.

[AMSZ12] Wameath S Abdul-Majeed, GM Serdaroglu, and William B Zimmerman. Application of liquid nitrogen cold trap for purification of hydrogen gas stream generated from NaBH4. *Journal of Chemical & Engineering*, 6(5):425–434, 2012.

[Bak00] Richard W Baker. *Membrane Technology and Applications*. John Wiley and Sons, 2000.

[BC96] Anthonie J Burggraaf and Louis Cot. *Fundamentals of Inorganic Membrane Science and Technology*, volume 4. Elsevier, 1996.

[BCMS02] M P Bernal, J Coronas, M Menéndez, and J Santamaría. Characterization of zeolite membranes by measurement of permeation fluxes in the presence of adsorbable species. *Industrial & Engineering Chemistry Research*, 41(20):5071–5078, 2002.

[BCNH03] N Bekris, C Caldwell-Nichols, and E Hutter. Cold trap and cryogenic molecular sieve adsorber: components for tritium extraction from the purge gas of the HCPB-breeder blanket for ITER. *Fusion Engineering and Design*, 69:21–25, 2003.

[BDKL13] O Borisevich, D Demange, M Kind, and X Lefebvre. Zeolite Membrane Cascade for Tritium Extraction and Recovery Systems. In *10th International Conference on Tritium Science and Technology*, 2013.

[BGG+05] B Bornschein, M Glugla, K Günther, TL Le, KH Simon, and S Welte. Successful experimental verification of the Tokamak exhaust processing concept of ITER with the CAPER facility. *Fusion Science and Technology*, 48:11 – 16, 2005.

[Bha91] Ramesh R Bhave. *Inorganic Membranes Synthesis, Characteristics, and Applications*, volume 312. Springer, 1991.

[BK13] R Bilato and R Kleiber. *IPP Summer University for Plasma Physics*. Max Planck Institut für Plasmaphysik, September 2013.

[Bur99] A J Burggraaf. Single gas permeation of thin zeolite (MFI) membranes: theory and analysis of experimental observations. *Journal of Membrane Science*, 155(1):45–65, 1999.

[BVDBKM97] W J W Bakker, L J P Van Den Broeke, F Kapteijn, and J A Moulijn. Temperature dependence of one-component permeation through a silicalite-1 membrane. *AIChE journal*, 43:2203–2214, 1997.

[BVKV98] AJ Burggraaf, Z.A.E.P. Vroon, K Keizer, and H Verweij. Permeation of single gases in thin zeolite MFI membranes. *Journal of Membrane Science*, 144(1):77–86, 1998.

[CAD+00] L Cot, A Ayral, J Durand, C Guizard, N Hovnanian, A Julbe, and A Larbot. Inorganic membranes and solid state sciences. *Solid State Sciences*, 2:313 – 334, 2000.

[CKV+08] H L Castricum, R Kreiter, H M Veen, D HA Blank, J F Vente, and J E ten Elshof. High-performance hybrid pervaporation membranes with superior hydrothermal and acid stability. *Journal of Membrane Science*, 324:111 – 118, 2008.

[CN08] J Caro and M Noack. Zeolite membranes - recent developments and progress. *Microporous and Mesoporous Materials*, 115:215 – 233, 2008.

[CNKS00] J Caro, M Noack, P Kölsch, and R Schäfer. Zeolite membranes–state of their development and perspective. *Microporous and Mesoporous Materials*, 38(1):3–24, 2000.

[Cor] Rotronic Instrument Corp. The rotronic humidity handbook.

[CSARR+13] JM Castillo, J Silvestre-Albero, F Rodriguez-Reinoso, TJ Vlugt, and S. Calero. Water adsorption in hydrophilic zeolites: Experiment and simulation. *Physical Chemistry Chemical Physics*, 15:17374–17382, 2013.

[CY91] YD Chen and RT Yang. Concentration dependence of surface diffusion and zeolitic diffusion. *AIChE journal*, (10):1579–1582, 1991.

[DBG+13] D Demange, O Borisevich, N Gramlich, R Wagner, and S Welte. Zeolite membranes and palladium membrane reactor for tritium extraction from the breeder blankets of ITER and DEMO. *Fusion Engineering and Design*, 88(9):2396–2399, 2013.

[DGG+08] D Demange, M Glugla, K Günther, TL Le, KH Simon, R Wagner, and S Welte. Tritium processing tests for the validation of upgraded PERMCAT mechanical design. *Fusion Science and Tchnology*, 54(1):14–17, 2008.

[DSK11] D Demange, S Stämmler, and M Kind. A new combination of membranes and membrane reactors for improved tritium management in breeder blanket of fusion machines. *Fusion Engineering and Design*, 86(9):2312–2316, 2011.

[Fre07] Jeffrey P Freidberg. *Plasma Physics and Fusion Energy.* Cambridge University Press, 2007.

[GCA+06] L Giancarli, V Chuyanov, M Abdou, M Akiba, BG Hong, R Lässer, C Pan, and Y Strebkov. Breeding blanket modules testing in ITER: an international program on the way to DEMO. *Fusion Engineering and Design*, 81(1):393–405, 2006.

[GCA+07] L Giancarli, V Chuyanov, M Abdou, M Akiba, BG Hong, R Lässer, C Pan, and Y Strebkov. Test blanket modules in ITER: an overview on proposed designs and required DEMO-relevant materials. *Journal of Nuclear Materials*, 367–370:1271–1280, 2007.

[GLELFdS02] T Gallego-Lizon, E Edwards, G Lobiundo, and L Freitas dos Santos. Dehydration of water/t-butanol mixtures by pervaporation: comparative study of commercially available polymeric, microporous silica and zeolite membranes. *Journal of Membrane Science*, 197:309–319, 2002.

[GRV13] C Günther, H Richter, and I Voigt. Zeolite membranes for hydrogen and water separation under harsh conditions. *Chemical Engineering Transactions*, 32:1963–1968, 2013.

[Har00] Archie A Harms. *Principles of Fusion Energy.* World Scientific, 2000.

[HGK+10] Ø Hatlevik, S K Gade, M K Keeling, P M Thoen, AP Davidson, and J D Way. Palladium and palladium alloy membranes for hydrogen separation and production: history, fabrication strategies, and current performance. *Separation and Purification Technology*, 73:59–64, 2010.

[Hir02] Yasuhiko Hirabayashi. Pervaporation membrane system for the removal of ammonia from water. *Materials Transactions*, 43(5):1074–1077, 2002.

[Hsi96] HP Hsieh. *Inorganic Membranes for Separation and Reaction.* Elsevier, 1996.

[ITE01] ITER EDA. Summary of the ITER Final Design Report. Technical report, International Atomic Energy Agency, 2001.

[Jar04] F. Jareman. *Properties and Modeling of MFI Membranes.* PhD thesis, Lulea University of Technology, 2004.

[Kan00] Nick K Kanellopoulos. *Recent advances in gas separation by microporous ceramic membranes.* Elsevier, 2000.

[KGH08] S Konishi, M Glugla, and T Hayashi. Fuel cycle design for ITER and its extrapolation to DEMO. *Fusion Engineering and Design*, 83(7):954–958, 2008.

[Kha10] Sheida Khajavi. *Separation of Process Water using Hydroxy Sodalite Membranes.* PhD thesis, Delft University of Technology, 2010.

[KJK07] S Khajavi, JC Jansen, and F Kapteijn. Preparation and performance of H-SOD membranes: a new synthesis procedure and absolute water separation. *Studies in Surface Science and Catalysis*, 170:1028–1035, 2007.

[Kra87] Kenneth S Krane. *Introductory Nuclear Physics.* John Wiley and Sons, 1987.

[LFN06] Shiguang Li, John L Falconer, and Richard D Noble. Improved SAPO-34 membranes for CO2/CH4 separations. *Advanced Materials*, 130(16):5412–5413, 2006.

[LKNA02] YS Lin, I Kumakiri, BN Nair, and H Alsyouri. Microporous inorganic membranes. *Separation & Purification Reviews*, 31(2):229–379, 2002.

[LU00] LL Lucas and MP Unterweger. Comprehensive review and critical evaluation of the half-life of tritium. *Journal of Research-National Institute of Standards and Technology*, 105(4):541–550, 2000.

[MPM10] S Maleksaeedi, Mohammad H Paydar, and J Ma. Centrifugal gel casting: a combined process for the consolidation of homogenous and reliable ceramics. *Journal of the American Ceramic Society*, 93(2):413–419, 2010.

[MT13] S Matsuda and K Tobita. Evolution of the ITER program and prospect for the next-step fusion DEMO reactors: status of the fusion energy R&D as ultimate source of energy. *Journal of Nuclear Science and Technology*, 50(4):321–345, 2013.

[NS95] Richard D Noble and S Alexander Stern. *Membrane separations technology: principles and applications.* Elsevier, 1995.

[Par11] M. T. Parracho. Permeance and selectivity of helium and hydrogen as single gases in nanocomposite-mfi membranes for tritium processes. Master's thesis, Instituto Superior Técnico, 2011.

[PC01] P Pandey and RS Chauhan. Membranes for gas separation. *Progress in Polymer Science*, 26(6):853–893, 2001.

[PTAN+09] M Pera-Titus, A Alshebani, C-H Nicolas, J-P Roumégoux, S Miachon, and J-A Dalmon. Nanocomposite MFI-alumina membranes: High-flux hollow fibers for CO2 capture from internal combustion vehicles. *Industrial & Engineering Chemistry Research*, 48(20):9215–9223, 2009.

[RC08] I Ricapito and A Ciampichetti. TBM-ITER tritium plant interfaces - Final Report. Technical report, ENEA, 2008.

[RCAB08] I Ricapito, A Ciampichetti, P Agostini, and G Benamati. Tritium processing systems for the helium cooled pebble bed test blanket module. *Fusion Engineering and Design*, 83(10):1461–1465, 2008.

[RSK+08] MP Rohde, G Schaub, S Khajavi, JC Jansen, and F Kapteijn. Fischer–tropsch synthesis with in situ H2O removal–directions of membrane development. *Microporous and Mesoporous Materials*, 115(1):123–136, 2008.

[RVFP03] H Richter, I Voigt, G Fischer, and P Puhlfürß. Preparation of zeolite membranes on the inner surface of ceramic tubes and capillaries. *Separation and Purification Technology*, 32(1):133–138, 2003.

[RVK06] H Richter, I Voigt, and JT Kühnert. Dewatering of ethanol by pervaporation and vapour permeation with industrial scale NaA-membranes. *Desalination*, 199(1):92–93, 2006.

[RVV+10] H Richter, H Voß, I Voigt, A Diefenbacher, G Schuch, F Steinbach, and J Caro. High-flux ZSM-5 membranes with an additional non-zeolite pore system by alcohol addition to the synthesis batch and their evaluation in the 1-butene/i-butene separation. *Separation and Purification Technology*, 72(3):388–394, 2010.

[SAB+14] M Simplício, M D Afonso, O Borisevich, X Lefebvre, and D Demange. Permeation of single gases and binary mixtures of hydrogen and helium through a MFI zeolite hollow fibres membrane for application in nuclear fusion. *Separation and Purification Technology*, 122:199–205, 2014.

[SD05] N Savage and M S Diallo. Nanomaterials and water purification: opportunities and challenges. *Journal of Nanoparticle Research*, 7(4):331–342, 2005.

[Sim12] M. Simplício. Experimental study of a MFI membrane for application in nuclear fusion. Master's thesis, Instituto Superior Técnico, 2012.

[Squ01] Gordon L Squires. *Practical Physics*. Cambridge University Press, 2001.

[Stä10] S Stämmler. Zeolite membranes for tritium processing in fusion machines. 2010.

[Szo92] Rosemarie Szostak. *Handbook Of Molecular Sieves: Structures*. Springer, 1992.

[Tay97] John Taylor. *Introduction to Error Analysis, the Study of Uncertainties in Physical Measurements*. University Science Books, 1997.

[TD99] A Tavolaro and E Drioli. Zeolite membranes. *Advanced materials*, 11(12):975–996, 1999.

[TDN09] Z Tang, J Dong, and T M Nenoff. Internal surface modification of MFI-type zeolite membranes for high selectivity and high flux for hydrogen. *Langmuir*, 25(9):4848–4852, 2009.

[Ver12] H Verweij. Inorganic membranes. *Current Opinion in Chemical Engineering*, 1(2):156–162, 2012.

[WBK+12] Y Wall, G Braun, N Kaltenborn, I Voigt, and G Brunner. Separation of CO2/N2 by means of a carbon membrane. *Chemical Engineering & Technology*, 35(3):508–512, 2012.

[WDSV10] J C White, P K Dutta, K Shqau, and H Verweij. Synthesis of ultrathin zeolite Y membranes and their application for separation of carbon dioxide and nitrogen gases. *Langmuir*, 26(12):10287–10293, 2010.

[WL12] H Wang and YS Lin. Effects of water vapor on gas permeation and separation properties of MFI zeolite membranes at high temperatures. *AIChE Journal*, 58(1):153–162, 2012.

[XBS+05] X Xu, Y Bao, C Song, W Yang, J Liu, and L Lin. Synthesis, characterization and single gas permeation properties of NaA zeolite membrane. *Journal of Membrane Science*, 249(1):51–64, 2005.

[Xia90] J. Xiao. *The Diffusion Mechanism of Hydrocarbones in Zeolites*. PhD thesis, East China Institute of Technology, 1990.

[YNF11] Miao Yu, Richard D Noble, and John L Falconer. Zeolite membranes: microstructure characterization and permeation mechanisms. *Accounts of Chemical Research*, 44(11):1196–1206, 2011.

[YPF06] Yuri P Yampolskii, Ingo Pinnau, and Benny D Freeman. *Materials Science of Membranes for Gas and Vapor Separation*. Wiley Online Library, 2006.

[ZSS+11] K Zhang, J Sunarso, Z Shao, W Zhou, C Sun, S Wang, and S Liu. Research progress and materials selection guidelines on mixed conducting perovskite-type ceramic membranes for oxygen production. *RSC advances*, 1(9):1661–1676, 2011.

A

Calibration of the Mass Flow Controllers

The MF1 series MFCs produced by MKS Instruments are calibrated for one specific gas i. In the instructions manual, gas correction factors g_{ij} are provided to convert the measured flow to the actual flow of the gas j being measured by the device. However, it was preferred to find these conversion factors experimentally: by imposing several flows of a gas j with a properly calibrated MFC and measuring it with another MFC (calibrated for i), a calibration curve could thus be found. Specifically, the calibrated MFC was the 1000 ml/min calibrated for He by default (here designated RF003). The resulting calibration curves with the respective equations for the nitrogen and hydrogen gases are presented below. The calibration fittting for both cases was more accurate when $b = 0$ in $y = ax + b$. The fitting was performed by using the data analysis framework ROOT.

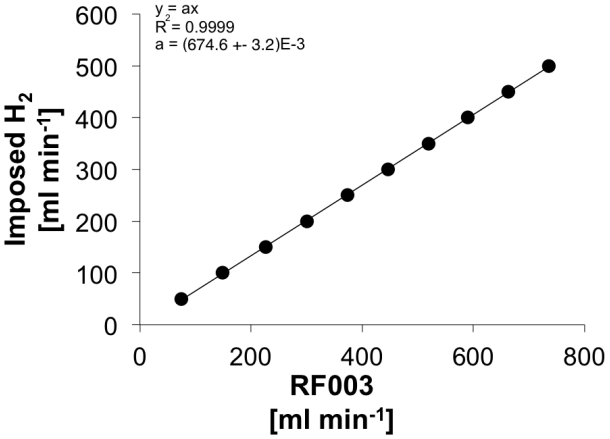

Figure A.1: Calibration plot of H_2. The hydrogen flow was imposed by a 500 ml/min MFC.

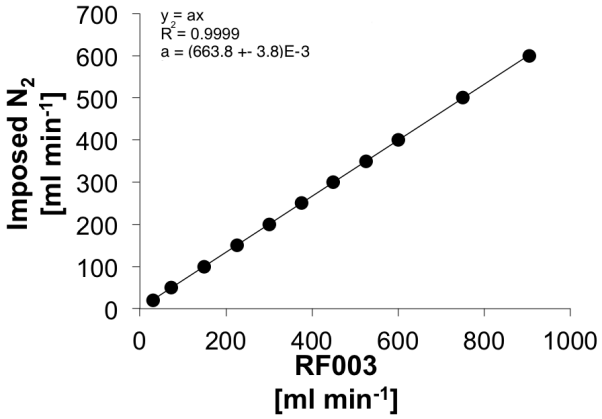

Figure A.2: Calibration plot of N_2. The nitrogen flow was imposed by a 1000 ml/min MFC.

B

The Quadera Software

The Quadera software is an user-friendly platform for capturing and visualizing measured data and parameter records. Complete measurement procedures can be programmed. Several different analysis modes are possible to perform, but only one was used for the determination of the H_2 in the H_2/He stream. The Faraday MID (Multiple Ion Detection) type of measurement allows the observation of the intensity/current signals respective to each mass as a function of time in a graph. The masses of the desired species to study are previously defined.

The signals are measured periodically in the course of the experiments until a steady-state is reached. An example of the interface of the software at this MID mode is presented in figure B.1, where the He, H_2 and N_2 species are being analysed. In this example, a s_{H_2}/s_{He} ratio of 5.6×10^{-3} is obtained. The signal relative to N_2 was also tracked since it is a good indicator of non-tight connections when its value reaches orders of magnitude above 10^{-11} A.

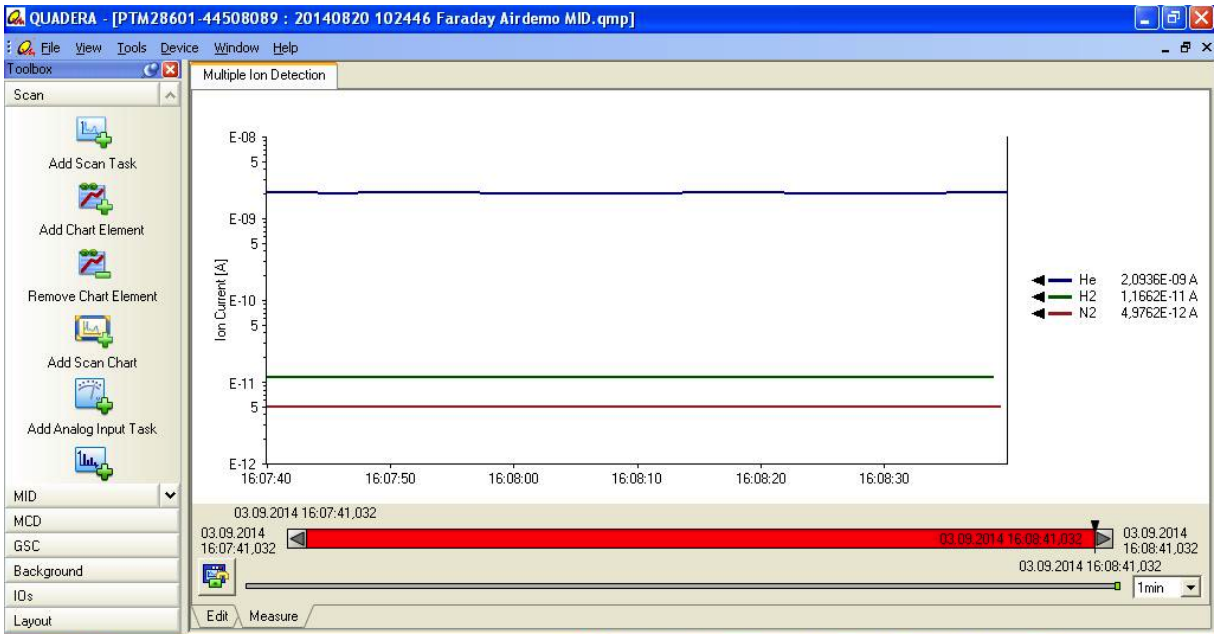

Figure B.1: Interface of the Quadera software operated in the MID mode.

C

Determination of the Uncertainties of the Quantities of Interest

The uncertainties associated with the experimental quantities calculated in this work were determined using the propagation of uncertainties for non-correlated quantities, given by the general formula:

$$\Delta f = \sqrt{\left|\frac{\partial f}{\partial a}\right|^2 \Delta a^2 + \left|\frac{\partial f}{\partial b}\right|^2 \Delta b^2 + ... + \left|\frac{\partial f}{\partial z}\right|^2 \Delta z^2} \tag{C.1}$$

where f is a function of the variables a, b, ..., z and $\Delta\rho$ is the uncertainty of the quantity ρ. This formula is also applicable when the uncertainties are calculated by using the specifications of the product (such as errors in accuracy or resolution, for example). However, as for example in the case of permeance (section C.0.2), where the permeate flow and pressure difference have some degree of correlation (although not exactly known) an upper limit can be obtained by using $\Delta f = \left|\frac{\partial f}{\partial a}\right| \Delta a + \left|\frac{\partial f}{\partial b}\right| \Delta b + ... + \left|\frac{\partial f}{\partial z}\right| \Delta z$ [Tay97].

C.0.1 Uncertainties of the measured (direct) quantities

In the experiments, the measured quantites are the pressures and flows (in feed, permeate and retentate[1] sides). Furthermore, the electrical current signals relative to the gas species in both permeate and retentate lines are obtained by the QUADERA software associated with the QMS. Relative and absolute humidity, temperatures of the pipes (given by the humidity sensor) and membrane module are also other quantities directly accessible from the experiments.

The uncertainties related with the MFC readings (in both measuring and controlling function) are calculated using the different sources of errors from the product specifications: accuracy (0.5% of the reading + 0.2% of the full scale), repeatability (0.20% of the full scale) and resolution (0.1% of the full scale). According to the product specifications, 1% of the reading is considered as accuracy uncertainty for pressures measurements, and it is somewhat in agreement to what is observed experimentally. The temperature measurements from the humidity sensor are considered to have ±0.05 °C of associated (resolution) error.

The determination of the H_2 concentration in both permeate and retentate sides was accomplished by measuring the He and H_2 electrical signals from the QMS, until the s_{H_2}/s_{He} reached a steady state. This steady state ratio was computed averaging the last measurements. The uncertainties associated with the current signals were determined by using the standard deviation of the mean: in a set $x_1, ..., x_N$ of N measurements, the best estimate for the quantity x is the average $\bar{x}$, whose uncertainty is given by the ratio $\sigma_x/\sqrt{N}$, where σ_x is the standard deviation [Tay97, Squ01]. The same procedure was done to obtain the uncertainties related to the RH and AH measured values.

C.0.2 Uncertainties of the computed (indirect) quantities

Using the measured quantities from the experiments, quantities of interest such as permeance, ideal selectivity or separation factor can be determined. Using the surface area A of the membrane, and permeate flow and pressure difference values, the permeance defined in section 2.3.2 can be computed. Moreover, using the permeation values of two gases (Π_i and Π_j for

[1] Applicable in both binary and ternary mixtures gas experiments, where the retentate is opened.

instance), the ideal selectivity $\alpha_{i,j} = \Pi_i/\Pi_j$, is readily obtained. The separation factor is obtained by using the molar fractions (concentrations) as defined in (2.5). Other quantities such as the cut or the ratio of the signals provided by the QMS for instance have also associated uncertainties that must be determined. By using the propagation of uncertainties formulae and the defining expressions of the several quantities, their uncertainties were computed applying the following equations:

- **Total flow,** F_F

$$\Delta F_F = \sqrt{\Delta F_{F,i}^2 + \Delta F_{F,j}^2 + ...} \tag{C.2}$$

  where $F_{F,a}$ is the flow in feed side of the specias a.

- **Permeance of species** i **in single gas experiments,** Π_i

$$\frac{\Delta \Pi_i}{\Pi_i} = \frac{\Delta F}{F} + \frac{\Delta(\Delta p)}{\Delta p} \tag{C.3}$$

- **Ideal Selectivity,** $\alpha_{i,j}$

$$\frac{\Delta \alpha_{i,j}}{\alpha_{i,j}} = \sqrt{\frac{\Delta \Pi_i^2}{\Pi_i^2} + \frac{\Delta \Pi_j^2}{\Pi_j^2}} \tag{C.4}$$

- **Concentration of species** i **in feed,** x_i

$$\frac{\Delta x_i}{x_i} = \sqrt{\frac{\Delta F_i^2}{F_i^2} + \frac{\Delta F_F^2}{F_F^2}} \tag{C.5}$$

- **Concentration of species** i **in permeate**[2]**,** y_i

  If $z_{i,j} = ay_i + b$ is the calibration equation of the QMS, where $z_{i,j}$ is the signal ratio of the signals relative to species i and j, and a and b have their own linear regression uncertainties, then

$$\Delta y_i = \sqrt{\left|-\frac{z_{i,j}-b}{a^2}\right|^2 \Delta a^2 + \left|-\frac{1}{a^2}\right|^2 \Delta b^2 + \left|\frac{1}{a^2}\right|^2 \Delta z_{i,j}^2} \tag{C.6}$$

- **Separation Factor,** $\alpha_{i,j}^*$

$$\frac{\Delta \alpha_{i,j}^*}{\alpha_{i,j}^*} = \sqrt{\frac{\Delta y_i^2}{y_i^2} + \frac{\Delta x_i^2}{x_i^2} + \frac{\Delta y_j^2}{y_j^2} + \frac{\Delta x_j^2}{x_j^2}} \tag{C.7}$$

- **Permeance of species** i **in binary and ternary gas experiments,** Π_i^*

$$\frac{\Delta \Pi_i^*}{\Pi_i^*} = \frac{\Delta x_i}{x_i} + \frac{\Delta F_F}{F_F} + \frac{\Delta w}{w} \tag{C.8}$$

  where $w \equiv x_i p_F - y_i p_P$ and thus $\Delta w = \sqrt{(x_i \Delta p_F)^2 + (p_F \Delta x_i)^2 + (y_i \Delta p_P)^2 + +(p_P \Delta y_i)^2}$.

[2]Also valid for computing the uncertainty of the concentration in retentate.

- **Cut, ν**

$$\frac{\Delta\nu}{\nu} = \sqrt{\frac{\Delta F_P^2}{F_P^2} + \frac{\Delta F_F^2}{F_F^2}} \tag{C.9}$$

- **Concentration of water vapor in a strem, $\mathbf{c_{H_2O}}$**

$$\frac{\Delta c_{\mathrm{H_2O}}}{c_{\mathrm{H_2O}}} = \sqrt{\frac{\Delta \mathrm{AH}^2}{\mathrm{AH}^2} + \frac{\Delta p^2}{p^2} + \frac{\Delta T^2}{T^2}} \tag{C.10}$$

D

Measured and Computed Data from the Single Gas Experiments on the MFI-ZSM5

In tables D.1 - D.3 the measured (flows and pressure differences) and computed (permeance and ideal selectivity) data for the MFI-ZSM5 membrane obtained from the single experiments within the $\sim$ RT – 130 °C temperature range are presented. See section 5.2.1.

$F_{F,\mathrm{He}}$ [ml/min]	$\Delta p_{\mathrm{He}} \pm 1\%$ [hPa]	$\mathrm{F}_{F,\mathrm{H_2}}$ [ml/min]	$\Delta p_{\mathrm{H_2}} \pm 1\%$ [hPa]	$\mathrm{F}_{F,\mathrm{N_2}}$ [ml/min]	$\Delta p_{\mathrm{N_2}} \pm 1\%$ [hPa]
		$T \sim 21$ °C			
126 ± 2.7%	506	260 ± 1.5%	500	200 ± 4.7%	496
253 ± 1.6%	997	536 ± 3.4%	1000	408 ± 3.5%	991
366 ± 1.2%	1440	674 ± 3.4%	1240	612 ± 3.3%	1490
		$T \sim 50$ °C			
115 ± 3.0%	502	233 ± 4.4%	500	166 ± 5.2%	491
235 ± 1.7%	1010	465 ± 3.5%	994	340 ± 3.7%	1000
335 ± 1.3%	1440	583 ± 3.4%	1240	509 ± 3.4%	1495
		$T \sim 75$ °C			
109 ± 3.1%	515	205 ± 4.7%	505	145 ± 5.7%	510
207 ± 1.8%	992	410 ± 3.5%	1005	282 ± 3.9%	989
299 ± 1.4%	1440	508 ± 3.4%	1240	425 ± 3.5%	1490
		$T \sim 100$ °C			
92.0 ± 3.6%	499	179 ± 5.1%	497	117 ± 3.6%	491
183 ± 2.0%	986	360 ± 3.7%	987	238 ± 4.2%	993
269 ± 1.5%	1440	454 ± 3.5%	1240	362 ± 3.6%	1500
		$T \sim 130$ °C			
89.9 ± 3.7%	506	173 ± 5.2%	500	103 ± 7.3%	507
177 ± 2.1%	992	347 ± 3.7%	997	205 ± 4.6%	993
268 ± 1.5%	1500	435 ± 3.5%	1239	313 ± 3.8%	1500

Table D.1: Helium, hydrogen and nitrogen permeation flows and pressure differences values measured in the single gas experiments for the MFI-ZSM5 membrane within the $\sim$ RT – 130 °C temperature range.

Π_{He} [10^{-7} mol/m^{2}sPa]	T [°C]	Π_{H_2} [10^{-7} mol/m^{2}sPa]	T [°C]	Π_{N_2} [10^{-7} mol/m^{2}sPa]	T [°C]
3.41 ± 2.8%	21.0 ± 0.56%	7.22 ± 3.8%	21.4 ± 0.54%	5.53 ± 4.8%	21.5 ± 0.16%
3.13 ± 3.0%	49.5 ± 0.26%	6.33 ± 4.7%	49.3 ± 0.24%	4.59 ± 5.1%	50.4 ± 0.28%
2.83 ± 3.1%	75.7 ± 0.53%	5.51 ± 4.9%	74.4 ± 0.13%	3.86 ± 5.4%	76.7 ± 0.50%
2.51 ± 3.4%	100.3 ± 0.14%	4.92 ± 5.1%	99.9 ± 0.72%	3.20 ± 5.8%	100.1 ± 0.23%
2.41 ± 3.4%	130.4 ± 0.25%	4.72 ± 5.1%	129.7 ± 0.14%	2.79 ± 6.2%	130.1 ± 0.12%

Table D.2: Helium, hydrogen and nitrogen permeance values obtained in the single gas experiments for the MFI-ZSM5 membrane within the ∼ RT – 130 °C temperature range.

$\alpha_{H_2/He}$	$\alpha_{N_2/He}$	α_{H_2/N_2}	T [°C]
2.11 ± 4.7%	1.62 ± 5.6%	1.31 ± 6.1%	∼ 21
2.02 ± 5.6%	1.47 ± 5.9%	1.38 ± 6.9%	∼ 50
1.95 ± 5.8%	1.36 ± 6.2%	1.43 ± 7.3%	∼ 75
1.96 ± 6.1%	1.29 ± 6.7%	1.52 ± 7.7%	∼ 100
1.95 ± 6.2%	1.16 ± 7.1%	1.69 ± 8.1%	∼ 130

Table D.3: H_2/He, N_2/He and H_2/N_2 ideal selectivity values obtained in the single gas experiments for the MFI-ZSM5 membrane within the ∼ RT – 130 °C temperature range. For simplicity the indicated temperatures are approximated values.

E

Parameters used for the fitting of the experimental single gas permeance of H_2

In table E.1 it is presented the parameters concerning the permeation of hydrogen through a MFI-type zeolite, used for fitting the experimental single gas permeances of that gas (section 5.2.1) [BVDBKM97]. In table E.2, the MFI-type zeolite structural parameters relevant for use to this fit are also provided.

	H_2
q_s [mmol g^{-1}]	5.4
$D_{0,s}$ [10^{-8} m^2 s^{-1}]	1.5
$E_{D,s}$ [kJ mol^{-1}]	2.1
ΔS [J mol^{-1} K^{-1}]	-43
ΔH [kJ mol^{-1}]	-5.9
$E_{D,\mathrm{GT}}$ [kJ mol^{-1}]	8.3
M [kg mol^{-1}]	2×10^{-3}
λ [m]	$9{\times}10^{-10}$

Table E.1: Hydrogen thermodynamic parameters for estimation of the permeation of this species through MFI-type zeolites as a function of the temperature. Based on the reference [BVDBKM97].

ρ_z [g cm^{-3}]	1.76
β	4

Table E.2: MFI-type physical parameters relevant for the fit of the experimental permeances. From the reference [BVDBKM97].

F

Measured and Computed Data from the H_2/He Binary Mixtures Gas Experiments on the MFI-ZSM5

In the tables F.1, and F.3, the relevant data concerning the binary experiments with the MFI-ZSM5 membrane are presented. Here, only the concentrations of hydrogen are presented, since these are the values obtained directly from the calibration curve of the QMS. The helium concentrations are promptly determined from those values. Note that the partial pressures Δp are absolute values (using the concentrations of helium or hydrogen the corresponding partial pressure differences are obtained). See section 5.3.1.1.

	$(\mathbf{0.1000 \pm 0.0039})\%$ **H_2**			
θ	0.10 ± 24%	0.27 ± 9.7%	0.43 ± 6.5%	0.67 ± 4.8%
y_{H_2}, %	0.14 ± 4.6%	0.17 ± 4.0%	0.16 ± 4.1%	0.12 ± 4.8%
w_{H_2}, %	0.12 ± 4.9%	0.11 ± 4.9%	0.092 ± 8.1%	0.066 ± 7.3%
F_P [ml/min]	129 ± 23%	335 ± 9.3%	537 ± 6.0%	836 ± 3.9%
F_R [ml/min]	1100 ± 3.1%	875 ± 3.8%	675 ± 4.7%	375 ± 8.3%
Δp [hPa]	363 ± 3.6%	906 ± 1.3%	1448 ± 1.7%	2224 ± 1.1%
$\alpha^*_{H_2/He}$	1.44 ± 6.0%	1.68 ± 5.6%	1.65 ± 5.7%	1.21 ± 6.2%

Table F.1: Parameters of interest obtained from the binary mixtures experiments at 0.10%.

	$(\mathbf{1.00 \pm 0.13})\%$ **H_2**			
θ	0.12 ± 20%	0.26 ± 9.9%	0.48 ± 6.0%	0.70 ± 4.7%
y_{H_2}, %	1.53 ± 4.9%	1.57 ± 5.0%	1.50 ± 5.1%	1.32 ± 6.3%
w_{H_2}, %	0.86 ± 8.4%	0.80 ± 9.1%	0.63 ± 12%	0.47 ± 15%
F_P [ml/min]	153 ± 20%	328 ± 9.5%	602 ± 5.3%	880 ± 3.8%
F_R [ml/min]	1114 ± 3.1%	875 ± 3.8%	625 ± 5.1%	400 ± 7.8%
Δp [hPa]	712 ± 1.4%	1412 ± 1.2%	1448 ± 1.2%	3610 ± 1.1%
$\alpha^*_{H_2/He}$	1.53 ± 13%	1.58 ± 13%	1.50 ± 13%	1.32 ± 14%

Table F.2: Parameters of interest obtained from the binary mixtures experiments at 1.0%.

In the graphics below, the helium and hydrogen partial flows as a function of the corresponding partial pressure differences at 0.10% (figure F.1), 1.0% (figure F.2) and 10% (figure F.3) H_2/He concentration are presented. The correlation factor R^2 is also presented in the plots to quantify the degree of linearity between the quantities. See section 5.3.1.1.

	$(\mathbf{10.00 \pm 0.32})\%$ $\mathbf{H_2}$			
θ	0.17 ± 15%	0.37 ± 7.3%	0.56 ± 5.3%	0.77 ± 4.4%
y_{H_2}, %	15.7 ± 2.0%	15.4 ± 2.0%	14.6 ± 1.4%	13.2 ± 1.5%
w_{H_2}, %	9.38 ± 1.6%	7.82 ± 1.5%	6.12 ± 1.8%	4.34 ± 2.1%
F_P [ml/min]	211 ± 15%	460 ± 7.0%	703 ± 4.6%	960 ± 3.4%
F_R [ml/min]	1115 ± 3.0%	875 ± 3.8%	625 ± 5.1%	375 ± 8.3%
Δp [hPa]	751 ± 1.5%	1620 ± 1.2%	2561 ± 1.1%	3528 ± 1.1%
$\alpha^*_{H_2/He}$	1.67 ± 3.8%	1.64 ± 3.8%	1.54 ± 3.5%	1.36 ± 3.5%

Table F.3: Parameters of interest obtained from the binary mixtures experiments at 10%.

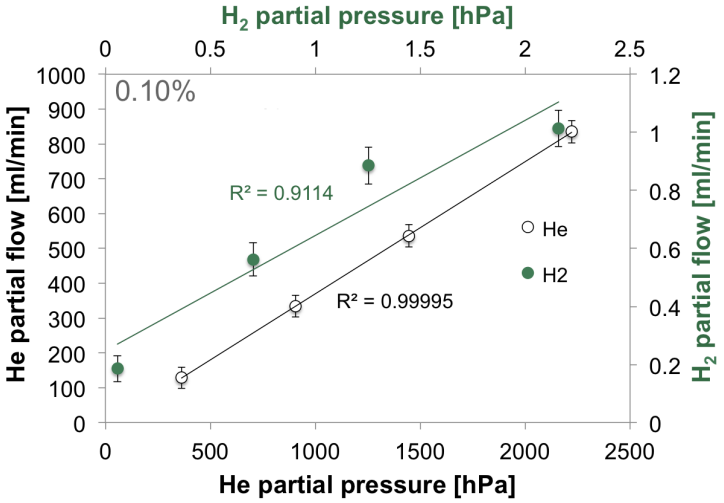

Figure F.1: Helium and hydrogen partial flows as a function of the corresponding partial pressures at 0.1% H_2/He, obtained from the binary mixtures experiments data. The green filled (empty) circes and the top (bottom) and right (left) axis correspond to the H_2 (He)

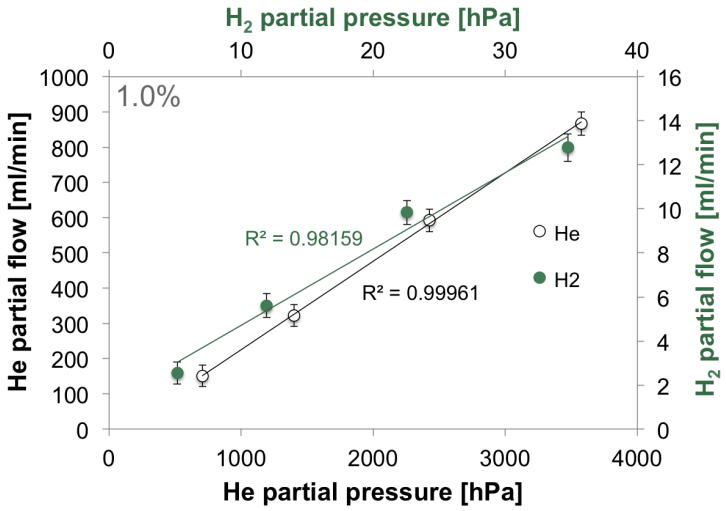

Figure F.2: Helium and hydrogen partial flows as a function of the corresponding partial pressures at 1.0% H_2/He, obtained from the binary mixtures experiments data. The green filled (empty) circes and the top (bottom) and right (left) axis correspond to the H_2 (He)

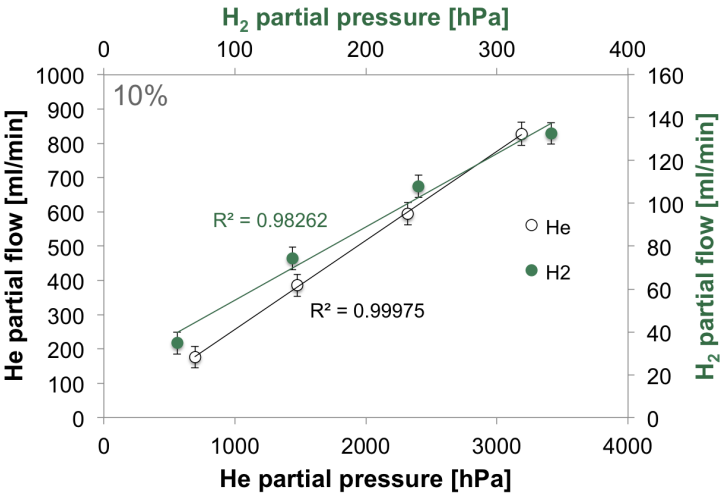

Figure F.3: Helium and hydrogen partial flows as a function of the corresponding partial pressures at 10% H_2/He, obtained from the binary mixtures experiments data. That the green filled (empty) circes and the top (bottom) and right (left) axis correspond to the H_2 (He).